

Daniel Schmid

**Laboratory Studies on
Aqueous Absorption and High
Temperature Chemistry of NO_x
and SO_x in Thermal Conversion
of Biomass Waste**



Laboratory Studies on Aqueous Absorption and High Temperature Chemistry of NO_x and SO_x in Thermal Conversion of Biomass Waste

Daniel Schmid

Inorganic Chemistry
Faculty of Science and Engineering
Åbo Akademi University
Åbo, Finland, 2023

Supervisor

Assoc. Prof. Oskar Karlström
Åbo Akademi University

Co-supervisor

Prof. Emerit. Mikko Hupa
Åbo Akademi University

Opponent and reviewer

Prof. Fredrik Normann
Chalmers University of Technology

Reviewer

Prof. Franz Winter
Technische Universität Wien

ISBN 978-952-12-4272-4 (printed)

ISBN 978-952-12-4273-1 (digital)

Painosalama, Turku, Finland 2023

PREFACE

The research presented in this thesis was carried out at the Laboratory of Inorganic Chemistry, Åbo Akademi, as part of the Johan Gadolin Process Chemistry Centre from 2019 to 2023. Funding for the projects was received from the EU project Horizon 2020 (“Highly efficient biomass CHP plants by handling ash related problems”), EU grant agreement 727616, as well as from the Academy of Finland (“Chemical challenges in gasification of biomass and waste”), Decision no. 353318 and 355914. Other research partners were Lund University, Technical University of Denmark, University of North Texas and Valmet Technologies Oy.

I want to thank everyone who has helped and supported me to carry out my research at Åbo Akademi University. First, I want to thank Prof. Leena Hupa for giving me the opportunity to carry out my research at the Laboratory of Inorganic Chemistry. A big thank you goes to Assoc. Prof. Oskar Karlström, my supervisor, for all the support and guidance during the last years, for the opportunity to conduct parts of my research in Sweden and Denmark, and for the freedom in my work to grow and develop own ideas. All the brainstorming and deep chemistry discussions in the office, the lab or on Zoom have been a real pleasure. I also want to thank Prof. Emerit. Mikko Hupa who has been attending many of these discussions, especially the discussions around Na-sulfation and NO₂ absorption. While sharing your great scientific experience in this research area, you always challenge others with your sharp questions, which always gives new ideas and inspiration. I am also grateful to D.Sc. Patrik Yrjas for his help and comments for the work on NO_x-release.

My stay at Lund University in 2020 ended abruptly due to the pandemic, but I am grateful that we managed to collect the experimental data for the Na-sulfation before I had to leave and that we could continue the modeling work online. I want to thank Prof. Marcus Aldén and the rest of the team at Lund University for inviting me and for the supervision in the lab. Peter Glarborg from DTU and Paul Marshall are gratefully acknowledged for their input for the modeling work.

From the laboratory service staff at Åbo Akademi University, I want to thank Tor Laurén for all the help and material provided in the lab. Whenever something was needed to start new experiments, I could trust on fast help. Another thanks goes to Luis Bezerra for carrying out all the ICP-OES analyses for my work. Discussions about sports and movies with you made the waiting time during long experiments more enjoyable.

I am also grateful for all the other colleagues in our research group. Teaching with Maria and Johan, discussions around beer after the CLUE meetings, games on the Christmas cruise, and lunch discussions with the other PhD students. All this has been a great balance to my research work.

I want to thank all my friends, especially from Brahe Djäkna and Florakörens who have been an important part of my life from the first day on after I came to Finland. Special thanks go to the Halikko gang for all the trips to the cottage and our “combustion experiments” there, Hanna Stål for your guidance and inspiration, Johnny Nykvist and Alexander Nykvist for all the serious or less serious discussions around a good beer, the board game group for all the nice evenings around board games, and the group involved in my “food chemistry experiments” around making own sausages.

Finally, I want to thank Rebekka for at least trying to listen to my chemistry (and other) monologues at home.

Turku, January 2023

Daniel Schmid

ABSTRACT

In order to fulfill the transition to a climate neutral economy and society, various renewable energy sources are needed to replace fossil fuels. Thermal conversion of biomass waste streams plays an important role in this transition. From a circular economy point of view, thermal conversion of valuable biomass materials, e.g. wood, is undesired. However, biomass waste streams, e.g. from agriculture and forest industry, which cannot be recycled or re-used can be valorized by recovering energy and valuable elements via thermal conversion. Thermal conversion of biomass waste is connected to various challenges due to their chemical and physical nature. Nitrogen and alkali metals are common components in biomass waste. In thermal conversion, nitrogen partly forms NO_x emissions, which are harmful to the environment. Hence, NO_x needs to be removed from the flue gases. The alkali in the biomass can cause deposit formation and corrosion on metal surfaces. In order to minimize high-temperature corrosion, biomass-fired boilers use lower steam temperatures as compared to e.g. coal fired boilers, which reduces the electrical efficiency of biomass-fired boilers. To reduce corrosion issues, corrosive alkali compounds such as alkali chlorides or hydroxides need to be captured in less corrosive forms, e.g. alkali sulfates.

The present work focuses on various aspects of the nitrogen and sulfur chemistry in thermal conversion processes using biomass waste streams. The formation of NO_x and NO_x precursors was studied for the thermal conversion of pre-treated bark and straw. The sulfation of sodium salts with SO_2 has been investigated in post-flame conditions. Regarding NO_x removal from flue gases, NO_2 absorption in aqueous solutions with sulfite and thiosulfate has been studied.

Combustion and devolatilization experiments for the investigation of NO_x emissions were performed in a single particle reactor consisting of an electrically heated quartz tube reactor. Single biomass particles were combusted (3% O_2 /rest N_2) or devolatilized (100% N_2) in the reactor. Pre-treated bark samples had a lower fuel-N to NO conversion as compared to the raw bark, while pre-treated straw samples had higher fuel-N to NO conversions. During the char conversion, washed samples had the highest conversion for both straw and bark. This was explained by the catalytic effect of ash forming elements in reducing NO emissions during char conversion. The ash forming elements also influenced the NO_x precursor formation during devolatilization. Samples with higher calcium contents showed higher NH_3 formation tendencies during devolatilization. The split between NH_3 and HCN also seems to be affected by the fuel-N and fuel-H content.

Sodium sulfation experiments were performed in a multi-jet burner, which provided well-controlled post-flame conditions at 850 to 1475 °C. NaOH(g) or

NaCl(g) and SO₂ were fed separately to the combustion environment where the sulfation reactions took place. The sodium salts were fed with a resulting gas phase concentration of 20 ppm, and SO₂ with 0–150 ppm. The concentrations of NaOH(g) and NaCl(g) were quantified using broadband UV absorption spectroscopy to follow the degree of sulfation. At temperatures above 1275 °C, almost no sulfation of NaOH(g) was observed, while most of the NaOH(g) was sulfated at 985 °C and below. The sulfation of NaCl(g) occurred to a much lower extent as compared to NaOH(g). At 850 °C, around half of the NaCl(g) was sulfated with 150 ppm SO₂. Chemical equilibrium calculations and kinetic modeling results were compared to the experimental results. At the highest investigated temperatures, the system could be described by chemical equilibrium. At 1115 °C and below, the measured concentrations were in good agreement with the kinetic model for NaOH(g). In the case of NaCl(g), the kinetic model over-predicted the degree of sulfation. The combined experimental data, chemical equilibrium calculations and kinetic modeling support that sulfation of alkali species can occur in the gas phase through homogenous reactions.

NO₂ absorption tests were performed by bubbling test gases with various NO₂ concentrations with and without air through aqueous solutions containing sulfur-containing additives. Without the additives, NO₂ was absorbed at low rates in water, i.e. 15% with 50 ppm NO₂ inlet concentration. When sulfite was present in the solution, NO₂ reacted with the sulfite to nitrite at increasingly higher rates. With 1 mM sulfite, the absorption rate increased by 200% as compared to water and by 500% with 10 mM at pH 8. The pH was shown to have a great impact on the performance of the sulfite additive due to the sulfite-bisulfite equilibrium. The absorption efficiency decreased with decreasing pH. Another factor that had a significant influence on the absorption efficiency was the presence of oxygen in the incoming gas. Without oxygen present, sulfite was consumed at a rate proportional to the NO₂ absorption, as sulfite only reacted with NO₂. In the presence of oxygen, however, sulfite was consumed at much higher rates due to radical chain reactions oxidizing sulfite to sulfate. While the sulfite oxidation rate was independent on the oxygen concentration for the investigated conditions (2–10% O₂), the rate increased linearly with the sulfite concentration in the absorption solution. The addition of thiosulfate to the sulfite solution has been shown to effectively reduce the sulfite oxidation, as thiosulfate acts as a radical scavenger. For a 10 mM sulfite solution, the sulfite oxidation rate decreased by 75% with 1 mM thiosulfate.

SVENSK SAMMANFATTNING

För att genomföra omställningen till en klimatneutral ekonomi behövs bättre förståelse för olika typerns förnybara energi. Termisk omvandling av biomassaavfallsströmmar spelar en viktig roll i denna omställning. Sett från en cirkulärekonomis synvinkel är termisk omvandling av värdefulla biomassamaterial såsom trä icke-önskvärt. Däremot kan biomassaavfallsströmmas bättre utnyttjas, t.ex. avfall från jordbruk och skogsindustri som inte kan återanvändas, genom att återvinna energi och värdefulla element via termisk omvandling. Termisk omvandling av biomassa har flera utmaningar på grund av deras kemiska och fysiska egenskaper. Kväve och alkalimetaller är vanliga komponenter i biomassa. Kväve i biomassan leder vid termisk omvandling till utsläpp av kväveoxider, som är skadligt för miljön. Därför måste kväveoxider avlägsnas från rökgaserna. Alkalimetaller i biomassan kan orsaka avlagringar och korrosion på metallytor. Biomassaeldade pannor använder lägre ångtemperaturer jämfört med t.ex. koleldade pannor för att minska på högtemperaturkorrosion, vilket också leder till en lägre verkningsgrad hos biomassaeldade pannor. För att minska korrosionsproblem måste korrosiva alkalikomponenter såsom alkaliklorider eller -hydroxider omvandlas till mindre korrosiva komponenter, såsom alkalisulfater.

Detta arbete fokuserar på olika aspekter av kväve- och svavelkemi relaterad till termisk omvandling av biomassaavfallsströmmar. Denna avhandling har studerat omvandlingen av bränslekväve till kväveoxider och mellanprodukter som leder till bildning av kväveoxider för termisk omvandling av förbehandlad bark och halm. Avhandlingen har även undersökt sulfateringen av natriumsalter med SO_2 i en förbränningsmiljö. För avlägsnande av kväveoxider från rökgaser studerades NO_2 -absorption i vattenlösningar med sulfat och tiosulfat.

Förbrännings- och termiska degraderingsexperiment för att undersöka utsläppet av kväveoxider utfördes i en elektriskt uppvärmd en-partikelreaktor gjord av kvartsglas. Biomassapartiklar förbrändes (3% O_2 /rest N_2) eller pyrolyserades (100% N_2) i reaktorn. Förbehandlade bark gav upphov till en lägre omvandling av bränsle-N till NO jämfört med obehandlad bark, medan förbehandlad halm gav upphov till en högre omvandling av bränsle-N till NO. Under koksförbränning uppgav tvättat bränsle den högsta omvandlingen av N till NO för både halm och bark. Detta förklarades av den katalytiska effekten av askbildande element vilken ger upphov till att NO-utsläppen minskar under koksförbränningen. De askbildande elementen påverkar också bildandet av kvävehaltiga mellanprodukter under pyrolysen. Prover med högre kalciumhalter uppvisade högre tendens att bilda NH_3 under pyrolysskedet. Fördelningen mellan NH_3 och HCN påverkades också av halterna av N och H i bränslet.

Natriumsulfateringsexperimenten utfördes i en förbränningsreaktor vid välkontrollerade förhållanden vid temperaturer mellan 850 och 1475 °C. NaOH(g) eller NaCl(g) och SO₂ matades separat till förbränningsmiljön där sulfateringsreaktionerna ägde rum. Ingångskoncentrationerna för natriumsalterna var 20 ppm och 0-150 ppm för SO₂. K NaOH(g) och NaCl(g)-koncentrationerna kvantifierades med hjälp av bredbands UV-absorptionsspektroskopi för att följa sulfateringen. Vid temperaturer över 1275 °C observerades nästan ingen sulfatering av NaOH(g), medan det mesta av NaOH(g) sulfaterades vid temperaturer lägre än 985 °C. Sulfateringen av NaCl(g) skedde i lägre utsträckning jämfört med NaOH(g). Vid 850 °C sulfaterades ungefär hälften av all NaCl(g) med 150 ppm SO₂. Kemiska jämviktsberäkningar och kinetiska modelleringsresultat jämfördes med de experimentella resultaten. Vid de högsta undersökta temperaturerna kunde systemet beskrivas väl med kemisk jämvikt. Vid temperaturer lägre än 1115 °C var de uppmätta koncentrationerna i god överensstämmelse med den kinetiska modellen för NaOH(g). I fallet med NaCl(g) förutspådde den kinetiska modellen högre grad av sulfatering än vad som observerades i experimenten. En kombination av experimentella data, kemiska jämviktsberäkningar och kinetisk modellering stödjer att sulfatering av alkalialter sker i gasfasen genom homogena reaktioner.

NO₂-absorptionstest utfördes genom att bubbla testgaser med olika NO₂-koncentrationer med och utan syre genom vattenlösningar innehållande svavelhaltiga tillsatser. Utan tillsatserna absorberades 15% av inkommande NO₂ i vatten. Med tillsatt sulfit i lösningen reagerade NO₂ med sulfiten till nitrit. Med tillsats av 1 mM sulfit ökade absorptionshastigheten med 200 % jämfört med vatten och med 10 mM ökade hastigheten med 500 % vid pH 8. Absorptionslösningens pH visade sig ha en stor inverkan på prestandan hos sulfittillsatsen vilket kunde förklaras med sulfit-bisulfid-jämviktstillståndet. Absorptionseffektiviteten minskade med sjunkande pH. En annan faktor som hade en betydande inverkan på absorptionseffektiviteten var ifall testgasen innehöll syre. I frånvaro av syre förbrukades sulfit proportionellt mot mängden absorberad NO₂ eftersom sulfit reagerade med NO₂. I närvaro av syre förbrukades sulfit däremot snabbare på grund av radikala kedjereaktioner som bidrog till att sulfit oxiderades till sulfat. Medan sulfitoxideringshastigheten var oberoende av syrekoncentrationen för de undersökta förhållandena (2, 5 och 10 % O₂), ökade oxidationshastigheten linjärt med sulfitkoncentrationen i absorptionslösningen. Tillsatsen av tiosulfat till sulfitlösningen har visat sig effektivt reducera sulfitoxideringen, eftersom tiosulfat fungerar som en radikalfångare. För en 10 mM sulfitlösning med 1 mM tiosulfat minskade sulfitoxideringshastigheten med 75 %.

LIST OF PUBLICATIONS

This dissertation is based on the following peer-reviewed scientific publications:

- I. **D. Schmid**, O. Karlström, P. Yrjas. Release of NH_3 , HCN and NO during devolatilization and combustion of washed and torrefied biomass. *Fuel* 280 (2020), 118583.
- II. O. Karlström, **D. Schmid**, M. Hupa, A. Brink. Role of CO_2 and H_2O on NO Formation during Biomass Char Oxidation. *Energ. Fuel* 35(9) (2021), 7058-7064.
- III. **D. Schmid**, W. Weng, S. Li, O. Karlström, M. Hupa, Z. Li, P. Glarborg, P. Marshall, M. Aldén. Optical in-situ measurements and modeling of post-flame sulfation of $\text{NaOH}(\text{g})$ and $\text{NaCl}(\text{g})$. *Fuel* 332(2) (2023), 126337.
- IV. **D. Schmid**, O. Karlström, V. Kuvaja, I. Vuorinen, M. Paavola, M. Hupa. Role of Sulfite Oxidation in NO_2 Absorption in a pH-Neutral Scrubber Solution. *Energ. Fuel* 36(5) (2022), 2666-2672.
- V. **D. Schmid**, M. Hupa, M. Paavola, I. Vuorinen, A. Lehikoinen, O. Karlström. Role of Thiosulfate in NO_2 Absorption in Aqueous Sulfite Solutions. *Ind. Eng. Chem. Res.* 62(1) (2023), 150-110.

CONTRIBUTION OF THE AUTHOR

- I. The author performed the experimental work and evaluated the data. The author was the main author of the publication.
- II. The author contributed to the experimental work. The author also participated in writing the publication.
- III. The author performed the experimental work, evaluated the data and performed the kinetic modeling and chemical equilibrium calculations. The author was the main author of the publication.
- IV. The author was responsible for planning and performing experimental work and analyses. The author was the main author of the publication.
- V. The author was responsible for planning and performing experimental work and analyses. The author was the main author of the publication.

TABLE OF CONTENTS

| | |
|---|------|
| PREFACE | IV |
| ABSTRACT | VI |
| SVENSK SAMMANFATTNING | VIII |
| LIST OF PUBLICATIONS | X |
| CONTRIBUTION OF THE AUTHOR | XI |
| 1. CONTEXT AND OBJECTIVES | 1 |
| 1.1 Context | 1 |
| 1.2. Objective..... | 2 |
| 2. INTRODUCTION | 3 |
| 2.1. Thermal conversion of biomass | 4 |
| 2.2. Pre-treatment of biomass | 5 |
| 2.3. NO _x formation | 6 |
| 2.4. NO _x removal..... | 7 |
| 2.5. Sodium sulfation..... | 11 |
| 3. EXPERIMENTAL | 14 |
| 3.1. NO _x and NO _x pre-cursor experiments | 14 |
| 3.1.1. <i>Biomass fuel samples</i> | 14 |
| 3.1.2. <i>Single particle reactor</i> | 15 |
| 3.2. NO ₂ absorption experiments | 16 |
| 3.3. Na-sulfation | 17 |
| 3.3.1. <i>Experimental setup</i> | 17 |
| 3.3.2. <i>Kinetic modelling and equilibrium calculations</i> | 19 |

| | |
|--|----|
| 4. RESULTS AND DISCUSSION | 21 |
| 4.1. NO _x and NO _x pre-cursor formation | 21 |
| 4.2. NO _x removal | 27 |
| 4.2.1. NO ₂ absorption in sulfite solutions (O ₂ -free flue gas) | 27 |
| 4.2.2. Sulfite oxidation during NO ₂ absorption (O ₂ -containing flue gas) | 30 |
| 4.2.3. NO ₂ absorption with thiosulfate | 33 |
| 4.2.4. Thiosulfate as sulfite oxidation inhibitor during NO ₂ absorption | 35 |
| 4.3. Na-sulfation | 40 |
| 4.3.1. NaOH(g) sulfation – experimental results and modelling | 40 |
| 4.3.2. NaCl(g) sulfation – experimental results and modelling | 43 |
| 5. CONCLUSIONS | 46 |
| 6. REFERENCES | 48 |
| Appendix I | 60 |
| Publications | 61 |

1. CONTEXT AND OBJECTIVES

1.1 Context

In December 2019, the European Commission presented the new European Green Deal, which aims to convert Europe to a climate neutral continent with no net emissions of greenhouse gases by 2050 [1]. Reducing the emissions of greenhouse gases requires a higher share of renewable energy sources in the European energy mix. For 2030, a new 40% renewable energy target was set. To reach this target, a variety of renewable energy sources is needed, such as wind-, hydro-, solar- and bioenergy.

Bioenergy is traditionally utilized via thermal conversion, e.g. the combustion of wood. Combustion of wood has been an important energy source in human history for hundreds of thousands of years. Even in the age of fossil fuels, it continued to be an important energy source. From a circular economy point of view, however, combustion of wood for energy production is undesired, as trees are a valuable resource. The European goal of re-forestation and restoring of natural environments also restricts the availability of wood as an energy source [1]. Biomass waste streams, on the other hand, e.g. from agriculture and forest industry, which cannot be recycled or re-used, can be valorized by recovering the energy and valuable elements via thermal conversion.

The thermal conversion of biomass waste streams is connected to various challenges due to their chemical nature and physical properties. High moisture contents and low grindability may require pre-treatments before the biomass waste can be used as a fuel. High NO_x emissions are a concern due high nitrogen contents in many biomass wastes. In addition, alkali halides present in the ash-forming fraction of the biomass waste can cause operational problems during the thermal conversion due to deposit formation and alkali induced corrosion in the boiler.

In order to increase the applicability of biomass waste streams for thermal conversion processes, it is important to address these challenges to reduce the environmental impact due to harmful emissions and to increase the efficiency of the thermal conversion by reducing ash-related issues.

1.2. Objective

The objective of this thesis is to shed more light on the nitrogen and sulfur chemistry in processes related to thermal conversion of biomass waste streams. Three different tasks are addressed in the reported work:

- Formation of nitrogen oxide and nitrogen oxide precursors during thermal conversion of from pre-treated biomass waste
- Gas-phase sulfation of corrosive sodium species with SO_2
- NO_x removal from flue gases by absorbing NO_2 in aqueous solutions with the sulfur-containing additives sulfite and thiosulfate

Biomass pre-treatment, such as washing and torrefaction, have gained increasingly more attention in order to improve physical and chemical properties of biomass wastes [2]. In the present work, the objective was to investigate how pre-treatment methods influence the fate of the fuel nitrogen during thermal conversion. The formation of NO , NH_3 and HCN during combustion and devolatilization has been investigated, as well as the correlation of their formation with changes in the fuel composition as a result of the pre-treatment

Sulfation of corrosive alkali species such as sodium hydroxide and sodium chloride is a method for reducing corrosion related problems on metal surfaces. The objective was to investigate the homogenous gas-phase reactions between the reactive alkali species and SO_2 at different temperatures between 850 and 1475 °C, which is a representative temperature range for most combustion processes. Optical in-situ measurements were performed to follow the sulfation reactions in post-flame conditions. Experimental results were also compared to an updated kinetic Na-Cl-S mechanism with novel thermodynamic data.

Stricter emission regulations require new technologies to reduce NO_x emissions from thermal conversion processes and other industrial processes [3]. The oxidation of NO to NO_2 with following absorption in aqueous solutions is a possible way to reduce NO_x emissions in flue gases. However, there are various challenges related to the goal of reaching high NO_2 absorption rates at reasonable costs. Additives such as sulfite can be used to improve the absorption rate. Sulfite, however, oxidizes rapidly to sulfate in the presence of oxygen. Sulfate does not influence the NO_2 absorption rates. In this thesis, the role of sulfite in NO_2 absorption has been studied under various well-controlled conditions to find optimal conditions for the NO_2 absorption, and to clarify the chemistry of the relevant reactions. Additionally, thiosulfate has been investigated as an additive to reduce sulfite oxidation in the presence of oxygen in the flue gas.

2. INTRODUCTION

In 2020, more than 80% of the world's primary energy consumption was based on fossil fuels, i.e. oil, gas and coal (see Fig. 1). Renewable energy sources such as wind, solar energy and biomass covered around 6% of the total primary energy consumption [4]. Energy conversion from biomass-based fuels has increased significantly during the last decades. While 162 TWh electricity was generated from biomass in 2000, the number increased to 655 TWh in 2019. This represents an increase from 1.2% to 2.7% of the total electricity production worldwide [5,6]. However, during the same period, the net global electricity consumption increased from 13,261 TWh to 23,921 TWh. In the transition to a carbon free future, the task is not only to replace fossil energy sources, but also to cover the increasing energy demand in the world. The development of a circular economy powered by renewable energies is worldwide one of the biggest challenges of the 21th century.

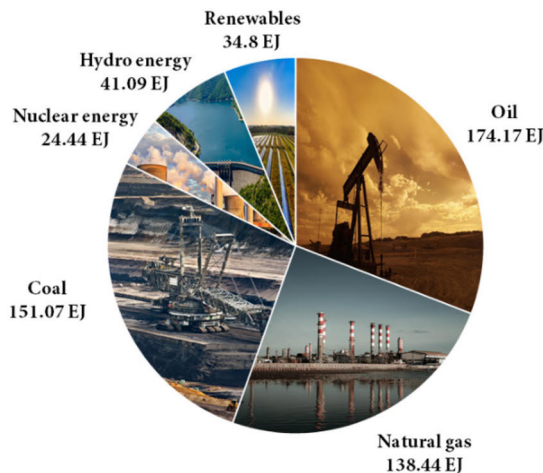


Figure 1. Primary energy consumption worldwide 2020 by fuel type.

In the EU, the usage of renewable energy sources increased steadily since the IPCC report in 1990 and the implementation of Kyoto I and Kyoto II. By 2030, 40% of the energy in the European Union should be generated from renewable sources. In 2020, Finland generated 50% of its electricity from renewable sources of which 30% was generated from wood-based fuels and black liquor, a wood-based side stream from paper industry (see Figure 2). In the same year, around two thirds of the district and industrial heat was based on renewable fuels, also mainly black liquor and other wood-based fuels [7].

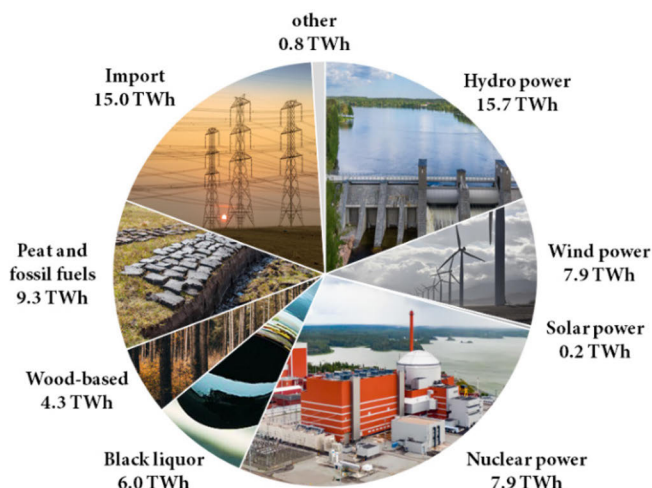


Figure 2. Electricity production Finland 2020.

While heat and power production from wood may not be considered carbon-neutral [8], thermal conversion of biomass waste (e.g. from forest industry and agriculture) is a preferred option that has increasingly gained more attention. However, various technical challenges are connected to the increased use of biomass fuels due to their chemical nature and physical nature. These challenges include NO_x emissions and ash-related issues, which are addressed in the present work.

2.1. Thermal conversion of biomass

Various thermal conversion methods can be utilized to generate heat from biomass for e.g. electricity production, but also to refine the biomass to liquid (pyrolysis) or gaseous (gasification) fuels that can be used in engines or for the production of valuable chemicals [9]. The oldest, and most used thermal conversion method is combustion.

During combustion, a biomass particle undergoes different combustion stages (see Figure 3). When entering a hot environment, e.g. in a boiler, the particle is drying and the water in the biomass particle starts to evaporate [10]. The next stage is the devolatilization, in which volatile compounds are released to the gas phase. In the presence of oxygen, these volatile gases and tars are oxidized to CO_2 and H_2O , and also partly to NO_x . The non-volatile compounds remain in the char. During the char conversion, the char is reacting with oxygen to mainly form CO and CO_2 and also NO_x . When the combustion is completed, the ash remains. The ash consists mainly of inorganic compounds.

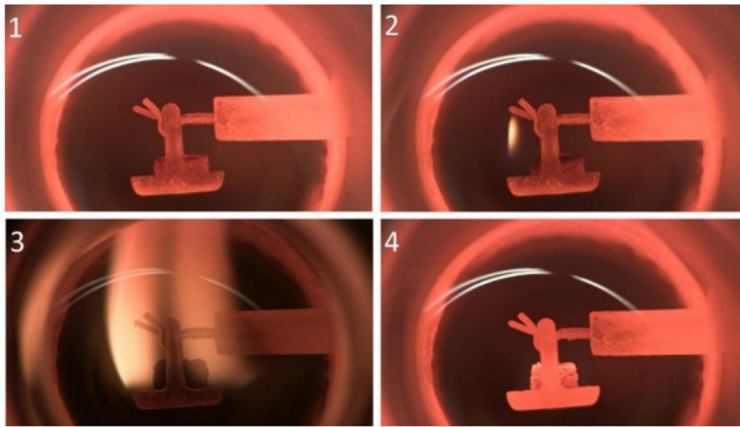


Figure 3. Stages during combustion of biomass particle: 1 – drying, 2/3- devolatilization and combustion of gases, 4 – char conversion. Figure from Åbo Akademi single particle reactor.

2.2. Pre-treatment of biomass

Biomass can be pre-treated to improve the chemical and physical properties of the biomass fuel. Biomass has beneficial properties such as high volatile content and reactive chars, which results in high thermal conversion rates and low residence times in the boiler. However, when comparing biomass fuels to coal, there are significant drawbacks in using biomass regarding the energy density, which also affects the economic feasibility of replacing coal with biomass [11]. While the lower heating value of coal ranges between 17–33 MJ/kg, it is only 16–17 MJ/kg for wood pellets [12]. Other drawbacks of biomass are the high moisture content, hygroscopicity and the high alkali content [13].

Torrefaction is a pre-treatment for upgrading biomass fuels to obtain a more homogenous fuel with higher quality [14]. For torrefaction, the biomass is heated to 200–300 °C to release moisture and parts of the volatile matter of the fuel. The volatile matter released at these temperatures has a lower heating value. The remaining solid biomass has a higher heating value as compared to the original biomass. Torrefaction can be performed in non-oxidative atmospheres (N₂ or CO₂ [15,16]) or oxidative atmospheres (air or flue gases [17,18]). Interestingly, torrefaction in oxidative atmospheres occur at a higher rate, but the solid yield is lower as compared to torrefaction in non-oxidative atmospheres.

Another common pre-treatment method is washing. The purpose of washing the biomass is to leach soluble alkali compounds from the biomass fuel to reduce alkali-

induced corrosion in the boiler. Depending on the biomass fuel, up to 30% of the alkali may be removed with water washing and around 70% with acid washing [19]. Especially for biomass fuels such as straw washing has been shown to be an effective pre-treatment [20].

2.3. NO_x formation

NO_x describes a group of nitrogen oxides of which NO (> 90%), NO₂ and N₂O are the most common ones that can be emitted from thermal conversion processes [21]. NO and NO₂ can form acidic rain when reacting with moisture in the atmosphere and cause smog, while N₂O is a potent greenhouse gas and ozone destroyer [22]. Due to their harmful nature, NO_x formation has been an important research topic in order to understand the chemical details of the formation needed to further reduce NO_x emissions [23,24].

NO_x is formed by oxidation of the fuel-bound nitrogen (fuel-N) and at higher temperature from reactions between O₂ and N₂ (thermal NO_x). The fuel-N is typically divided into two categories: volatile nitrogen (vol-N) and char nitrogen (char-N). The vol-N describes the fraction of nitrogen that is released during devolatilization, and the char-N is the nitrogen that remains in the char. Vol-N consists of compounds like NH₃, HCN, N₂, NO and HNCO. For some fuels, a significant fraction of the vol-N is bound to tars [23]. For biomass however, tar-N is generally observed at lower temperatures than typical of biomass combustion, i.e. above 800 °C.

NH₃ and HCN are NO_x pre-cursors, i.e. they can be oxidized to NO during the combustion process. At the same time, they can also react with NO and O₂, reducing the NO to N₂. NH₃ has a higher tendency to reduce NO to N₂ [21]. Due to the importance of NH₃ and HCN in NO_x formation, the formation of these NO_x pre-cursors has been studied extensively. While some studies investigated their formation during thermal conversion of a range of fuels [25–28], other studies have been looking into model compounds representing N-containing species similar to those found in biomass [29–31].

The ratio (split) and release of NH₃ and HCN depends on several factors, such as the fuel type. For instance, in spruce bark, NH₃ has been reported to be the main NO_x precursor, while NH₃ and HCN were equally formed during the devolatilization of wheat straw [32]. Another important factor are the conditions of the thermal conversion process, i.e. the temperature and the heating rate of the fuel particles. At high heating rates, HCN formation is enhanced, while lower heating rates promote NH₃ formation [33].

The NH_3 and HCN formation tendencies may be attributed to the chemical composition of the fuels. In biomass, the majority of the fuel-N is bound in proteins, which consist of a great variety of amino acids [30]. Carbohydrates (cellulose, hemicellulose and lignin) in the biomass have different effects on the amino acids during devolatilization [32]. In addition, ash forming elements such as calcium and potassium have shown catalytic effects on the HCN and NH_3 formation [28,31,34,35]. A study by Zhou et al. revealed that potassium promoted the NH_3 formation during fast pyrolysis of 2,5-diketopiperazine while it inhibited the HCN formation [31]. Calcium, on the other hand had the opposite effect, suppressing the NH_3 formation. In a study by Yi et al., calcium had an enhancing effect on the NH_3 formation during pyrolysis of amino acids and proteins [35]. For the pyrolysis of straw and corncob, it was found that potassium promoted both NH_3 and HCN formation, while calcium inhibited the formation [36]. The great variety of results in these kind of studies show the complexity of the NH_3 and HCN formation during devolatilization and the lack of consensus in this area.

Besides the NO_x precursor formation from vol-N, ash-forming matter also affects the NO_x chemistry during char conversion. During char conversion, char-N is oxidized to mainly NO. Char conversion is a heterogeneous reaction between the oxidizing gas and the solid char particle. Before the NO is released, it can be reduced to N_2 in the pores of the char, due to the catalytic activity of the char [37,38]. The degree of the reduction of NO to N_2 is dependent on various factors such as particle size and the availability of catalytically active elements in the char, e.g. potassium [39–41].

2.4. NO_x removal

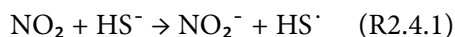
NO_x emissions can be reduced using several different techniques that either aim to reduce the NO_x during the thermal conversion process or to remove the NO_x from the flue gas. A brief description of the most common techniques follows:

1. Fuel staging, also known as re-burning, has been introduced around a semi-century ago [42,43]. In re-burning, oxidizing and reducing zones are created in the furnace by combustion with excess air and followed re-burn fuel addition. NO_x that is formed during the initial combustion can be reduced to N_2 in the reducing zone. An additional burn-out zone is needed to fully oxidized re-burn fuel. Usually, around 50-70% NO_x reduction can be obtained using re-burning.

2. Air staging intends to reduce the formation of NO_x by limiting the availability of O₂, O and OH, which are NO_x promoters. Air staging reduces NO_x emissions by around 50% [44].
3. Selective non-catalytic reduction (SNCR) reduces NO_x by injecting ammonia or urea in the presence of oxygen. SNCR has the disadvantage of possible ammonia slip, little or no hydrocarbons or CO should be present in the flue gas, and the narrow temperature range for high efficiency (900 – 1050 °C when using urea) [45–47].
4. Selective catalytic reduction (SCR) also uses ammonia to reduce NO_x to N₂. In SCR, the ammonia is chemisorbed on a catalyst. This enables operation at lower temperature (250 – 400 °C), but poisoning of the catalyst due to fly ash and dust from the combustion process limits the application [48,49].
5. In wet scrubbing NO_x (and also other gases) are removed from the flue gas by absorption of the gases into a liquid [50,51]. Additives may be required to achieve a desired absorption efficiency. The chemistry of NO_x absorption with sulfur additive is topic of the present thesis.

As mentioned in section 2.3, NO is the main NO_x species that is formed during thermal conversion of biomass waste. NO, however, has a low solubility in water. Various additives have been investigated to improve the absorption of NO into aqueous solutions, e.g. by liquid phase oxidation [52,53]. Oxidizing agents like NaClO₃, NaClO₂, NaClO, ClO₂ [53–56], ozone [57,58] KMnO₄ [59] or persulfate [60]. NO is oxidized to NO₂ to improve the absorption efficiency as NO₂ has a higher solubility in water [61]. NO can also be selectively oxidized in the flue gas with the described oxidizing agents, so that the flue gas mainly contains NO₂ when it enters the scrubber.

Despite the higher solubility of NO₂ as compared to NO, absorption rates may still be too low to achieve the required NO_x removal. A range of additives, mainly sulfur additives, has been investigated to improve NO₂ absorption in aqueous solutions. One of these additives is sodium sulfide (Na₂S), which proved being effective also on large scale [62–64]. When dissolved in water, sulfide hydrolyzes almost completely to HS⁻ and reacts with NO₂:

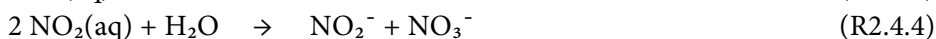
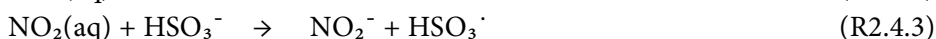
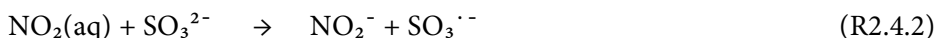


Shen and Rochelle demonstrated that > 95% of the NO₂ in a stirred cell reactor with sulfide solutions containing 0.1 M Na₂S or higher. The experiments were performed with inlet concentrations of 20 – 500 ppm NO₂ [63]. While sulfide is highly effective for enhancing the NO₂ absorption, it has the huge disadvantage that it requires a

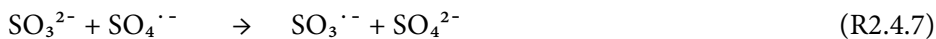
high pH to be stable. If the pH of the absorption solution is below pH 9, H₂S will be formed [65]. The formation of H₂S should be avoided as H₂S is a poisonous gas [66]. The high pH that is required for safe NO₂ absorption with H₂S may cause other operational problems such as that CO₂ (which is present in flue gases) will start to absorb and clogs may form due to carbonate deposit formation.

Another additive that has been demonstrated to enhance NO₂ absorption is sulfite (SO₃²⁻). Sulfite improves NO₂ absorption rates and in contrast to sulfide, it is stable at lower pH [67–69]. Similar to the experiments with sulfide, Shen and Rochelle investigated the NO₂ absorption in a stirred cell reactor using aqueous solutions containing 1 – 100 mM sulfite [67]. At pH > 7.5, 80% NO₂ absorption was achieved with 10 mM sulfite.

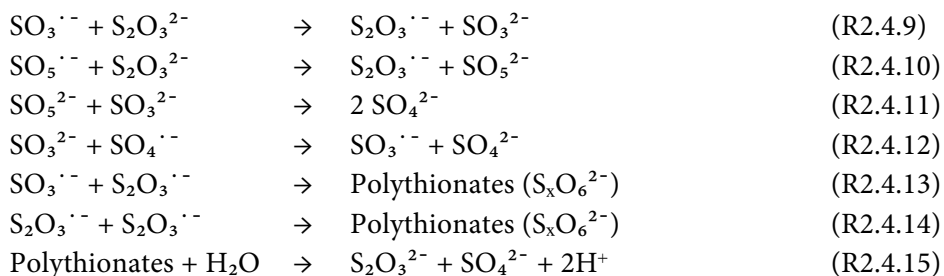
NO₂ absorption in aqueous sulfite solutions consists of a complex series of diffusion and chemical reaction steps. The first two steps are the diffusion of NO₂ through the gas-liquid film and the reaction NO₂(g) → NO₂(aq). NO₂(aq) will then react with water molecules or the sulfite additive via charge transfer reactions [70]. Dependent on the pH, sulfite is either present as SO₃²⁻ (sulfite) or HSO₃⁻ (bisulfite).



When NO₂ is reacting with water, equimolar amounts of nitrite (NO₂⁻) and nitrate (NO₃⁻) are formed. In the reaction with sulfite, only nitrite is formed and the sulfite ion reacts to a sulfite radical. In the presence of oxygen, the sulfite radical will initiate a radical chain reaction which consumes further sulfite ions through oxidation to sulfate [61,71,72].



The oxidation of sulfite via this radical chain mechanism is not desired as it reduces the sulfite concentration in the absorption solution rapidly and thereby decreases the absorption efficiency. To prevent sulfite from being oxidized by O₂, radical scavengers may be added to the solution to terminate the radical chain reaction. Thiosulfate (S₂O₃²⁻) is a known sulfite oxidation inhibitor [73], but also organic radical scavengers like hydroquinone, thiourea, ascorbic acid, p-phenylenediamine or tert-butylhydroquinone may be used for that purpose [74].

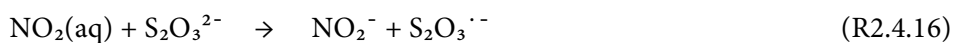


R2.4.9 – R.2.4.15 describe reactions that possibly take place when thiosulfate is used to reduce the sulfite oxidation. Some studies proposed that the radical chain mechanism is terminated by thiosulfate reacting with the $\text{SO}_5^{\cdot -}$ radical formed in R2.4.5 [61,67]. Other suggested the reaction of thiosulfate with the sulfite radical [75,76]. According to these reactions, the sulfite radical is re-converted to a sulfite ion (R2.4.9). The thiosulfate radical, which is formed in this reaction, will react further with sulfite radicals or another thiosulfate radical forming polythionates (R 2.4.13 and R2.4.14). Hydrolysis of the polythionates partially regains thiosulfate, which can participate again in the sulfite oxidation inhibition mechanism.

Sapkota et al. investigated the kinetics of sulfite oxidation with thiosulfate as a sulfite oxidation inhibitor [61]. In their study, low NO_2 concentrations (2 – 10 ppm) were used for absorption experiments with sulfite concentrations of around 40 mM and 25 – 100 mM thiosulfate. The addition of 25 mM thiosulfate reduced the sulfite oxidation rate by one order of magnitude. The further increase of the thiosulfate concentration to 100 mM showed only minor improvements.

Another study on the sulfite oxidation inhibition and thiosulfate consumption was performed by Mo et al. on an industrial scale [76]. It should be mentioned that the study aimed to reduce sulfite oxidation in a desulfurization scrubber to avoid sulfate formation and NO_2 was not present in this study. Nevertheless, the study demonstrated inhibition effects of sulfite oxidation with thiosulfate concentrations as low as 2 mM.

The study of Mo et al. [76] suggested that self-oxidation of thiosulfate may be ignored for the thiosulfate consumption when used as a sulfite oxidation inhibitor in the absence of NO_2 . In the presence of NO_2 , however, this might not be the case. Similar to sulfite oxidation, thiosulfate consumption might also be promoted through the reaction with NO_2 [67]. NO_2 reacts with thiosulfate to nitrite and a thiosulfate radical. However, according to Shen and Rochelle, this reaction is significantly slower as compared to the reaction of NO_2 with sulfite.



Several studies have been looking into the simultaneous absorption of NO_x and SO_x , hence using absorbed SO_2 in the scrubber solution as a sulfite source [77–83]. However, in contrast to e.g. coal, many biomass- and waste-derived fuels contain low contents of sulfur, hence the flue gas contains only small concentrations of SO_2 [84]. NO_2 removal under these conditions may require the addition of sulfite [83]. To reduce the consumption of the used chemicals (sulfite and thiosulfate), it is crucial to understand the chemical details of the process. In terms of NO_x removal, the aim of this thesis was to shed light on the NO_2 absorption process by investigating various reaction conditions (varying sulfite and thiosulfate concentrations, the oxygen and NO_2 concentrations in the test gas and the pH of the absorption solution) and following the consumption of the additives.

2.5. Sodium sulfation

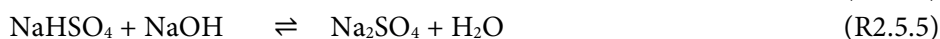
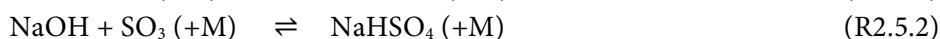
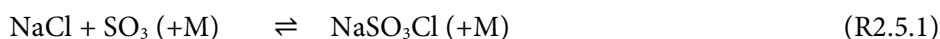
Some inorganic compounds, especially those with low melting points, are a main concern in thermal conversion of biomass waste. Biomass, black liquor or other waste side streams often contain high amounts of alkali, sulfur and chlorine, which can be released as alkali chloride or hydroxide, hydrogen chloride (HCl) and sulfur dioxide (SO_2) [85–88]. The alkali compounds contribute to aerosol formation [89–91] and to slagging [92], fouling [93] and corrosion in the boiler [94]. A study by Enestam et al. showed that potassium chloride and sodium chloride are equally corrosive towards conventional heat exchanger materials [95]. In most biomass fuels, potassium is the dominant alkali species [96] as potassium is an important nutrient for plants [97]. Sodium is not a nutrient for plants but is still present in the fuel, e.g. in biomasses that have been treated with lye [93], painted waste wood [98], black liquor [99] or biomasses exposed to seawater and road salting [100].

The corrosivity of the alkali compounds that are released during the thermal conversion process can be reduced by converting those alkali compounds to less corrosive ones. Alkali chlorides, which have a lower melting point, strongly accelerate the high temperature corrosion of metal surfaces in a boiler [101]. Alkali sulfates, on the other hand, have higher melting points and are less corrosive. Another corrosive sodium salt with a low melting point is sodium hydroxide. In absence of chlorine, sodium hydroxide is the main compound released to the gas phase that is stable in combustion gases, i.e. moist and oxidizing conditions [102].

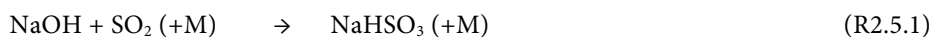
Sulfation of alkali compounds can occur in the combustion gas in the presence of SO_2 . The SO_2 content in flue gases from thermal conversion of biomass are generally low [103]. Additional sulfur may be added to enable the sulfation reactions. Sulfur can be added in its elemental form, which is oxidized to SO_2 during the combustion process [104]. Sulfur can also be added by mixing the biomass fuel

with sulfur-rich fuels like peat [105]. Another alternative is the addition of sulfate salts, e.g. ammonium sulfate. The sulfate salts decomposes to SO₃ at high temperatures, which can then react with the alkali compounds to form alkali sulfate. This has been shown to be more efficient for sulfation reactions as compared to SO₂ [106–108].

The sulfation reactions may occur in the gas phase and in the condensed phase, depending on the conditions in the combustion gas [109–111]. However, sulfation reactions in the gas phase are expected to occur at higher rates as compared to sulfation reactions in the condensed phase [109]. A detailed kinetic mechanism for the sulfation of alkali (here shown for sodium) to alkali sulfate in the gas phase has been proposed by Glarborg and Marshall [112].



Kinetic modeling based on this mechanism was in good agreement with experimental results for the sulfation of KCl in an entrained flow reactor at 900 – 1100 °C [109]. To initiate the sulfation reaction, SO₂ has to be converted to SO₃ [109,112]. The kinetics of the oxidation of SO₂ to SO₃ is important for a complete description of the sulfate formation, which has been emphasized by Jiménez and Ballester [113]. Hindiyarti et al. suggested alternative reaction paths for lower temperatures, as the oxidation of SO₂ to SO₃ may be too slow under such conditions [89]. This reaction path includes the direct reaction of NaOH and SO₂ to sulfite. The sulfite is then oxidized in an additional reaction step to sulfate, which has been described as the rate-limiting step for this reaction path.



The sulfation reactions of potassium and the details of the K-Cl-S mechanism have been investigated in numerous studies, in laboratory scale and larger scale and under different combustion conditions [114–116]. Weng et al. developed a novel multi-jet burner to investigate the K-Cl-S chemistry and kinetics using optical in-situ measurement methods [117–119]. KOH, KCl and K were quantified in the gas phase to follow the degree of sulfation under various post-flame conditions.

One objective of this thesis was to clarify the gas phase chemistry and kinetics of the Na-Cl-S system at high temperatures between 850 and 1475 °C. The experiments

were performed under the same conditions as for potassium in the above-mentioned studies by Weng et al. Even though similarities have been measured for elementary reactions of potassium and sodium, there has been no evidence so far that the gas-phase sulfation behavior of K and Na species is the same. The aim was therefore to collect experimental data for Na-sulfation and compare the data to experimental results from K-sulfation. Predictions from a newly updated kinetic Na-S-Cl model were compared to the experimental data to verify whether the model gives a satisfying description of the Na-sulfation in the gas phase. In addition, results of chemical equilibrium calculations were compared to the experimental data. In this context, it is not common to compare the behavior of both a kinetic model and an equilibrium model.

3. EXPERIMENTAL

3.1. NO_x and NO_x pre-cursor experiments

3.1.1. Biomass fuel samples

The biomass samples used for the devolatilization and combustion experiments were raw and pre-treated spruce bark and wheat straw. The pre-treated samples were either torrefied (torrefied bark = TB, torrefied straw = TS) or washed and torrefied (washed and torrefied bark = WTB, washed and torrefied straw = WTS).

Table 1. Analysis of the biomass samples used bark and straw samples.

| | RB | TB | WTB | RS | TS | WTS |
|--------------------------------|-------|--------|--------|--------|--------|--------|
| Volatile matter | 79.4 | 68.1 | 68.3 | 85.0 | 78.2 | 78.7 |
| Ultimate analysis, wt.-% | | | | | | |
| C | 51.6 | 55.1 | 54.5 | 43.1 | 44.6 | 44.5 |
| H | 6.0 | 5.3 | 5.4 | 5.5 | 5.3 | 5.4 |
| N | 0.38 | 0.47 | 0.45 | 0.67 | 0.72 | 0.51 |
| S | 0.022 | 0.023 | 0.021 | 0.106 | 0.107 | 0.063 |
| O | 40.4 | 37.1 | 37.9 | 44.3 | 42.8 | 43.8 |
| Ash forming elements, mg/kg | | | | | | |
| Si | 2,640 | 1,490 | 550 | 44,900 | 49,300 | 46,900 |
| Al | 434 | 329 | 178 | 396 | 385 | 226 |
| Ca | 8,880 | 14,200 | 13,700 | 3,660 | 4,180 | 4,100 |
| Fe | 227 | 194 | 120 | 245 | 233 | 140 |
| K | 1,760 | 2,010 | 1,120 | 7,390 | 7,780 | 3,290 |
| Mg | 602 | 895 | 829 | 790 | 890 | 720 |
| Mn | 529 | 525 | 530 | 16 | 14 | 13 |
| Na | 148 | 109 | 203 | 760 | 721 | 575 |
| P | 398 | 491 | 436 | 760 | 721 | 575 |
| Cl | 110 | < 80 | < 80 | 1320 | 956 | 248 |

In the washing step, the biomass samples were washed in hot tap water at 50 °C for 60 min. After removing the biomass from the hot water, it was sprayed with additional tap water and kept for drying until the moisture content was below 15%. In the torrefaction step, bark was pre-dried at 150 °C and straw at 180 °C. Afterwards, the samples were torrefied at 230 and 250 °C respectively. The mass loss during the torrefaction was 35% for bark and 31% for the straw. The biomass samples were used as received, pulverized and pressed to pellets with a diameter of 8 mm and a mass of 100 mg. Table 1 presents fuel analysis for the raw and pre-treated biomass samples.

3.1.2. Single particle reactor

The combustion and devolatilization experiments for investigating the NO_x and NO_x pre-cursor formation from the biomass samples were performed in an electrically heated single particle reactor (SPR) made of quartz glass (see Fig. 4). The quartz tubes had an inner diameter of 44 mm. The reactor was fed with N_2 from the sides with a flow rate of 120 Nl/h and N_2 (devolatilization experiments) or $\text{N}_2 + \text{air}$ (combustion experiments) from the bottom of the reactor with a flow rate of 100 Nl/h , resulting in a total flow rate of 220 Nl/h . Single biomass particles were inserted through an insertion tube to the center of the reactor where the devolatilization or combustion reactions took place. The temperature in the center of the reactor was 850 $^\circ\text{C}$.

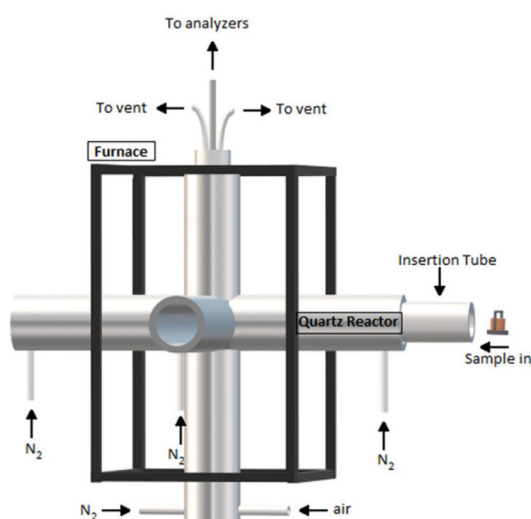


Figure 4. Quartz glass Single Particle Reactor with electrically heated furnace (Reprinted with permission from Publication I. ©2020 Elsevier).

Concentrations of O_2 , NO , CO and CO_2 in the flue gas were analyzed continuously. O_2 was analyzed with a gas analyzer from Servomex, model 4900, using a paramagnetic sensor. NO was quantified using a chemiluminescence analyzer from Teledyne, model 200EM. CO and CO_2 were measured with a gas analyzer from ABB, model AO2020, using an on-dispersive infrared analyzer.

For the combustion experiments, air was fed to the reactor resulting in a concentration of 10% O_2 in the center of the reactor. The biomass particles were kept in the reactor until no more CO_2 was released. At this stage, the combustion was considered finished. Each combustion experiment was repeated three times. Devolatilization experiments were performed in 100% N_2 atmosphere and the

samples were kept for 60 s in the reactor. In the devolatilization experiments, the flue gas was bubbled through alkaline or acidic solutions to capture NH_3 and HCN. A 1M HCl solution was used to capture NH_3 in form of NH_4^+ and a 1M NaOH solution was used to capture HCN as CN^- . Ammonium and cyanide ions were then quantified with spectroscopic methods. To collect sufficient amounts of NH_3 and HCN, each experiment was repeated 30 times.

3.2. NO_2 absorption experiments

Figure 5 shows the setup for the NO_2 absorption experiments, which consists of a gas-mixing unit, a gas washing bottle and a continuous NO/NO_2 analyzer. The NO_2 was purchased from Air Products (200 ppm NO_2 , N_2 as balance gas). The gas was diluted with N_2 to vary the inlet concentrations in the experiments between 25 and 150 ppm NO_2 . Air was added for the experiments with oxygen, using concentrations of 2 – 10% O_2 . The gas flows were controlled with EL-FLOW mass flow controllers from Bronkhorst. The total gas flow was either 2.0 NL/min (experiments related to publication II) or 2.3 NL/min (experiments related to publication III). The total flow used in the experiments is mentioned in the figure descriptions in the results part.

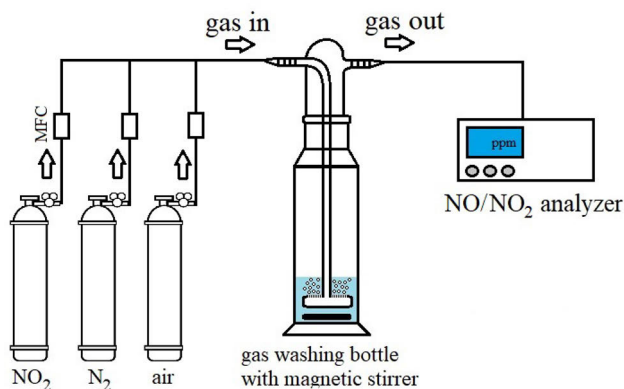


Figure 5. Experimental setup for NO_2 absorption experiments (Reprinted with permission from Publication IV. ©2022 American Chemical Society).

After mixing, the gas was bubbled through an absorption solution in a gas-washing bottle made of glass. The end part of the inlet tube in the bottom of the bottle consisted of a sintered glass filter to increase the contact area between the gas and the liquid. The solution was stirred with a magnetic stirrer at 300 rpm to avoid concentration gradients in the solution. The absorption solution contained either pure water or various concentrations of either sulfite (0–20 mM) or thiosulfate (0–100 mM) or both sulfite and thiosulfate mixed together.

All solutions were buffered with a phosphate buffer (Sørensen-buffer) using $\text{Na}_2\text{HPO}_4 \cdot 2\text{H}_2\text{O}$ (analytical grade, purchased from Honeywell) and KH_2PO_4 (analytical grade, purchased from Merck) at various ratios to obtain pH values between 6 and 8. For selected experiments, ion chromatography was performed to quantify concentrations of the additives and reaction products before and after the experiments. For the analysis of nitrite and nitrate, a Metrosep A SUPP 4 column from Metrohm was used and a carbonate/bicarbonate eluent (1.8 mM/ 1.7 mM).

3.3. Na-sulfation

3.3.1. Experimental setup

A multi-jet burner, as presented in Fig. 6a, was used to create well-controlled combustion environment in which the sodium sulfation experiments took place. The burner consists of 181 jet tubes with a diameter of 1.6 mm. The fuel, CH_4 , is pre-mixed with oxygen in the jets and above each jet a laminar conical flame is formed. A top view of the pre-mixed flames is shown in Fig. 6b. Between the jets, a co-flow is introduced through a bed of glass beads with a diameter of 1 mm. The gas from the co-flow and the flue gases are mixed evenly, creating a fairly homogenous hot flue gas environment above the burner outlet. The temperature and oxygen concentration in the hot flue gas environment can be adjusted by changing the composition of the jet flow and the co-flow. The temperature in the area where the measurements took place, and the O_2 , CO_2 and H_2O concentrations for the investigated conditions are shown in Tab. 2. The temperatures measured along the vertical axis from the jet tubes, as well as the calculated adiabatic temperatures for the used gas mixtures are shown in Fig. 7.

Table 2. Temperature and flue gas composition 5 mm above the burner outlet.

| Temp. [°C] | Fuel- O_2 ratio φ | O_2 | CO_2 | H_2O |
|------------|------------------------------------|--------------|---------------|----------------------|
| 1475 | 0.74 | 4.5 | 6.5 | 13.2 |
| 1275 | 0.70 | 4.6 | 5.4 | 11.0 |
| 1115 | 0.67 | 4.6 | 4.6 | 9.4 |
| 985 | 0.63 | 5.2 | 3.9 | 7.9 |
| 850 | 0.60 | 4.6 | 3.4 | 6.9 |

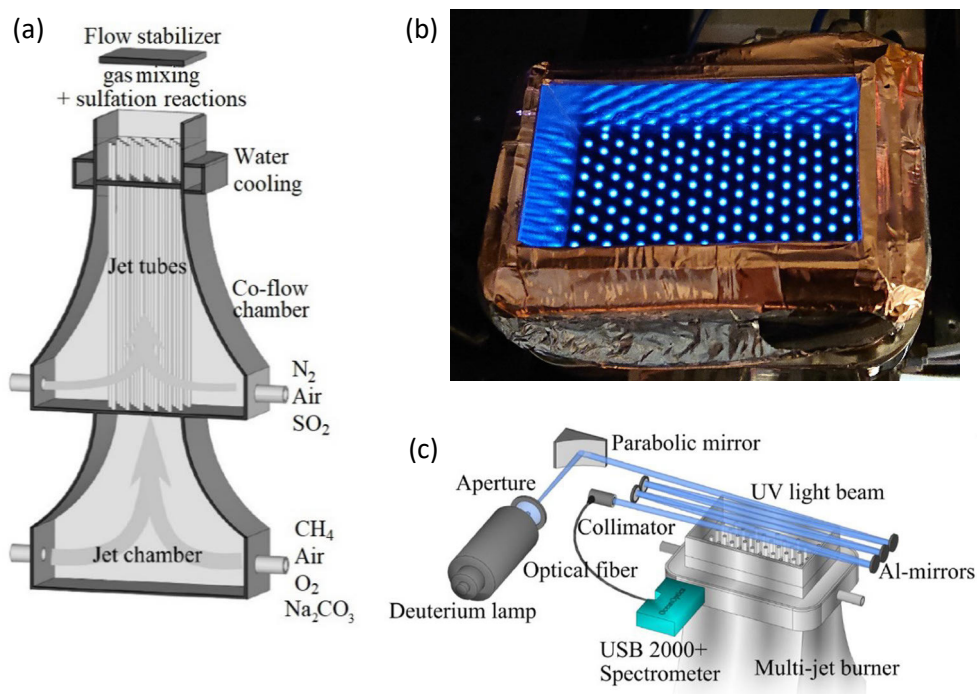


Figure 6. Schematic picture of the Multi-Jet Burner at Lund University (a), top view on pre-mixed flames and setup for broadband UV absorption spectroscopy. (Reprinted with permission from Publication III. ©2022 Elsevier).

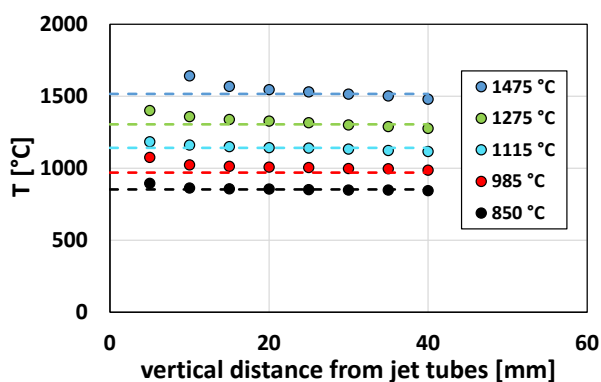


Figure 7. Temperatures measured along the vertical axis of the burner (dots) with a B-type thermocouple and two-line atomic fluorescence thermometry, and adiabatic temperatures for the used gas mixtures (dotted lines) (Reprinted with permission from Publication III. ©2022 Elsevier).

The quantification of gaseous NaOH and NaCl was done 5 mm above the outlet of the burner, at a distance of around 4 cm downstream from the jet flames. Broadband UV absorption spectroscopy was used to quantify NaOH(g) and NaCl(g) with the setup describe in Fig xc. A deuterium lamp was used to create an UV beam with a diameter of 10 mm. With the help of mirrors, the UV beam passed five times through the hot flue gas to increase the optical path length to achieve a higher sensitivity of the signal. After passing the flue gas, the UV light was collected and analyzed with a spectrometer (USB 2000+, Ocean Optics). One measurement included 200 scans and the integration time for one scan was 2 ms. For each experimental condition 20 measurements were performed.

The concentrations of NaOH(g) and NaCl(g) were determined from the optical signal using the Beer-Lambert law:

$$\text{Absorbance}(\lambda) = N_A \sigma_A(\lambda)L = -\ln\left(\frac{I_s(\lambda)}{I_0(\lambda)}\right) \quad (1)$$

with λ being the wavelength, N_A the number density of the gaseous species, $\sigma_A(\lambda)$ the absorption cross section as a function of the wavelength, L the optical path length, $I_s(\lambda)$ the measured intensity of the UV beam in the experiment and $I_0(\lambda)$ the intensity of the UV light source at a given wavelength. The absorption cross sections for NaOH(g) and NaCl(g) used in this work were determined by Weng et al. The absorption cross sections were determined at temperatures between 1125 and 1575 °C. Due to the low temperature dependence of the absorption cross section in this temperature range, it was assumed that the absorption cross section also can be used for the measurements at 850 and 985 °C.

3.3.2. Kinetic modelling and equilibrium calculations

The thermodynamic data and the reaction mechanisms for the sulfation of the investigated species, sodium hydroxide and sodium chloride were based on the work by Glarborg and Marshall [112]. Thermodynamic data for hydrogen sulfates and chlorinated intermediates from ab initio computations were estimated by Glarborg et al., which were emphasized as important alkali sulfate gas-phase pre-cursors. Recent modifications which were made for the potassium subset for the alkali sulfation [116,117,119] were applied to the sodium subset in the present work. Properties for the species NaHSO₃ and NaOSO₃ were calculated and added to the model, and data for NaSO₃Cl was updated.

The kinetic modeling was performed with the Ansys Chemkin-Pro software. A one-dimensional free propagation model was used to determine the composition of

the post-flame gases from the methane combustion. The mixture of the post-flame gases and the co-flow together with 20 ppm NaOH or NaCl and 0–150 ppm SO₂ was used as the input for a plug flow reactor model that was used to model the sulfation reactions. The temperature profile in the model used the temperatures that have been measured using two-line atomic fluorescence and a B-type thermocouple.

FACTSAGE 7.3 was used for the chemical equilibrium calculations. Equilibrium concentrations were calculated by minimizing the Gibbs energy, using the “Equilib” module within the FACTSAGE software. For the equilibrium calculations, a data set was created using existing databases from FACTSAGE, extended with thermodynamic data from [112] and new data from the present work for the following species: NaSO₂, NaSO₃, NaSO₄, NaHSO₄, NaSO₃Cl.

4. RESULTS AND DISCUSSION

4.1. NO_x and NO_x pre-cursor formation

Figure 8 shows the distribution of the volatile nitrogen (vol-N) and the char nitrogen (char-N) in the raw and pre-treated biomass samples based on a percentage of the original nitrogen content in the raw biomass sample. The share of the volatile content was determined for devolatilization in pure N₂ at 850 °C. The removed nitrogen here is the nitrogen that has been removed from the biomass samples during the pre-treatment. For raw bark, around 70% of the fuel-N was released during devolatilization while 30% remained in the char. For raw straw, the ratio was 90% and 10%, respectively. For both bark and straw, the vol-N content was generally lower in the pre-treated samples, while the char-N content was less affected by the pre-treatments.

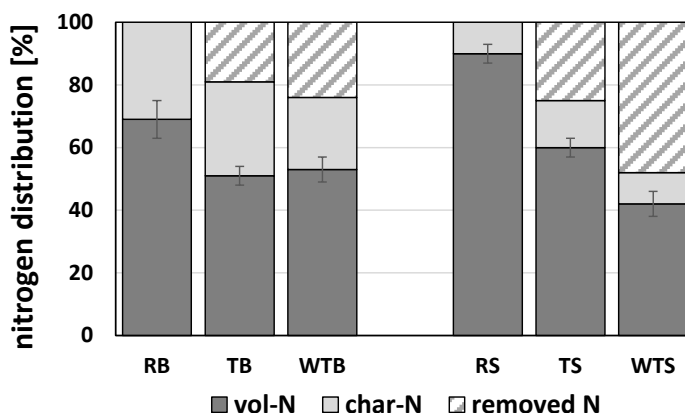


Figure 8. Nitrogen distribution in biomass samples: volatile nitrogen, char nitrogen and nitrogen removed during pre-treatment. RB = raw bark, TB = torrefied bark, WTB = washed and torrefied bark, RS = raw straw, TS = torrefied straw, WTS = washed and torrefied straw (Reprinted with permission from Publication I. ©2020 Elsevier).

The conversion of fuel-N to NO was determined for the combustion of the biomass pellets at 850 °C in a 10% O₂ (rest N₂) atmosphere. The share of fuel-N oxidized to NO during the combustion is shown in Fig. 9a. Around 50% of the fuel-N in raw bark was oxidized to NO under these conditions, and around 45% of the fuel-N in the pre-treated bark samples. The fuel-N to NO conversion for all straw samples was lower as compared to the bark samples. 23% of the fuel-N in raw straw formed NO,

27% in torrefied straw and 31% in washed& torrefied straw. Figure 9b and 9c show the conversion to NO separately for the vol-N (from the devolatilization step) and the char-N (from the char conversion). For the devolatilization, different trends were observed for the vol-N to NO conversion. Raw bark had the highest conversion of the bark samples, and washed and torrefied bark had the lowest conversion. For straw, the opposite trend was observed. For the char conversion, however, the same trends were observed for both fuel types. While the torrefied samples had a lower char-N to NO conversion, washed and torrefied samples had the highest conversions.

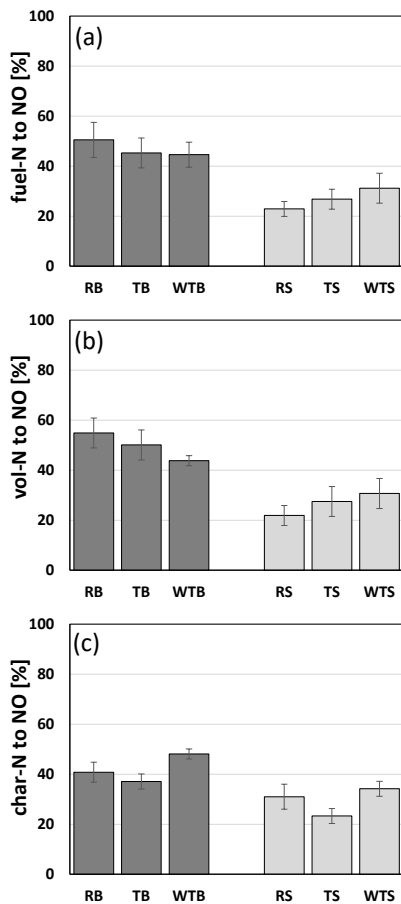


Figure 9. Conversion of total fuel-N (a), volatile-N (b) and char-N (c) to NO during combustion in 10% O₂ at 850 °C. RB = raw bark, TB = torrefied bark, WTB = washed and torrefied bark, RS = raw straw, TS = torrefied straw, WTS = washed and torrefied straw (Reprinted with permission from Publication I. ©2020 Elsevier).

The observations made for the char-N to NO conversion during the char combustion is in line with observations made in earlier studies [120]. Catalytically active elements in the ash such as K [121], Ca [122], Mg [123] and Fe [124] can reduce NO to N₂ in the char. As shown in Tab. 1 (section 3.1.1.), the concentration of these elements vary for the differently pre-treated samples. For both bark and straw, an enrichment of these elements was observed in the torrefied samples. In the washed and torrefied samples, however, those catalytically active elements were present at lower concentrations. The higher concentrations of those elements in torrefied samples may explain the reduced char-N to NO conversion. Vice versa, the decreased concentrations of the catalytically active elements leads to less NO reduction in the char, hence the higher NO conversion.

This effect of ash forming elements on reducing the NO emissions during char conversion is demonstrated in Fig. 10. Char from straw and softwood were combusted in various atmospheres. The chars were produced from raw and acid washed biomass. In the acid washed samples, almost all of K, Ca, Mg or Fe has been leached from the fuel. Under all conditions, the char-N to NO conversion was significantly higher for the acid washed samples. For softwood char, up to 86% of the char-N was released as NO, while it was less than 40% for the raw softwood char. For straw char, NO formation was generally lower, but the same trend, i.e. a higher NO formation for the acid washed samples, was observed.

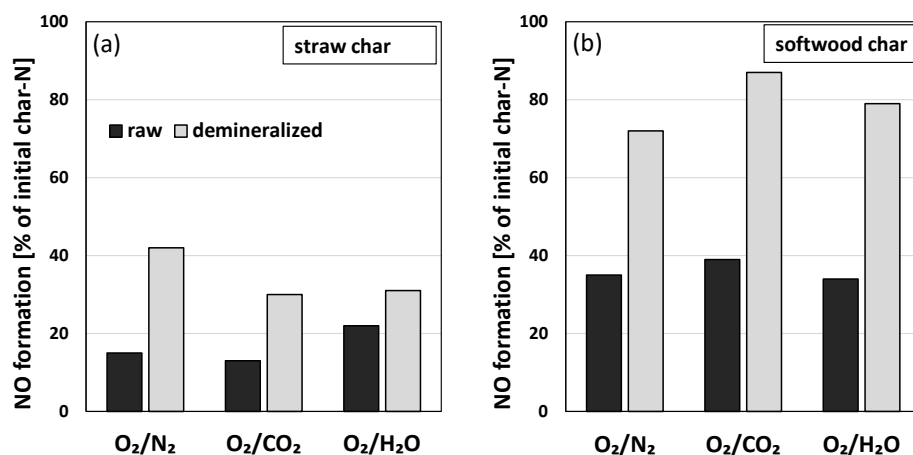


Figure 10. Total conversion of char-N to NO during oxidation of straw char (a) and softwood char (b) in O₂/N₂ (3/97 vol.-%), O₂/CO₂/N₂ (3/34/63 vol.-%) and O₂/H₂O/N₂ (3/17/80 vol.-%) at 900 °C. (Reprinted with permission from Publication II. ©2020 American Chemical Society.)

Figure 11 illustrates the formation of NH_3 , HCN and NO during the devolatilization in inert atmosphere (100 % N_2) at 850 °C. For the bark samples, NH_3 was the main product formed while the conversion of vol-N to NH_3 and HCN was similar for the straw samples. For the pre-treated samples, the same trends could be observed for both bark and straw. The torrefied samples showed the highest NH_3 and HCN formation. For the washed and torrefied samples, the NO precursor formation increased only slightly as compared to the raw samples.

Here it should be noted that the NO pre-cursor formation would not necessarily correlate with the NO formation during devolatilization in oxidizing conditions due to the complex gas phase chemistry. The lack of measurements of other vol-N-species like tar-N or N_2 may also cause some uncertainty as the mass balance for N cannot be closed. However, the formation of NO pre-cursors may still give indication to a certain degree from which samples a high NO formation might be expected during combustion. Figure 12 shows the total amount of N in the NO precursors formed during the devolatilization experiments in inert atmosphere vs the total amount of NO formed during the combustion experiments in oxidizing conditions.

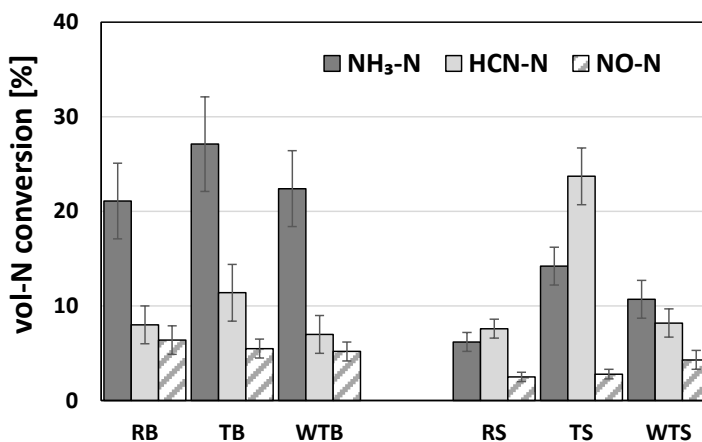


Figure 11. Conversion of volatile-N to NH_3 , HCN and NO during devolatilization in 100% N_2 at 850 °C. RB = raw bark, TB = torrefied bark, WTB = washed and torrefied bark, RS = raw straw, TS = torrefied straw, WTS = washed and torrefied straw (Reprinted with permission from Publication I. ©2020 Elsevier).

The molar ratios between the total amounts of HCN and NH_3 correlated well with the nitrogen and hydrogen content, as shown in Fig. 13. This is in line with previous findings reported in literature [25]. Samples with a higher fuel-N content had a

higher HCN to NH_3 ratio while samples with a higher H/N ratio had a lower HCN to NH_3 formation ratio.

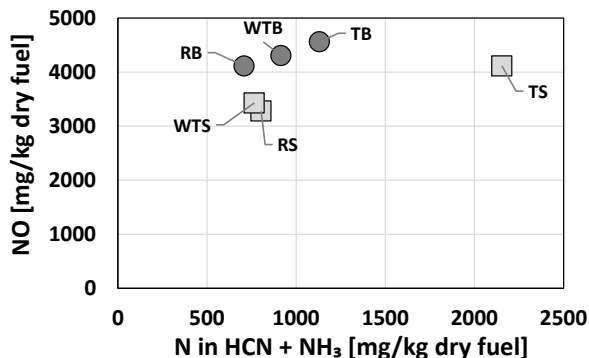


Figure 12. NO pre-cursor formation from devolatilization experiments (100% N_2) vs NO formation from combustion experiments (10% O_2 , rest N_2). RB = raw bark, TB = torrefied bark, WTB = washed and torrefied bark, RS = raw straw, TS = torrefied straw, WTS = washed and torrefied straw (Publication I).

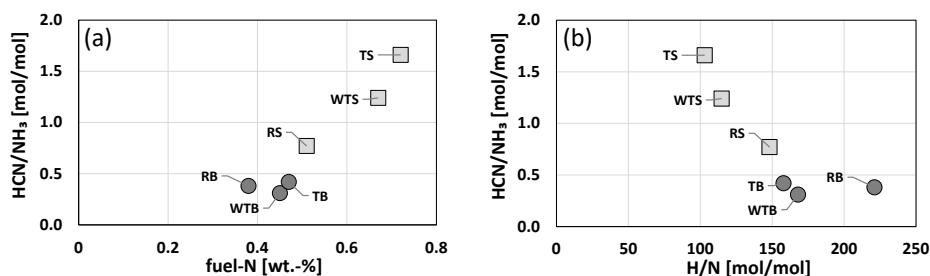


Figure 13. Molar ratio of HCN and NH_3 versus fuel-N (a) and molar ratio of H/N in fuel (b). RB = raw bark, TB = torrefied bark, WTB = washed and torrefied bark, RS = raw straw, TS = torrefied straw, WTS = washed and torrefied straw (Reprinted with permission from Publication I. ©2020 Elsevier).

Besides the nitrogen and hydrogen content in the fuel, variations in the amount of cellulose, hemicellulose and lignin may also contribute to the different HCN to NH_3 ratios. A study by Chen et al. investigated the effects of torrefaction on hemicellulose, cellulose and lignin [125]. It was found that mostly hemicellulose is removed during the torrefaction, while the share of cellulose and lignin in the biomass increase. A higher lignin content may promote polymerization reactions between cellulose, hemicellulose and proteins [126]. Heterocyclic nitrogen is more likely to form HCN as compared to nitrogen in amino acids, which has a higher

tendency to form NH_3 . The polymerization reactions could also explain why the straw samples in general had a higher HCN to NH_3 ratio, as straw contains significantly more lignin than bark [127,128].

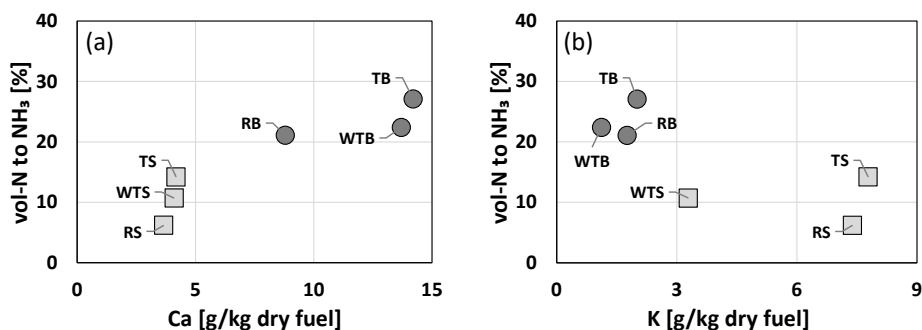


Figure 14. Conversion of vol-N to NH_3 versus calcium content (a) and potassium content (b) in the fuel samples. RB = raw bark, TB = torrefied bark, WTB = washed and torrefied bark, RS = raw straw, TS = torrefied straw, WTS = washed and torrefied straw (Reprinted with permission from Publication I. ©2020 Elsevier).

Another factor that may influence the HCN and NH_3 formation during devolatilization is the ash forming matter in the biomass fuel. Opposing observations have been reported in literature regarding the catalytic effects of K and Ca on the HCN and NH_3 formation tendency for various N-containing compounds (compare section 2.3.). For the biomass samples that have been used in the present work, Ca seemed to have a promoting effect on the NH_3 formation, as shown in Figure 14. Raw straw, which had the lowest amount of Ca, had the lowest NH_3 formation tendency, while torrefied bark had the higher amount of Ca and the highest NH_3 formation tendency. Regarding the potassium content in the fuel samples, the opposite effect was observed. No correlation was found between the HCN formation tendency and Ca and K contents in the samples.

Due to the complexity of the biomass samples and the various factors that may influence the HCN and NH_3 formation, it cannot be clarified based on the presented results to which extend each factor contributes to the overall reactions. Nevertheless, the results may give insight into how different pre-treatment methods may affect different types of biomass and consequently help to understand the different NO_x formation tendencies for pre-treated fuel samples.

4.2. NO_x removal

The NO_x removal has been investigated by absorbing NO₂ in aqueous solutions containing the sulfur additives sulfite and thiosulfate (Papers III and IV). With sulfite in the solution, the NO₂ absorption increased significantly. However, under oxidizing conditions sulfite oxidized rapidly to sulfate. The NO₂ absorption efficiency of sulfite solutions decreased with decreasing pH. With thiosulfate in the solution, the NO₂ absorption also improved. However, the effect of thiosulfate was significantly smaller as compared to sulfite. When used as a sulfite inhibitor, thiosulfate was shown to reduce the sulfite consumption drastically. The experimental results are discussed in detail in the following sections.

4.2.1. NO₂ absorption in sulfite solutions (O₂-free flue gas)

NO₂ concentrations measured during the absorption experiments with sulfite are shown in Fig. 15. The corresponding NO₂ absorption rates are presented in Tab. 3. The input concentration of the test gas was 50 ppm NO₂ (N₂ as balance). The absorption solutions were buffered with a phosphate buffer at pH 8. With 0 mM sulfite, the NO₂ concentration decreased to 43 ppm, i.e. 14% of the NO₂ was absorbed. This is in agreement with previous absorption tests of NO₂ in pure water [69]. In the case of pure water, the measured NO₂ concentration was constant throughout the experiment. In the case of 0.5 mM, the NO₂ concentration initially decreased to 35 ppm, which means that twice as much NO₂ was absorbed as compared to when pure water was used. With further increases in the sulfite concentration, a further decrease in the NO₂ concentration was observed. However, the higher the sulfite concentration, the smaller was the effect of a further increase of the sulfite concentration. At the highest investigated sulfite concentration, 20 mM, more than 80% of the NO₂ was absorbed.

In all cases with sulfite, the NO₂ concentration increased with time, i.e. less NO₂ was absorbed. This observation was explained by reaction R2.4.2, describing the consumption of sulfite by NO₂. In the case with 0.5 mM sulfite, the NO₂ concentration eventually reached the same level as in the test with pure water (0 mM sulfite) at 1200 s. At this point, it can be assumed that all sulfite had been consumed and only the reaction with water takes place. At higher concentrations, the NO₂ concentrations increased at a lower rate as the experiment proceeded.

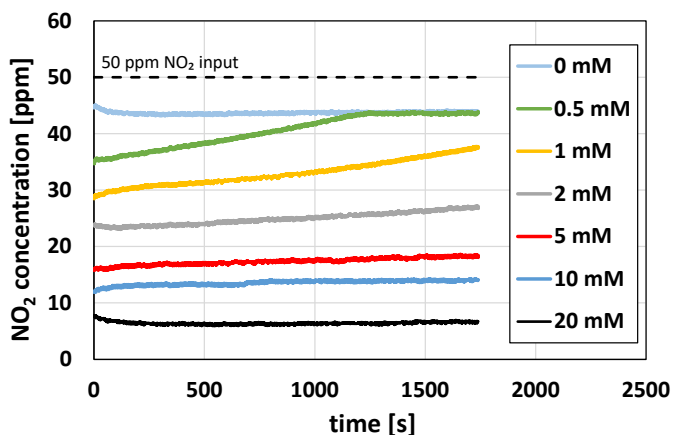


Figure 15. NO_2 concentrations for absorption tests with 0 – 20 mM sulfite (pH 8, no oxygen); initial concentration 50 ppm NO_2 (N_2 as balance gas), flow rate 2.0 NL/min (Reprinted with permission from Publication IV. ©2022 American Chemical Society).

Table 3. NO_2 absorption rates for various sulfite concentrations.

| sulfite concentration [mM] | NO_2 absorption rate [$\mu\text{mol}\cdot\text{L}^{-1}\cdot\text{min}^{-1}$] |
|----------------------------|---|
| 0 | 11.3 |
| 0.5 | 25.4 |
| 1 | 35.7 |
| 2 | 44.7 |
| 5 | 56.7 |
| 10 | 63.2 |
| 20 | 75.6 |

After the absorption experiments, selected absorption solutions were analyzed on their nitrite and nitrate content to clarify to which extend reactions R2.4.2 and R2.4.4 took place. The total amounts of nitrite and nitrate found in the absorption solution are listed in Tab. 4. Uncertainties in the mass balance might be caused by uncertainties of the ion chromatography analysis or the quantification of NO_2 in the gas phase. In the absorption solution without sulfite, roughly equal amounts of nitrite and nitrate were found, which was expected from reaction R2.4.4. In the case with 1 mM sulfite, 10 times more nitrite was found as compared to nitrate. This indicates that already with 1 mM sulfite, mostly R2.4.2 took place while R2.4.4 only contributed to a minor extend. In the solution from the experiment with 10 mM sulfite, only nitrite was identified and nitrate was below the detection limit. Based on these findings, the reaction of NO_2 with water may be neglected for the overall NO_2 absorption when using sufficient high sulfite concentrations.

Table 4. Mass balance for NO_2 , NO_2^- and NO_3^- .

| SO_3^{2-} [mM] | NO_2 in [mol] | NO_2 abs. [μmol] | NO_2^- [μmol] | NO_3^- [μmol] | mass balance |
|----------------------------|---------------------------|---|--|--|-----------------|
| 0 | 87.7 ^b | 18.6 | 9.3 | 8.3 | 0.95 |
| 1 | 122.6 | 40.4 | 45 | 4 | 1.2 |
| 10 | 122.6 | 87 | 107 | < 1 | 1.2 |

^blower NO_2 in due to shorter time for experiment with 0 mM sulfite

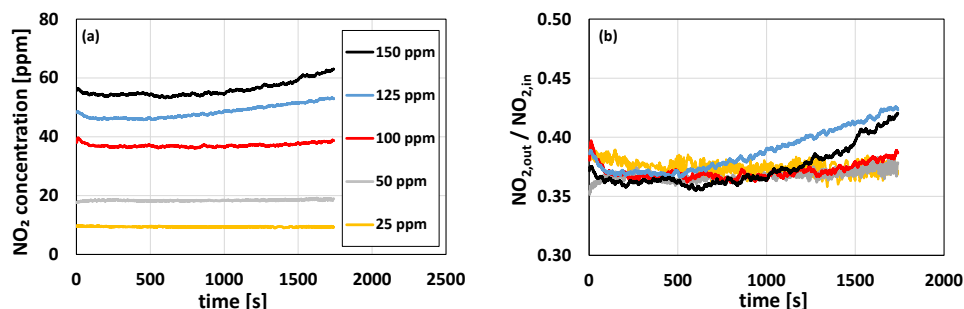


Figure 16. NO_2 concentrations (a) and $\text{NO}_{2,\text{out}}/\text{NO}_{2,\text{in}}$ ratio (b) for absorption test with 5 mM sulfite solution (pH 8, no oxygen); initial concentration 25 – 150 ppm NO_2 (N_2 as balance gas), flow rate 2.0 NL/min (Fig. 16a reprinted with permission from Publication IV. ©2022 American Chemical Society).

Figure 16 shows NO_2 concentrations for absorption tests with 5 mM sulfite for NO_2 input concentrations between 25 and 150 ppm. The corresponding absorption rates are shown in Fig. 17. For the experiments with 25–100 ppm NO_2 , the NO_2 concentration was constant throughout the 30 min experiment. With 125 and 150 ppm, the NO_2 concentration increased towards the end of the experiment, which may be explained by the higher sulfite consumption due to the higher initial concentration of NO_2 . Nevertheless, the initial NO_2 absorption was almost the same for all input concentrations. The initial $\text{NO}_{2,\text{out}}/\text{NO}_{2,\text{in}}$ ratio was around 0.37 for all cases (63% absorption). The NO_2 absorption rates increased linearly with the NO_2 input concentration.

The influence of the pH on the NO_2 absorption with sulfite solutions is illustrated in Fig. 18. For these tests, phosphate buffers were used with varying $\text{HPO}_3^{2-}/\text{H}_2\text{PO}_3^-$ ratios to vary the pH between 6 and 8. The sulfite concentration in these tests was 5 mM. The results show the relative NO_2 absorption for varying pH values as a percentage compared to the base case that is represented by pH 8. When decreasing the pH, the sulfite equilibrium shifts towards bisulfite [129]. Interestingly, the relative NO_2 absorption was in close correlation with the decreasing share of sulfite at lower pH values.

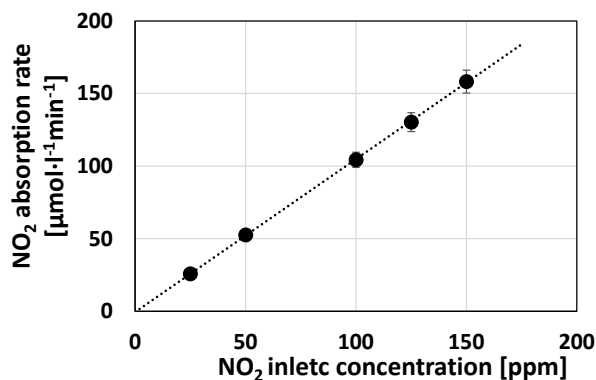


Figure 17. NO₂ absorption rate with 5 mM sulfite solution (pH8, no oxygen) vs NO₂ inlet concentration (N₂ as balance gas); flow rate 2.0 NL/min (Reprinted with permission from Publication IV. ©2022 American Chemical Society).

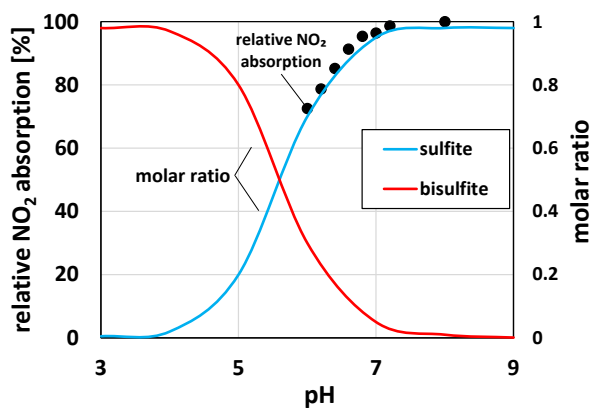


Figure 18. Relative NO₂ absorption for pH 6 – 8 with 5 mM sulfite (no oxygen), relative absorption at pH 8 = 1; initial concentration 50 ppm NO₂ (N₂ as balance gas), flow rate 2.0 NL/min (Reprinted with permission from Publication IV. ©2022 American Chemical Society).

4.2.2. Sulfite oxidation during NO₂ absorption (O₂-containing flue gas)

In addition to the tests with varying sulfite concentrations and inert atmosphere presented in 4.2.1., the same tests were also repeated with 5% in the inlet gas. The NO₂ concentrations from these tests are shown in Fig. 19. In the presence of oxygen, the measured NO₂ concentrations increased significantly faster as compared to the NO₂ concentrations shown in Fig. 15. In the case of 1 mM sulfite, the NO₂

concentration increases to the level of 0 mM sulfite after around 100 s, implying that all sulfite is consumed within 100 s. Compared to this, in the test without oxygen and 1 mM sulfite, the sulfite was not entirely consumed after 1800 s. Even in the case with 20 mM sulfite, a high NO_2 could not be obtained in the presence of oxygen. Under these conditions, all sulfite was consumed within 500 s.

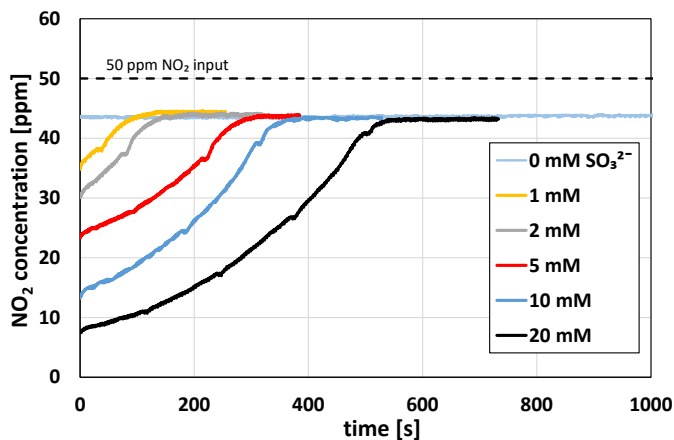


Figure 19. NO_2 concentrations for absorption tests with 0 – 20 mM sulfite (pH8); initial concentration 50 ppm NO_2 + 5% O_2 (N_2 as balance gas), flow rate 2.0 NL/min (Reprinted with permission from Publication IV. ©2022 American Chemical Society).

The significantly higher sulfite consumption in the presence of oxygen can be explained by the radical mechanism, described by the reactions R2.4.5–R2.4.8. Since the mechanism is rather complicated, a method was developed to quantify the overall sulfite oxidation due to the presence of oxygen. The sulfite oxidation rates describe in the following exclude the sulfite consumption by NO_2 , as this reaction is desired for the NO_2 absorption. The sulfite oxidation rate describes the sulfite consumption beyond the consumption through the desired reaction.

The following assumptions were made to determine the sulfite oxidation rates:

1. The sulfite concentration at each time point was calculated based on the NO_2 absorption using the results from Fig. 15.
2. The sulfite consumption by NO_2 was calculated by integrating the NO_2 absorption curves, assuming that 2 moles of absorbed NO_2 will consume 1 mole of sulfite ($2 \text{NO}_2 + \text{SO}_3^{2-} + \text{H}_2\text{O} \rightarrow 2 \text{NO}_2^- + \text{SO}_4^{2-} + 2 \text{H}^+$).
3. The difference between the total sulfite consumption and the sulfite consumed by NO_2 is assumed to be oxidized due to the presence of O_2 . As

the oxidation mechanism of sulfite in NO_2 absorption is rather complex and involves several steps, the estimated sulfite oxidation rate describes the combined phenomena of the various reactions caused by the presence of oxygen.

4. The oxidation rate was observed to decrease with decreasing sulfite concentrations in the absorption solution. As a result of this, sulfite oxidation rates were calculated based on the initial consumption rates in the beginning of the experiment when the sulfite concentration is close to the initial concentration.

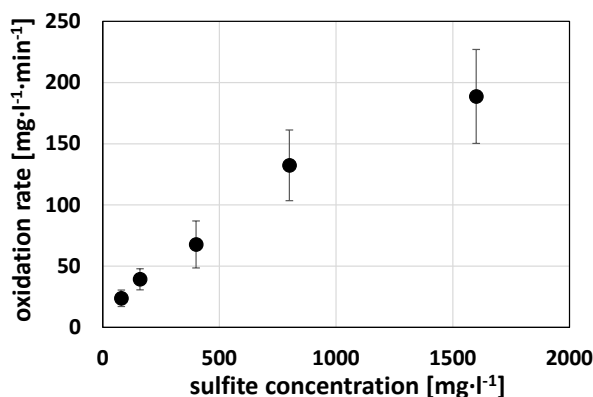


Figure 20. Sulfite oxidation rate (excluding oxidation by NO_2) vs sulfite concentration for absorption tests with 1 – 20 mM sulfite (pH 8); initial concentration 50 ppm NO_2 + 5% O_2 (N_2 as balance gas), flow rate 2.0 NL/min (Reprinted with permission from Publication IV. ©2022 American Chemical Society).

Figure 20 shows the sulfite oxidation rates estimated on the above described method versus the initial sulfite concentrations in the absorption solution. The sulfite oxidation rate increased almost linearly with the sulfite concentration in the solution for the investigated range of concentrations. Similar observations were also reported by Sapkota et al [61]. The fact that the sulfite oxidation increases with increasing sulfite concentrations poses a relevant problem for large scale applications. Depending on the statutory limits, higher sulfite concentrations in the absorption solution are needed to remove NO_x sufficiently from the flue gas. Using higher concentrations, however, will increase the sulfite consumption disproportionately to its benefit for NO_x when the sulfite oxidation cannot be prevented.

4.2.3. NO₂ absorption with thiosulfate

NO₂ absorption with thiosulfate as an additive in the absorption solution was investigated for the concentration range 0–100 mM thiosulfate. The NO₂ measured in these experiments are shown in Fig. 21. With 1 mM thiosulfate, the NO₂ concentration decreased to 42 ppm, representing a NO₂ absorption of 16%. This is significantly less than the 40% that was achieved with the same concentration of sulfite. Increasing the thiosulfate concentration to 2 mM did not result in any observable improvement. Only when the thiosulfate concentration was increased to 10 or 100 mM, the NO₂ absorption improved notably. Nevertheless, even with 100 mM thiosulfate in the absorption solution, the NO₂ absorption was still lower as compared to the case with 1 mM sulfite. Although the reactions are similar (compare R2.4.16 and R2.4.2), the kinetics of the reaction between NO₂ and sulfite or thiosulfate differs significantly. Similar observations were also made by Shen and Rochelle, who investigated the kinetics of these reactions at elevated temperatures [67].

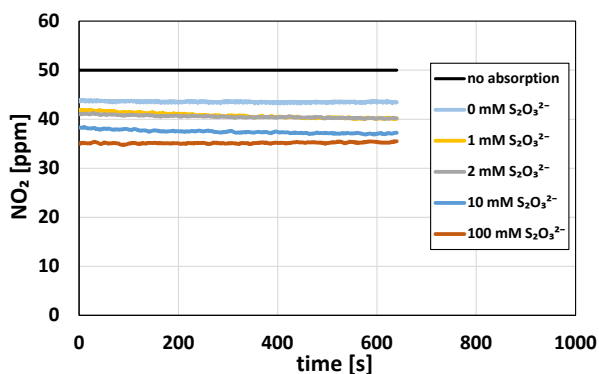


Figure 21. NO₂ concentrations for absorption tests with 0 – 100 mM thiosulfate (pH 7, no oxygen); initial concentration 50 ppm NO₂ (N₂ as balance gas), flow rate 2.3 Nl/min (Reprinted with permission from Publication V. ©2022 American Chemical Society).

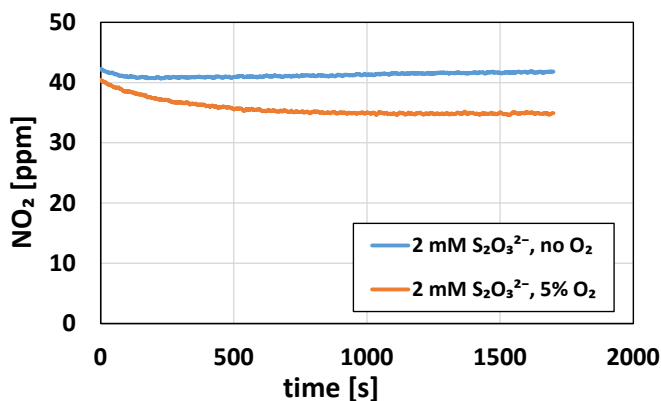


Figure 22. NO₂ concentrations for absorption tests with 2 mM thiosulfate (pH 7) with and without oxygen; initial concentration 50 ppm NO₂ (N₂ as balance gas), flow rate 2.3 NL/min (Reprinted with permission from Publication V. ©2022 American Chemical Society).

NO₂ concentrations for absorption tests with thiosulfate in absence or presence of oxygen in the test gas are shown in Fig. 22. Without oxygen, the NO₂ concentration was relatively constant throughout the 30 min test. Only a slight increase of the NO₂ concentration was observed as the experiment proceeded, which can be explained by the slow consumption of thiosulfate by the reaction with NO₂. Ion chromatography analysis revealed that around 6% of the thiosulfate was consumed during the 30 min test without oxygen (see Tab. 5). This also indicates that the reaction between NO₂ and water plays a significant role when using small concentrations of thiosulfate, as the thiosulfate consumption is too low to explain the NO₂ absorption in this test.

In the experiment with 50 ppm NO₂ + 5% O₂, the initial NO₂ absorption was similar to the test without oxygen. However, the NO₂ concentration decreased with time before reaching a constant level at 35 ppm after around 700 s. The thiosulfate consumption in this experiment was also higher. 17% of the thiosulfate was consumed during the 30 min experiment. The 17% consumption roughly represents a 2:1 molar ratio between absorbed NO₂ and consumed S(IV), indicating that NO₂ is mainly reacting with the sulfur additive and not water, which has been observed for the sulfite solutions. One possible explanation for the increased absorption in the presence of oxygen could be the partial oxidation of thiosulfate to sulfite. The oxidation of thiosulfate is generally a slow process, with sulfate being the final oxidation product [76,130]. Sulfate does not react with NO₂. Sulfite, however, might be formed as an intermediate during the oxidation. As sulfite is reacting much faster

with NO₂ than thiosulfate, already a small amount of sulfite would be sufficient to increase the NO₂ absorption significantly. Sulfite can also be formed as a decomposition product from thiosulfate. This, however, has only been described for acidic solution in literature [131]. Another decomposition product that could explain the increased NO₂ absorption is sulfide [132]. Sulfide formation at this pH would likely lead to the release of H₂S under the investigated conditions at pH 7, which was not detected during the experiment.

Table 5. Thiosulfate consumption during NO₂ absorption with and without oxygen determined by ion chromatography (Publication IV).

| gas inlet conc. | S ₂ O ₃ ²⁻ [mM] | | S ₂ O ₃ ²⁻ consumed [%] |
|--|--|--------------|--|
| | initial | after 30 min | |
| 50 ppm NO ₂ | 2.08 | 1.96 | 5.8 |
| 50 ppm NO ₂ + 5% O ₂ | 2.10 | 1.74 | 17.1 |

4.2.4. Thiosulfate as sulfite oxidation inhibitor during NO₂ absorption

The properties of thiosulfate as a sulfite oxidation inhibitor was studied by following the sulfite and thiosulfate consumption during NO₂ absorption experiments with various ratios of the two additives in the absorption solution. Experiments were performed with 2, 5 or 10 mM sulfite with 0–5 mM thiosulfate. Figure 23 shows results for tests with 2, 5 or 10 mM sulfite and 2 or 5 mM thiosulfate. When comparing the results with Fig. 15, it can be noted that the initial NO₂ concentrations are the same for the corresponding sulfite concentrations. Based on this, and the results from section 4.2.3., it can be concluded that thiosulfate has no notable effect on the overall NO₂ absorption when added at such small concentrations.

The comparison of the results presented in Fig. 15 and Fig. 19 show the clear improvement of enhanced NO₂ absorption over extended periods of time. When no thiosulfate was added to a solution with 10 mM sulfite, all sulfite was consumed within less than 400 s and the NO₂ increased to 42 ppm. With 2 mM thiosulfate and 10 mM sulfite, the NO₂ was still at 55% after 800 s, and at 70% with 5 mM thiosulfate.

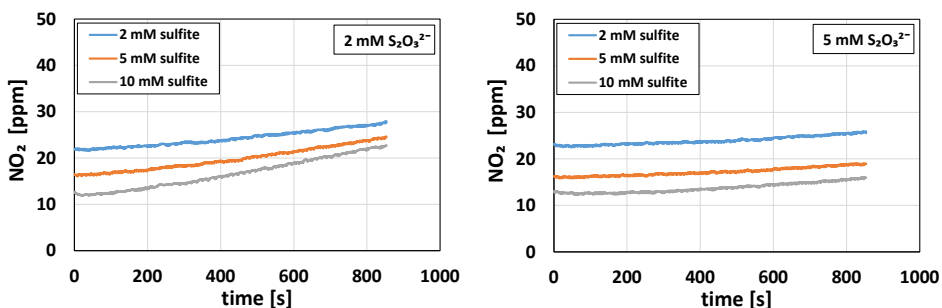


Figure 23. NO_2 concentrations for absorption tests with 2 – 10 mM sulfite and 2 or 5 mM thiosulfate (pH 7); inlet gas 50 ppm NO_2 + 5% O_2 (N_2 as balance gas), flow rate 2.3 NL/min (Reprinted with permission from Publication V. ©2022 American Chemical Society).

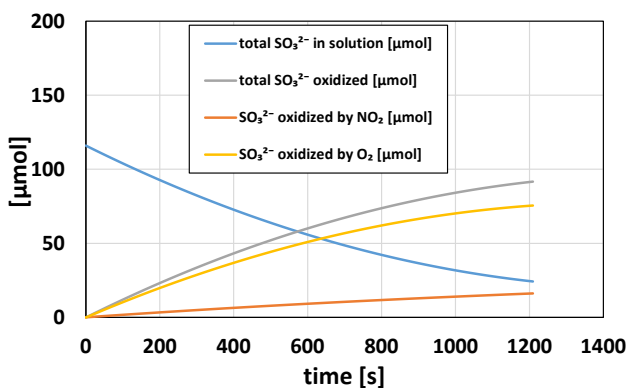


Figure 24. Total amount of sulfite in absorption solution (blue line) as function of time and amount of consumed sulfite: total consumption (grey line), consumed by O_2 (yellow line) and consumes by NO_2 (red line); illustrated for test with 2 mM sulfite and 1 mM thiosulfate, inlet gas 50 ppm NO_2 + 5% NO_2 (N_2 as balance gas), flow rate 2.3 NL/min (Reprinted with permission from Publication V. ©2022 American Chemical Society).

The oxidation rates for sulfite in the experiments with thiosulfate as an oxidation inhibitor were determined using the same method as described in section 4.2.2. Since it was shown that thiosulfate has no effect on the NO_2 absorption under these conditions, it was assumed that NO_2 only reacts with sulfite. Figure 24 illustrates the consumption of sulfite as a function of time from the test with 2 mM sulfite and 1 mM thiosulfate as an example. The red curve is the theoretical amount of sulfite consumed by NO_2 , based on the measurements of the NO_2 concentration during the experiment. The blue curve shows the sulfite concentration as a function of time.

The grey curve is the total sulfite consumption, given by the difference between the initial sulfite amount and the blue curve. The yellow curve represents the sulfite that is oxidized due to the presence of O₂ in the test gas, calculated by the difference between the total sulfite consumption and sulfite consumption by NO₂. In spite of the thiosulfate addition, the majority of sulfite is still lost due to undesired oxidation and only a minor part has reacted with NO₂. The sulfite oxidation rates were determined from the slope of the yellow curve in the beginning of the experiments.

The sulfite oxidation rates determined for all investigated sulfite/thiosulfate ratios are shown in Fig. 25. In the test with 10 mM sulfite without thiosulfate, the sulfite oxidation rate was 130 mg·l⁻¹·min⁻¹. With 1 mM thiosulfate, this oxidation rate decreased to 31 mg·l⁻¹·min⁻¹, a decrease of 75%. With 2 mM thiosulfate, the sulfite oxidation rate decreased even further to 16 mg·l⁻¹·min⁻¹. In the case of 2 and 5 mM sulfite, 1 mM thiosulfate reduced the sulfite oxidation rate by 70-80%.

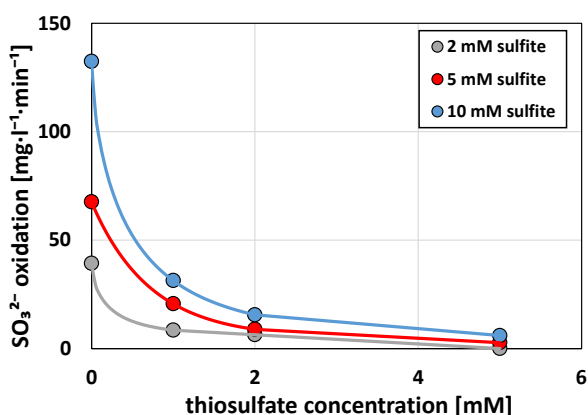


Figure 25. Sulfite oxidation rate (excluding oxidation by NO₂) vs sulfite concentration for absorption tests with 2 – 10 mM sulfite and 0 – 5 mM thiosulfate (pH 7); inlet gas 50 ppm NO₂ + 5% O₂ (N₂ as balance gas), flow rate 2.3 NL/min (Reprinted with permission from Publication V. ©2022 American Chemical Society).

Table 6. Thiosulfate consumption as sulfite oxidation inhibitor during NO₂ absorption determined by ion chromatography (Publication IV).

| gas inlet conc. | SO ₃ ²⁻ [mM] | S ₂ O ₃ ²⁻ [mM] | | S ₂ O ₃ ²⁻ consumed [%] |
|---|------------------------------------|--|--------------|--|
| | | initial | after 30 min | |
| 50 ppm NO ₂ + 5% O ₂ | 2 | 2.00 | 1.24 | 38.0 |
| 50 ppm NO ₂ + 5% O ₂ | 5 | 2.01 | 1.14 | 44.1 |

The thiosulfate consumption has been quantified with ion chromatography for two 30 min tests with 2 or 5 mM sulfite and 2 mM thiosulfate. The results are shown in Tab. 6. It was noted that the thiosulfate consumption was similar for both cases. From reactions R2.4.9 – R2.4.15 it would be expected that a higher sulfite concentration would lead to a higher thiosulfate consumption as more radicals are present. The regeneration of thiosulfate in the mechanism may partly explain the observations. However, based on the presented results it cannot be estimated how much each single reaction contributes to the total thiosulfate consumption (consuming and regenerating reactions).

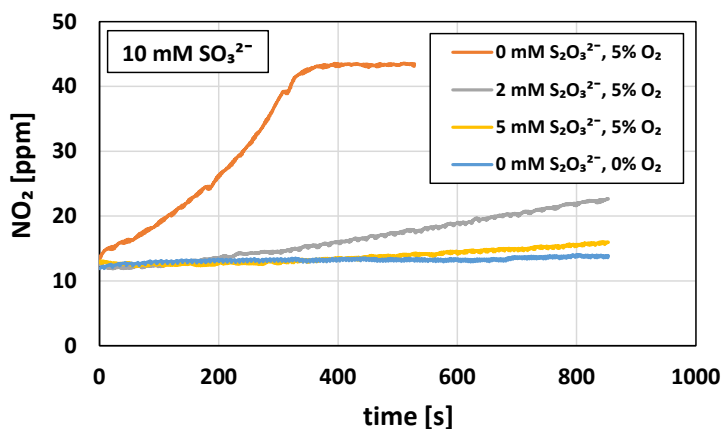


Figure 26. Comparison of NO_2 absorption experiments with 10 mM sulfite and 0 – 5 mM thiosulfate with and without oxygen; inlet gas 50 ppm NO_2 or 50 ppm NO_2 + 5% O_2 (N_2 as balance gas). (Reprinted with permission from Publication V. ©2022 American Chemical Society).

It can be concluded that thiosulfate is an effective sulfite oxidation inhibitor at already at low concentrations. Figure 26 summarizes four experiments under different conditions with 10 mM sulfite to illustrate the effect of thiosulfate. In the experiment with 5% oxygen in the test gas and no addition of thiosulfate, the NO_2 concentrations increases fast, i.e. the NO_2 decreases fast as sulfite is oxidized rapidly. When small amounts of thiosulfate are added (here 2 mM thiosulfate), the oxidation can be slowed down significantly. When adding sufficient amounts of thiosulfate (here 5 mM), the sulfite oxidation can be slowed down to such an extent that the NO_2 absorption rate is similar as compared to oxygen-free conditions.

The influence of the oxygen concentration seems to have no influence on the absorption process under the investigated conditions. Tests with 2–10% oxygen in the test gas were performed, using 10 mM sulfite and 6 mM thiosulfate in the absorption solution. For all investigated conditions, the NO_2 concentrations were almost identical.

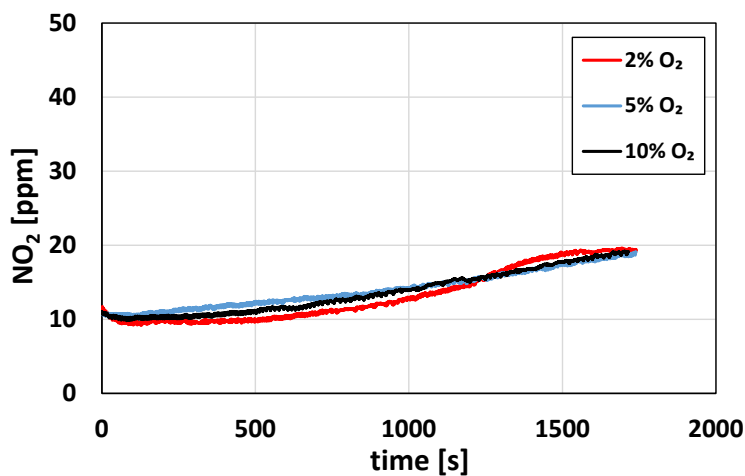


Figure 27. NO_2 concentrations for absorption tests with 10 mM sulfite and 6 mM thiosulfate with varying oxygen concentrations; inlet gas 50 ppm NO_2 + 2, 5 or 10% O_2 (N_2 as balance gas), flow rate 2.0 NL/min (Reprinted with permission from Publication IV. ©2022 American Chemical Society).

4.3. Na-sulfation

The sulfation of the sodium salts sodium hydroxide and sodium chloride has been investigated by using optical measurement methods to quantify the sodium species in the gas phase under post-flame conditions (paper V). Besides experimental work, kinetic modeling and equilibrium calculations were performed. The equilibrium calculations indicated that the system was at equilibrium at the highest temperatures (1275 and 1475 °C), while the system was still controlled by kinetics at the lower temperatures (850 – 1115 °C). Sodium hydroxide sulfation took place to a significant degree at 1115 and lower °C, while sulfation of sodium chloride was only observed at 985 °C and lower. The experimental results for the sulfation of sodium hydroxide were in good agreement with the kinetic modeling. For sodium chloride, the kinetic model could not accurately describe the reactions at the lowest temperature of 850 °C. The experimental results and the modeling are discussed separately for sodium hydroxide and sodium chloride in the following sections.

4.3.1. NaOH(g) sulfation – experimental results and modelling

The concentrations of sodium hydroxide in the gas phase measured during the sulfation experiments are shown in Fig. 28a. All measurements took place 5 mm above the burner outlet. The experiments were performed at 850 – 1475 °C under the post-flame conditions described in the experimental part (section 2.5). The SO₂ concentration in the gas mixture varied between 0–150 ppm. At the highest investigated temperature, 1475 °C, the NaOH(g) concentration was 20 ppm for all investigated SO₂ concentrations. No sulfation reaction took place at this temperature. At 1275 °C, a slight decrease in the NaOH(g) concentration was observed and 18 ppm was measured with > 50 ppm SO₂. At 1115 °C only a small decrease in the concentration of NaOH(g) was measured, but the concentration dropped further with increasing SO₂. With 100 and 150 ppm SO₂, around 40% of the NaOH(g) was consumed. Also at 985 and 850 °C, an increased NaOH(g) consumption was observed with increasing SO₂ concentrations. At the lowest investigated temperature, 850 °C, almost all of the NaOH(g) reacted with > 50 ppm SO₂.

Figure 28b shows KOH(g) concentrations from potassium sulfation experiments from a recent study by Weng et al. under the same conditions as the sodium sulfation experiments [119]. The measured KOH(g) are close to the measured NaOH(g) concentrations for the same conditions, showing that the chemistry and the kinetics of the sulfation of those alkali species in the gas phase is similar.

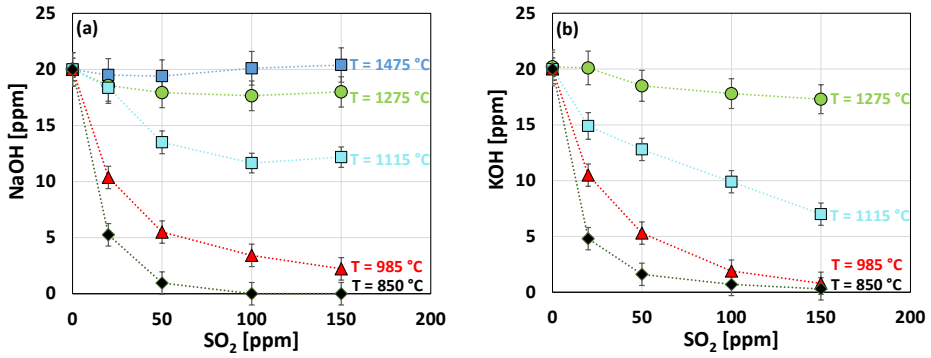


Figure 28. (a) NaOH concentrations from sulfation experiments at 850 – 1475 °C, inlet concentration 20 ppm NaOH and 0 – 150 ppm SO₂ and (b) KOH concentrations from sulfation experiments under same condition for comparison (reproduced from [117]) (Reprinted with permission from Publication III. ©2022 Elsevier).

The reduction of the NaOH(g) concentration can be explained by the formation of gaseous Na₂SO₄ and Na₂SO₄ aerosols, as proposed by Glarborg and Marshall [112]. The aerosol formation from sulfation of KOH(g) has been observed by Weng et al. at 985 and 850 °C [119]. Due to the similar experiments for sodium hydroxide and potassium hydroxide, it is assumed that aerosol formation from sodium hydroxide sulfation also takes place at these temperatures. This is also in line with a study by Jiménez and Ballester, reporting the nucleation of K₂SO₄ in presence of KOH(g) and SO₂ at temperatures below 1000 °C.

Figure 29 compares the experimental results from the sodium hydroxide sulfation experiments with chemical equilibrium concentrations and concentrations predicted from the kinetic modeling. At the highest temperatures, 1275 and 1475 °C, the kinetic model and the chemical equilibrium predict the same concentrations, indicating that the system is already at equilibrium under these conditions. Neither the chemical equilibrium nor the kinetic modeling predicted that sulfation took place at 1475 °C, and only some sulfation took place at 1275 °C, which was also observed in the experiment. At 1115 °C, the chemical equilibrium predicted lower NaOH(g) concentrations than the kinetic modeling, indicating that the system is not at equilibrium at these temperatures. The experimentally measured NaOH(g) concentrations were close to the one predicted from the kinetic model. Also at 850 and 985 °C, the kinetic modeling was in satisfactory agreement with the data obtained from the experimental measurements.

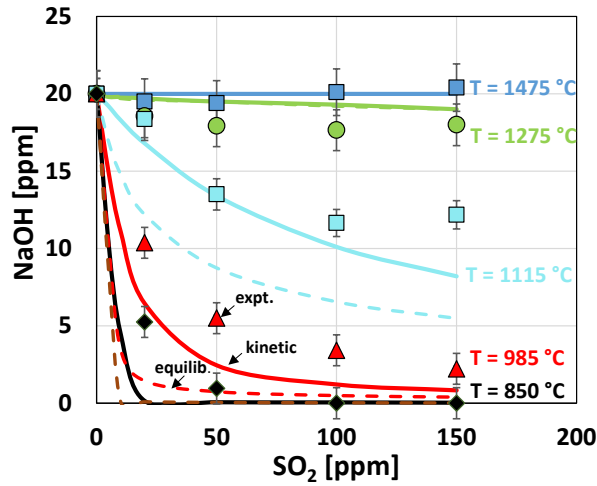


Figure 29. NaOH concentrations from sulfation experiments at 850 – 1475 °C, inlet concentration 20 ppm NaOH and 0 – 150 ppm SO₂: measured (symbols), kinetic modeling (continuous lines) and chemical equilibrium (dotted lines) (Reprinted with permission from Publication III. ©2022 Elsevier).

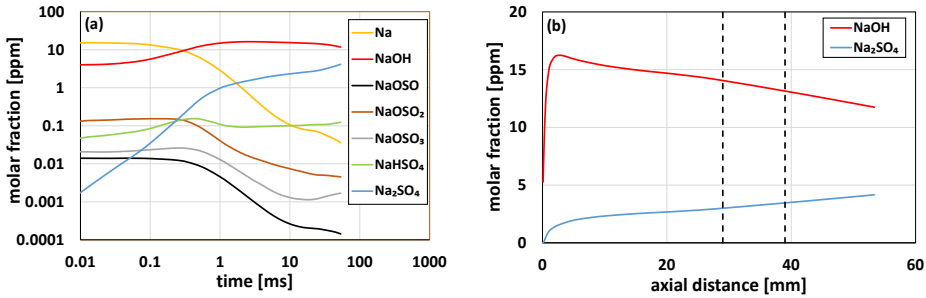


Figure 30. (a) Molar fractions of relevant species as a function of time (logarithmic scale) and (b) molar fraction of NaOH and Na₂SO₄ (linear scale) from kinetic modeling of the sulfation experiments at 1115 °C as a function of the vertical distance from the jet-tubes; inlet concentrations 20 ppm NaOH and 50 ppm SO₂. (Reprinted with permission from Publication III. ©2022 Elsevier).

Details of the kinetic modeling are presented in Fig. 30, showing concentrations of selected species as a function of time (molar fraction and time on a logarithmic scale) or the axial distance from the jets (linear scale). The dotted lines in Fig. 30b indicate the area in which the optical measurement took place. The concentrations shown are from the kinetic modeling of the sodium hydroxide sulfation at 1115 °C

with 50 ppm SO₂. According to the kinetic model, many reactions occur rapidly within the first 1 ms/ the first few millimeters above the burner outlet. NaOH is slowly consumed, while the concentration of Na₂SO₄ increases steadily.

To clarify whether the sulfation reactions actually can occur in the gas phase and if stable gaseous products can be formed under the investigated conditions, chemical equilibrium calculations were made. Figure 31 shows the split between gaseous and condensed Na₂SO₄ over the temperature range of 890 – 1130 °C in post-flame conditions as in the experiments. Above 1080 °C, only gaseous Na₂SO₄ seems to be stable. Below 1000 °C, most of the Na₂SO₄ is expected to be in the condensed phase, which is in line with the above discussed aerosol formation. The combined experimental data together with kinetic modeling and equilibrium calculations support that sulfation of alkali species can take place in the gas phase through homogenous reactions, as sodium sulfation was observed at temperatures where only gaseous Na₂SO₄ is a stable product. These findings are in contrast to earlier reports, suggesting that Na₂SO₄ formation cannot be a significant gas phase flame product and that most Na₂SO₄ likely forms through heterogeneous reactions [133].

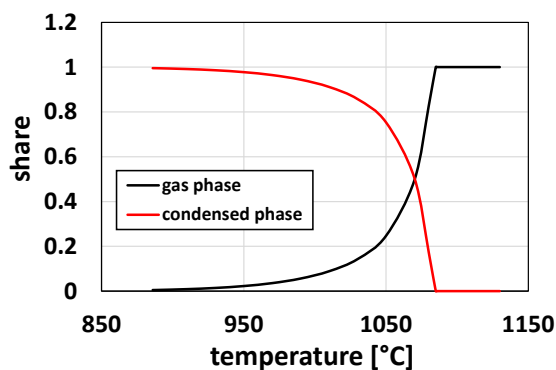


Figure 31. Equilibrium ratio of Na₂SO₄(g) and Na₂SO₄(l) for NaOH sulfation at 890 – 1130 °C; inlet concentration 20 ppm NaOH, 50 ppm SO₂, 4.7% CH₄ and 13.9% O₂ (N₂ as balance) (Reprinted with permission from Publication III. ©2022 Elsevier).

4.3.2. NaCl(g) sulfation – experimental results and modelling

For the investigation of the sulfation reactions of sodium chloride, the NaCl – NaOH equilibrium had to be taken into account (see Fig. 32). At low temperatures, most of the fed NaCl remained at NaCl(g) in the gas. At higher temperatures, however, NaCl partly converted to NaOH(g). At 1475 °C, NaCl(g) and NaOH(g) were present at equal ratios.

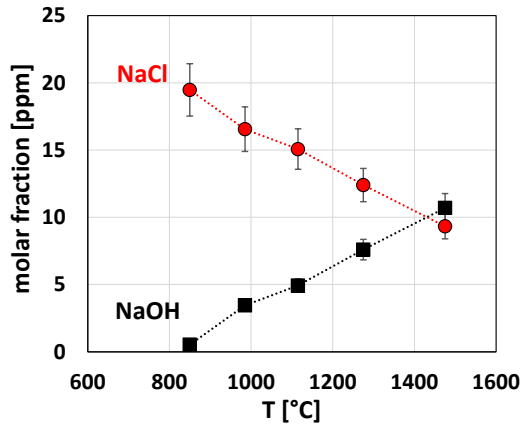


Figure 32. Molar fraction of NaCl and NaOH at 850 – 1475 °C measured in tests without SO₂; inlet concentration 20 ppm NaCl (Reprinted with permission from Publication III. ©2022 Elsevier).

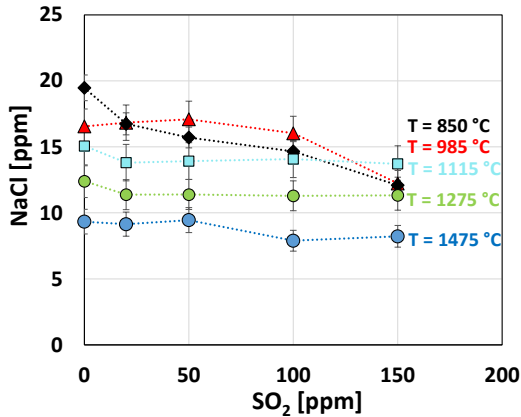


Figure 33. NaCl concentrations from sulfation experiments at 850 – 1475 °C; inlet concentration 20 ppm NaCl and 0 – 150 ppm SO₂ (dotted lines for clarity only) (Reprinted with permission from Publication III. ©2022 Elsevier).

The NaCl(g) concentrations measured during the sulfation experiments are shown in Fig. 33. At the higher temperatures, 1115 – 1475 °C, the NaCl(g) remained constant with SO₂ addition; no sulfation reactions took place at these temperatures. At 985 °C, the NaCl(g) concentration remained constant with 0- 100 ppm SO₂. With 150 ppm SO₂, a decrease in the NaCl(g) concentration was observed from around 17 ppm to 12 ppm. At the lowest temperature, 850 °C, the NaCl(g) concentration

decreased continuously with increasing SO_2 concentrations from 20 ppm without SO_2 addition to 12 ppm with 150 ppm SO_2 . This corresponds to a $\text{NaCl}(\text{g})$ reduction of around 40% under these conditions.

Figure 34 compares kinetic modeling and the chemical equilibrium calculations with the experimental data for the $\text{NaCl}(\text{g})$ sulfation. The data is shown for 850 and 985 °C, the cases in which sulfation reactions were observed. A comparison for experimental data and modeling for all investigated cases can be found in the Appendix I. At 985 °C, the system is close to equilibrium, but at 850 °C the system is far from equilibrium. Similar findings have been reported by Christensen and Livbjerg for the sulfation of KCl in a field study, showing that the alkali chloride sulfation was far from equilibrium according to their model [134].

For 985 °C, the kinetic model predictions were close to the concentrations measured in the experiment. For 850 °C, a significant deviation between the kinetic modeling predictions and the experiment was observed.

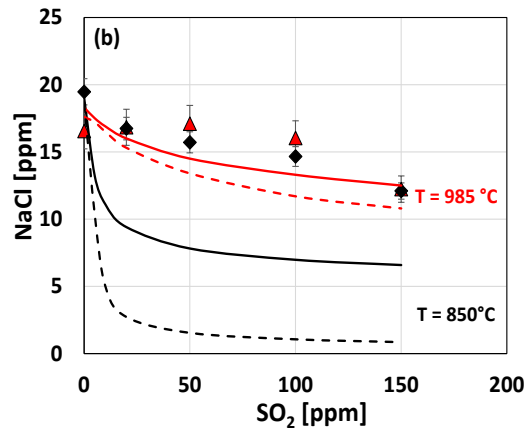


Figure 34. NaCl concentrations from sulfation experiments at 850 and 985 °C, inlet concentration 20 ppm NaCl and 0 – 150 ppm SO_2 : measured (symbols), kinetic modeling (continuous lines) and chemical equilibrium (dotted lines) (Reprinted with permission from Publication III. ©2022 Elsevier).

5. CONCLUSIONS

This thesis investigated the nitrogen and sulfur chemistry in processes related to thermal conversion of biomass waste streams. The three main tasks addressed were:

- Formation of nitrogen oxide and nitrogen oxide precursors during thermal conversion of from pre-treated biomass waste
- Gas-phase sulfation of corrosive sodium species with SO_2
- NO_x removal from flue gases by absorbing NO_2 in aqueous solutions with the sulfur-containing additives sulfite and thiosulfate

The formation of NO , NH_3 and HCN during devolatilization and combustion of raw and pre-treated bark and straw has been studied. For both biomass fuels, pre-treated samples had a higher vol-N to NH_3 and HCN formation during devolatilization (in 100% N_2 , 800 °C) as compared to the raw biomass samples. The highest NO precursor formation was found for the torrefied samples. During combustion (in 3% O_2 , rest N_2 , 800 °C), opposite effects were observed for bark and straw. While the fuel-N to NO conversion was lower for the pre-treated bark samples as compared to raw bark, a higher conversion was observed for the pre-treated straw samples. During char conversion, washed samples had the highest NO formation, and torrefied samples the lowest. The NO formation correlated with the amount of potassium in the samples. Ash forming matter also correlated with the vol-N to NH_3 conversion during devolatilization. Samples with higher calcium concentrations had a higher vol-N to NH_3 conversion, while samples with higher potassium contents had a lower vol-N to NH_3 conversion. A correlation between the presence of ash-forming elements and HCN formation was not observed. The ratio between NH_3 and HCN formed during devolatilization was significantly influenced by the fuel-N content and H/N ratio in the fuel. Samples with a higher fuel-N content and a lower H/N ratio showed a higher HCN/NH_3 ratio, while samples with less fuel-N and a higher H/N ratio showed a lower HCN/NH_3 ratio.

The homogenous gas-phase sulfation reactions of sodium hydroxide and sodium chloride were investigated in post-flame conditions at 850 – 1475 °C. The experiments were performed under oxidizing conditions with inlet concentrations of 20 ppm $\text{NaOH}(\text{g})$ or $\text{NaCl}(\text{g})$ and 0–150 ppm SO_2 . At 1275 °C and higher, almost no sulfation of $\text{NaOH}(\text{g})$ was observed. At 985 °C, almost all $\text{NaOH}(\text{g})$ was consumed with sufficiently high SO_2 concentrations. Sulfation of $\text{NaCl}(\text{g})$ occurred to a lower extent as compared to $\text{NaOH}(\text{g})$ under the investigated conditions. Almost no sulfation was observed for $\text{NaCl}(\text{g})$ above 985 °C. At the lowest investigated temperature, 850 °C, around 50% of the $\text{NaCl}(\text{g})$ was sulfated with 150 ppm SO_2 . Kinetic modeling and

chemical equilibrium calculations were done and results were compared to the experimental results. Above 1275 °C, the system can be described by chemical equilibrium. At 1115 °C and below, the measured NaOH(g) concentrations in the experiment were close to the concentrations predicted by the kinetic model. For NaCl(g), however, the kinetic model over-predicted the degree of sulfation. The combined experimental data, chemical equilibrium calculations and the kinetic modeling results support that sulfation reactions of reactive alkali species can occur in the gas phase through homogeneous reactions.

For NO₂ absorption in aqueous solutions with sulfur-containing additives, various factors such as additive concentration, pH, oxygen concentration and NO₂ concentrations were investigated. In absorption tests without oxygen, the NO₂ removal efficiency increased with increasing sulfite concentration in the absorption solution. With 0 mM sulfite, around 15% of the NO₂ was absorbed, 40% with 1 mM and 80% with 20 mM sulfite. Absorption rates were the highest at pH 8. With decreasing pH, lower absorption rates were observed, indicating that bisulfite is less reactive towards NO₂ as compared to sulfite. When the NO₂ inlet concentration was varied between 25 and 150 ppm, a linear increase of the absorption rate was observed. In the absorption tests with oxygen in the test gas, NO₂ absorption rates were initially the same as in the tests without oxygen. However, the rates dropped rapidly due to the consumption of sulfite by oxygen through a radical chain mechanism. Sulfite oxidation rates increased with increasing sulfite concentration in the absorption solution. The oxygen concentration, on the other hand, had no influence on the oxidation rate in the investigated range of 2 – 10%. Similar to sulfite, thiosulfate was also shown to promote NO₂ absorption rates, but to a much lower extent as compared to sulfite. The addition of 100 mM thiosulfate resulted in a lower absorption rate as compared to 1 mM sulfite. In the tests with both sulfite and thiosulfate, thiosulfate was shown to be an effective sulfite oxidation inhibitor, already at low concentrations of 1 mM. For a 10 mM sulfite solution, 1 mM thiosulfate decreased the sulfite oxidation rate by 75%. Thiosulfate was consumed at similar rates in tests with 2 and 5 mM sulfite. Around 38% and 44%, respectively, were consumed after a 30 min test.

6. REFERENCES

- [1] European Commission, European green deal : delivering on our targets, Publications Office of the European Union, 2021.
- [2] J.M.C. Ribeiro, R. Godina, J.C. de O. Matias, L.J.R. Nunes, Future Perspectives of Biomass Torrefaction: Review of the Current State-Of-The-Art and Research Development, *Sustainability* 2018, Vol. 10, Page 2323. 10 (2018) 2323.
- [3] N. Petrov, M. Mladenović, Legal limits for NOx emissions related to biomass in EU countries and Serbia, *Innovative Mechanical Engineering*. 1 (2022) 93–102.
- [4] bp, *Statistical Review of World Energy* 71st edition, 2022.
- [5] EIA, Net electricity consumption worldwide in select years from 1980 to 2021, (2022). <https://www.statista.com/statistics/280704/world-power-consumption/> (accessed December 16, 2022).
- [6] GLOBAL BIOENERGY STATISTICS 2021 World Bioenergy Association, 2021.
- [7] Official Statistics of Finland (OSF): Production of electricity and heat, (2021). http://www.stat.fi/til/salatuo/2020/salatuo_2020_2021-11-02_tie_001_en.html (accessed December 16, 2022).
- [8] B. Holtsmark, Harvesting in boreal forests and the biofuel carbon debt, *Clim Change*. 112 (2012) 415–428.
- [9] W.M. Lewandowski, M. Ryms, W. Kosakowski, Thermal biomass conversion: A review, *Processes*. 8 (2020).
- [10] J. Saastamoinen, J. Richard, Drying, Pyrolysis and Combustion of Biomass Particles, in: A. v Bridgwater, J.L. Kuester (Eds.), *Research in Thermochemical Biomass Conversion*, Springer Netherlands, Dordrecht, 1988: pp. 221–235.
- [11] A. Uslu, A.P.C. Faaij, P.C.A. Bergman, Pre-treatment technologies, and their effect on international bioenergy supply chain logistics. Techno-economic evaluation of torrefaction, fast pyrolysis and pelletisation, *Energy*. 33 (2008) 1206–1223.
- [12] B. Batidzirai, A.P.R. Mignot, W.B. Schakel, H.M. Junginger, A.P.C. Faaij, Biomass torrefaction technology: Techno-economic status and future prospects, *Energy*. 62 (2013) 196–214.

- [13] J.S. Tumuluru, S. Sokhansanj, J.R. Hess, C.T. Wright, R.D. Boardman, A review on biomass torrefaction process and product properties for energy applications, *Industrial Biotechnology*. 7 (2011) 348–401.
- [14] W.H. Chen, B.J. Lin, Y.Y. Lin, Y.S. Chu, A.T. Ubando, P.L. Show, H.C. Ong, J.S. Chang, S.H. Ho, A.B. Culaba, A. Pétrissans, M. Pétrissans, Progress in biomass torrefaction: Principles, applications and challenges, *Prog Energy Combust Sci*. 82 (2021) 100887.
- [15] S.S. Thanapal, W. Chen, K. Annamalai, N. Carlin, R.J. Ansley, D. Ranjan, Carbon dioxide torrefaction of woody biomass, *Energy and Fuels*. 28 (2014) 1147–1157.
- [16] W.H. Chen, P.C. Kuo, A study on torrefaction of various biomass materials and its impact on lignocellulosic structure simulated by a thermogravimetry, *Energy*. 35 (2010) 2580–2586.
- [17] Y. Mei, R. Liu, Q. Yang, H. Yang, J. Shao, C. Draper, S. Zhang, H. Chen, Torrefaction of cedarwood in a pilot scale rotary kiln and the influence of industrial flue gas, *Bioresour Technol*. 177 (2015) 355–360.
- [18] W.H. Chen, K.M. Lu, S.H. Liu, C.M. Tsai, W.J. Lee, T.C. Lin, Biomass torrefaction characteristics in inert and oxidative atmospheres at various superficial velocities, *Bioresour Technol*. 146 (2013) 152–160.
- [19] K.O. Davidsson, J.G. Korsgren, J.B.C. Pettersson, U. Jäglid, The effects of fuel washing techniques on alkali release from biomass, *Fuel*. 81 (2002) 137–142.
- [20] L. Deng, X. Jin, J. Long, D. Che, Ash deposition behaviors during combustion of raw and water washed biomass fuels, *Journal of the Energy Institute*. 92 (2019) 959–970.
- [21] M.R. Mladenović, D. v. Dakić, S. Nemoda, M.J. Paprika, M.S. Komatina, B.S. Repić, A.M. Erić, The combustion of biomass - The impact of its types and combustion technologies on the emission of nitrogen oxide, *Hem Ind*. 70 (2016) 287–298.
- [22] K.M. Hansson, J. Samuelsson, C. Tullin, L.E. Åmand, Formation of HNCO, HCN, and NH₃ from the pyrolysis of bark and nitrogen-containing model compounds, *Combust Flame*. 137 (2004) 265–277.
- [23] P. Glarborg, A.D. Jensen, J.E. Johnsson, Fuel nitrogen conversion in solid fuel fired systems, *Prog Energy Combust Sci*. 29 (2003) 89–113.

- [24] J. Giuntoli, W. de Jong, A.H.M. Verkooijen, P. Piotrowska, M. Zevenhoven, M. Hupa, Combustion characteristics of biomass residues and biowastes: Fate of fuel nitrogen, *Energy and Fuels*. 24 (2010) 5309–5319.
- [25] A. Anca-Couce, P. Sommersacher, N. Evic, R. Mehrabian, R. Scharler, Experiments and modelling of NO_x precursors release (NH₃ and HCN) in fixed-bed biomass combustion conditions, *Fuel*. 222 (2018) 529–537.
- [26] M. Becidan, Ø. Skreiberg, J.E. Hustad, NO_x and N₂O precursors (NH₃ and HCN) in pyrolysis of biomass residues, *Energy and Fuels*. 21 (2007) 1173–1180.
- [27] J. Leppälahti, Formation of NH₃ and HCN in slow-heating-rate inert pyrolysis of peat, coal and bark, *Fuel*. 74 (1995) 1363–1368.
- [28] H. Liu, L. Yi, H. Hu, K. Xu, Q. Zhang, G. Lu, H. Yao, Emission control of NO_x precursors during sewage sludge pyrolysis using an integrated pretreatment of Fenton peroxidation and CaO conditioning, *Fuel*. 195 (2017) 208–216.
- [29] K.M. Hansson, L.E. Åmand, A. Habermann, F. Winter, Pyrolysis of poly-L-leucine under combustion-like conditions, *Fuel*. 82 (2003) 653–660.
- [30] H. Chen, Y. Si, Y. Chen, H. Yang, D. Chen, W. Chen, NO_x precursors from biomass pyrolysis: Distribution of amino acids in biomass and Tar-N during devolatilization using model compounds, *Fuel*. 187 (2017) 367–375.
- [31] J. Zhou, P. Gao, C. Dong, Y. Yang, Effect of temperature and mineral matter on the formation of NO_x precursors during fast pyrolysis of 2,5-diketopiperazine, *Energies (Basel)*. 11 (2018).
- [32] Q. Ren, C. Zhao, Evolution of fuel-N in gas phase during biomass pyrolysis, *Renewable and Sustainable Energy Reviews*. 50 (2015) 408–418.
- [33] K.M. Hansson, J. Samuelsson, C. Tullin, L.E. Åmand, Formation of HNCO, HCN, and NH₃ from the pyrolysis of bark and nitrogen-containing model compounds, *Combust Flame*. 137 (2004) 265–277.
- [34] Q. Ren, C. Zhao, NO_x and N₂O precursors (NH₃ and HCN) from biomass pyrolysis: Interaction between amino acid and mineral matter, *Appl Energy*. 112 (2013) 170–174.
- [35] L. Yi, H. Liu, G. Lu, Q. Zhang, J. Wang, H. Hu, H. Yao, Effect of Mixed Fe/Ca Additives on Nitrogen Transformation during Protein and Amino Acid Pyrolysis, *Energy and Fuels*. 31 (2017) 9484–9490.

- [36] Q. Ren, C. Zhao, X. Wu, C. Liang, X. Chen, J. Shen, G. Tang, Z. Wang, Effect of mineral matter on the formation of NO_x precursors during biomass pyrolysis, *J Anal Appl Pyrolysis*. 85 (2009) 447–453.
- [37] G.G. de Soete, Heterogeneous N₂O and NO formation from bound nitrogen atoms during coal char combustion, *Symposium (International) on Combustion*. 23 (1991) 1257–1264.
- [38] A.F. Sarofim, J.M. Beer, Y.H. Song, Oxidation and devolatilization of nitrogen in coal char, *Combustion Science and Technology*. 28 (1982) 177–183.
- [39] B. Ulusoy, W. Lin, O. Karlström, S. Li, W. Song, P. Glarborg, K. Dam-Johansen, H. Wu, Formation of NO and N₂O during Raw and Demineralized Biomass Char Combustion, *Energy and Fuels*. 33 (2019) 5304–5315.
- [40] O. Karlström, A. Brink, M. Hupa, Biomass char nitrogen oxidation - Single particle model, *Energy and Fuels*. 27 (2013) 1410–1418.
- [41] O. Karlström, A. Brink, M. Hupa, Time dependent production of NO from combustion of large biomass char particles, *Fuel*. 103 (2013) 524–532.
- [42] J.O.L. Wendt, C. v. Sternling, M.A. Matovich, Reduction of sulfur trioxide and nitrogen oxides by secondary fuel injection, *Symposium (International) on Combustion*. 14 (1973) 897–904.
- [43] J.H. Fernandez, J.D. Sensenbaugh, D.G. Peterson, Boiler emissions and their control, *Proc. Air Pollution Control*. (1966).
- [44] E. Coda Zabetta, M. Hupa, K. Saviharju, Reducing NO_x Emissions Using Fuel Staging, Air Staging, and Selective Noncatalytic Reduction in Synergy, *Ind. Eng. Chem. Res*. 44 (2005) 4552–4561.
- [45] S.N. Anichkov, A.M. Zykov, A.G. Tumanovskii, O.N. Kulish, K.I. Zaporozhskii, Development of SNCR Technology and Prospects of Its Application, *Thermal Engineering* . 68 (2021) 510–515.
- [46] S.S. Daood, M.T. Javed, B.M. Gibbs, W. Nimmo, NO_x control in coal combustion by combining biomass co-firing, oxygen enrichment and SNCR, *Fuel*. 105 (2013) 283–292.
- [47] S. Mahmoudi, J. Baeyens, J.P.K. Seville, NO_x formation and selective non-catalytic reduction (SNCR) in a fluidized bed combustor of biomass, *Biomass Bioenergy*. 34 (2010) 1393–1409.

- [48] M. Mladenović, M. Paprika, A. Marinković, Denitrification techniques for biomass combustion, *Renewable and Sustainable Energy Reviews*. 82 (2018) 3350–3364.
- [49] Y. Zheng, A.D. Jensen, J.E. Johnsson, Deactivation of V₂O₅-WO₃-TiO₂ SCR catalyst at a biomass-fired combined heat and power plant, *Appl Catal B*. 60 (2005) 253–264.
- [50] H.M.A. Sharif, N. Mahmood, S. Wang, I. Hussain, Y.N. Hou, L.H. Yang, X. Zhao, B. Yang, Recent advances in hybrid wet scrubbing techniques for NO_x and SO₂ removal: State of the art and future research, *Chemosphere*. 273 (2021) 129695.
- [51] M. Zhao, P. Xue, J. Liu, J. Liao, J. Guo, A review of removing SO₂ and NO_x by wet scrubbing, *Sustainable Energy Technologies and Assessments*. 47 (2021) 101451.
- [52] R.T. Guo, J.K. Hao, W.G. Pan, Y.L. Yu, Liquid Phase Oxidation and Absorption of NO from Flue Gas: A Review, *Separation Science and Technology (Philadelphia)*. 50 (2015) 310–321.
- [53] B.R. Deshwal, S.H. Lee, J.H. Jung, B.H. Shon, H.K. Lee, Study on the removal of NO_x from simulated flue gas using acidic NaClO₂ solution, *Journal of Environmental Sciences*. 20 (2008) 33–38.
- [54] C. Brogren, H.T. Karlsson, I. Bjerle, Absorption of NO in an Aqueous Solution of NaClO₂, *Chem. Eng. Technol.* 21 (1998) 61–70.
- [55] D.S. Jin, B.R. Deshwal, Y.S. Park, H.K. Lee, Simultaneous removal of SO₂ and NO by wet scrubbing using aqueous chlorine dioxide solution, *J Hazard Mater*. 135 (2006) 412–417.
- [56] J. Wei, Y. Luo, P. Yu, B. Cai, H. Tan, Removal of NO from flue gas by wet scrubbing with NaClO₂/(NH₂)₂CO solutions, *Journal of Industrial and Engineering Chemistry*. 15 (2009) 16–22.
- [57] H.J. Yoon, H.W. Park, D.W. Park, Simultaneous Oxidation and Absorption of NO_x and SO₂ in an Integrated O₃ Oxidation/Wet Atomizing System, *Energy and Fuels*. 30 (2016) 3289–3297.
- [58] Y.S. Mok, Absorption-reduction technique assisted by ozone injection and sodium sulfide for NO_x removal from exhaust gas, *Chemical Engineering Journal*. 118 (2006) 63–67.

- [59] H. Chu, T.W. Chien, S.Y. Li, Simultaneous absorption of SO₂ and NO from flue gas with KMnO₄/NaOH solutions, *Sci Total Environ.* 275 (2001) 127–135.
- [60] Y.G. Adewuyi, N.Y. Sakyi, Simultaneous absorption and oxidation of nitric oxide and sulfur dioxide by aqueous solutions of sodium persulfate activated by temperature, *Ind Eng Chem Res.* 52 (2013) 11702–11711.
- [61] V.N.A. Sapkota, N.A. Fine, G.T. Rochelle, NO₂-catalyzed sulfite oxidation, *Ind Eng Chem Res.* 54 (2015) 4815–4822.
- [62] J.J. Kaczur, Oxidation chemistry of chloric acid in NO_x/SO_x and air toxic metal removal from gas streams, *Environmental Progress.* 15 (1996) 245–254.
- [63] C.H. Shen, G.T. Rochelle, Nitrogen dioxide absorption and sulfide oxidation in aqueous sulfide, *J Air Waste Manage Assoc.* 49 (1999) 332–338.
- [64] X. Gao, R.T. Guo, H.L. Ding, Z.Y. Luo, K.F. Cen, Absorption of NO₂ into Na₂S solution in a stirred tank reactor, *Journal of Zhejiang University: Science A.* 10 (2009) 434–438.
- [65] Y. Lee, J.H. Sung, B. Han, Y.J. Kim, H.J. Kim, Minimizing the consumption of reducing agents for NO_x removal in a wet scrubber without H₂S formation, *Sep Purif Technol.* 282 (2022) 120101.
- [66] W.P. Yant, R.R. Sayers, Hydrogen Sulfide as an Industrial Poison 613 HYDROGEN SULFIDE AS A LABORATORY AND INDUSTRIAL POISON*, *J Chem Educ.* 4 (1927) 613.
- [67] C.H. Shen, G.T. Rochelle, Nitrogen Dioxide Absorption and Sulfite Oxidation in Aqueous Sulfite, *Environ. Sci. Technol.* 32 (1998) 1994–2013. <https://pubs.acs.org/sharingguidelines>.
- [68] H. Takeuchi, M. Ando, N. Kizawa, Absorption of Nitrogen Oxides in Aqueous Sodium Sulfite and Bisulfite Solutions, *Ind. Eng. Chem. Process Des. Dev.* 16 (1977) 303–308.
- [69] Y. Kameoka, R.L. Pigford, Absorption of Nitrogen Dioxide into Water, Sulfuric Acid, Sodium Hydroxide, and Alkaline Sodium Sulfite Aqueous Solutions, *Ind. Eng. Chem., Fundam.* 16 (1977) 163–169.
- [70] T. Nash, The effect of Nitrogen Dioxide and some Transition Metals of dilute Bisulphite Solutions, *Atmos. Environ.* 13 (1967) 1149–154.

- [71] P. Neta, R.E. Huie, Free-Radical Chemistry of Sulfite, *Environ Health Perspect.* 64 (1985) 209–217.
- [72] R.E. Huie, P. Neta, Chemical behaviour of SO_3^- and SO_5^- radicals in aqueous solutions, *J. Phys. Chem.* 88 (1984) 5665–5669.
- [73] G.T. Rochelle, D.R. Owens, J.C.S. Chang, T.G. Bma, Thiosulfate as an oxidation inhibitor in flue gas desulfurization processes: A review of r&d results, *J Air Pollut Control Assoc.* 36 (1986) 1138–1146.
- [74] S. Li, W. Huang, H. Xu, K. Liu, J. nan Wang, Y. Sun, Z. Qu, N. Yan, Enhanced simultaneous absorption of NO_x and SO_2 in oxidation-reduction-absorption process with a compounded system based on Na_2SO_3 , *J Environ Sci (China)*. 111 (2021) 1–10.
- [75] J.C.S. Chang, T.G. Brna, Pilot testing of sodium thiosulfate, *Environmental Progress.* 5 (1986) 225–233.
- [76] J.-S. Mo, W.U. Zhong-Biao, C.-J. Cheng, B.-H. Guan, Z. Wei-Rong, Oxidation inhibition of sulfite in dual alkali flue gas desulfurization system, *J. Environ. Sci.* 19 (2007) 226–231. www.jesc.ac.cn.
- [77] Q. Guo, Y. He, T. Sun, Y. Wang, J. Jia, Simultaneous removal of NO_x and SO_2 from flue gas using combined Na_2SO_3 assisted electrochemical reduction and direct electrochemical reduction, *J Hazard Mater.* 276 (2014) 371–376.
- [78] F. Shi, K. Li, J. Li, D. Ying, J. Jia, T. Sun, N. Yan, X. Zhang, Simultaneous wet absorption of SO_2 and NO_x with mixed Na_2SO_3 and $(\text{NH}_4)_2\text{SO}_3$: Effects of mass concentration ratio and pH, *Chemical Engineering Journal.* 421 (2021).
- [79] S. Li, H. Xu, W. Huang, Y. Sun, J. Wang, Z. Qu, N. Yan, NO_x Absorption Enhancement and Sulfite Oxidation Inhibition via a Match Strategy in Na_2SO_3 Solution from a Wet Flue Gas Denitration System, *ACS EST Engg.* 1 (2021) 100–109.
- [80] Y. Sun, X. Hong, T. Zhu, X. Guo, D. Xie, The chemical behaviors of nitrogen dioxide absorption in sulfite solution, *Appl. Sci.* 7 (2017) 377.
- [81] T.Z. Tumsa, S.H. Lee, F. Normann, K. Andersson, S. Ajdari, W. Yang, Concomitant removal of NO_x and SO_x from a pressurized oxy-fuel combustion process using a direct contact column, *Chemical Engineering Research and Design.* 131 (2018) 626–634.
- [82] J. Johansson, F. Normann, N. Sarajlic, K. Andersson, Technical-Scale Evaluation of Scrubber-Based, Co-Removal of NO_x and SO_x Species from

Flue Gases via Gas-Phase Oxidation, *Ind Eng Chem Res.* 58 (2019) 21904–21912.

- [83] J. Johansson, F. Normann, K. Andersson, Techno-economic evaluation of co-removal of NO_x and SO_x species from flue gases via enhanced oxidation of NO by ClO₂—case studies of implementation at a pulp and paper mill, waste-to-heat plant and a cruise ship, *Energies (Basel)*. 14 (2021).
- [84] W. Moroń, W. Rybak, NO_x and SO₂ emissions of coals, biomass and their blends under different oxy-fuel atmospheres, *Atmos Environ.* 116 (2015) 65–71.
- [85] R. Paulauskas, N. Striūgas, M. Sadeckas, P. Sommersacher, S. Retschitzegger, N. Kienzl, Online determination of potassium and sodium release behaviour during single particle biomass combustion by FES and ICP-MS, *Science of the Total Environment*. 746 (2020).
- [86] J.G. Olsson, J.B.C. Pettersson, P. Hald, Alkali Metal Emission during Pyrolysis of Biomass, *Energ. Fuel.* 11 (1997) 779–784.
<https://pubs.acs.org/sharingguidelines>.
- [87] R. Backman, W.J. Frederick, M. Hupa, Basic studies on black-liquor pyrolysis and char gasification, *Bioresour Technol.* 46 (1993) 153–158.
- [88] D.C. Dayton, W.J. Frederick, Direct Observation of Alkali Vapor Release during Biomass Combustion and Gasification. 2. Black Liquor Combustion at 1100 °C, *Energ. Fuel.* 10 (1996) 284–292.
- [89] L. Hindiyarti, F. Frandsen, H. Livbjerg, P. Glarborg, P. Marshall, An exploratory study of alkali sulfate aerosol formation during biomass combustion, *Fuel.* 87 (2008) 1591–1600.
- [90] K.A. Christensen, H. Livbjerg, A plug flow model for chemical reactions and aerosol nucleation and growth in an alkali-containing flue gas, *Aerosol Science and Technology*. 33 (2000) 470–489.
- [91] J.R. Jensen, L.B. Nielsen, C. Schultz-Møller, S. Wedel, H. Livbjerg, The nucleation of aerosols in flue gases with a high content of alkali - A laboratory study, *Aerosol Science and Technology*. 33 (2000) 490–509.
- [92] C. Gilbe, M. Öhman, E. Lindström, D. Boström, R. Backman, R. Samuelsson, J. Burvall, Slagging characteristics during residential combustion of biomass pellets, *Energy and Fuels*. 22 (2008) 3536–3543.

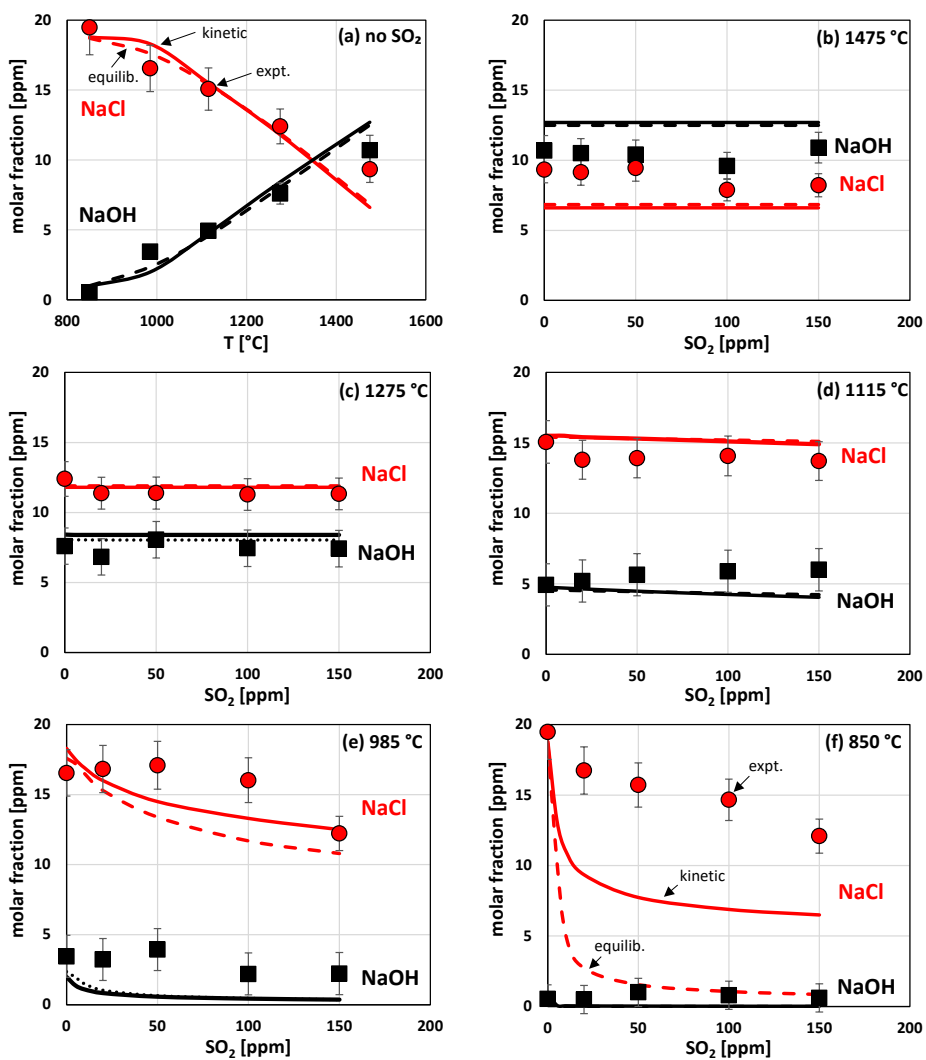
- [93] M. Lapuerta, A. Acosta, A. Pazo, Fouling Deposits from Residual Biomass with High Sodium Content in Power Plants, *Energy and Fuels*. 29 (2015) 5007–5017.
- [94] Y. Niu, H. Tan, S. Hui, Ash-related issues during biomass combustion: Alkali-induced slagging, silicate melt-induced slagging (ash fusion), agglomeration, corrosion, ash utilization, and related countermeasures, *Prog Energy Combust Sci*. 52 (2016) 1–61.
- [95] S. Enestam, D. Bankiewicz, J. Tuiremo, K. Mäkelä, M. Hupa, Are NaCl and KCl equally corrosive on superheater materials of steam boilers?, *Fuel*. 104 (2013) 294–306.
- [96] B.M. Jenkins, L.L. Baxter, T.R. Miles, T.R. Miles, Combustion properties of biomass, *Fuel Processing Technology*. 54 (1998) 17–46.
- [97] J. Sardans, J. Peñuelas, Potassium: A neglected nutrient in global change, *Global Ecology and Biogeography*. 24 (2015) 261–275.
- [98] J. Jermer, A. Ekvall, C. Tullin, Inventory of contaminants in waste wood; Inventering av foeroreningar i reurtrae, 2001.
- [99] L. Pola, S. Collado, P. Oulego, M. Díaz, Kraft black liquor as a renewable source of value-added chemicals, *Chemical Engineering Journal*. 448 (2022) 137728.
- [100] P. Grammelis, European Standards for Fuel Specification and Classes of Solid Biofuels, *Green Energy and Technology*. 28 (2010) 21–41.
- [101] S. Karlsson, J. Pettersson, L.G. Johansson, J.E. Svensson, Alkali induced high temperature corrosion of stainless steel: The influence of NaCl, KCl and CaCl₂, *Oxidation of Metals*. 78 (2012) 83–102.
- [102] A.A. Khan, W. de Jong, P.J. Jansens, H. Spliethoff, Biomass combustion in fluidized bed boilers: Potential problems and remedies, *Fuel Processing Technology*. 90 (2009) 21–50.
- [103] S. Karlsson, L.E. Åmand, J. Liske, Reducing high-temperature corrosion on high-alloyed stainless steel superheaters by co-combustion of municipal sewage sludge in a fluidised bed boiler, *Fuel*. 139 (2015) 482–493.
- [104] H. Wu, P. Yrjas, P. Vainikka, D. Lindberg, M. Hupa, Sulfation of alkali halides in a bench-scale bubbling fluidized bed reactor, *Fuel*. 177 (2016) 173–179.

- [105] H. Kassman, J. Pettersson, B.M. Steenari, L.E. Åmand, Two strategies to reduce gaseous KCl and chlorine in deposits during biomass combustion - Injection of ammonium sulphate and co-combustion with peat, in: *Fuel Processing Technology*, 2013: pp. 170–180.
- [106] H. Wu, G. Wang, P.A. Jensen, F. Jappe Frandsen, P. Glarborg, Reactive additives for alkali capture in biomass combustion *Reactive Additives for Alkali Capture in Biomass Combustion*, 2019.
- [107] M. Aho, K. Paakkinen, R. Taipale, Destruction of alkali chlorides using sulphur and ferric sulphate during grate combustion of corn stover and wood chip blends, in: *Fuel*, 2013: pp. 562–569.
- [108] M. Aho, P. Vainikka, R. Taipale, P. Yrjas, Effective new chemicals to prevent corrosion due to chlorine in power plant superheaters, *Fuel*. 87 (2008) 647–654.
- [109] K. Iisa, Y. Lu, K. Salmenoja, Sulfation of potassium chloride at combustion conditions, *Energy and Fuels*. 13 (1999) 1184–1190.
- [110] L. Boonsongsup, K. Iisa, W.J. Frederick, Kinetics of the Sulfation of NaCl at Combustion Conditions, *Ind. Eng. Chem. Res.* 36 (1997) 4212–4216.
<https://pubs.acs.org/sharingguidelines>.
- [111] J. Capablo, J. Ballester, Experimental study of the kinetics of sulfation of alkali chloride deposits, *Fuel Processing Technology*. 140 (2015) 215–221.
- [112] P. Glarborg, P. Marshall, Mechanism and modeling of the formation of gaseous alkali sulfates, *Combust Flame*. 141 (2005) 22–39.
- [113] S. Jiménez, J. Ballester, Influence of operating conditions and the role of sulfur in the formation of aerosols from biomass combustion, *Combust Flame*. 140 (2005) 346–358.
- [114] T. Ekvall, K. Andersson, T. Leffler, M. Berg, K-Cl-S chemistry in air and oxy-combustion atmospheres, *Proceedings of the Combustion Institute*. 36 (2017) 4011–4018.
- [115] T. Ekvall, F. Normann, K. Andersson, F. Johnsson, Modeling the alkali sulfation chemistry of biomass and coal co-firing in oxy-fuel atmospheres, *Energy and Fuels*. 28 (2014) 3486–3494.
- [116] B. Li, Z. Sun, Z. Li, M. Aldén, J.G. Jakobsen, S. Hansen, P. Glarborg, Post-flame gas-phase sulfation of potassium chloride, *Combust Flame*. 160 (2013) 959–969.

- [117] W. Weng, S. Chen, H. Wu, P. Glarborg, Z. Li, Optical investigation of gas-phase KCl/KOH sulfation in post flame conditions, *Fuel*. 224 (2018) 461–468.
- [118] W. Weng, T. Leffler, C. Brackmann, M. Aldén, Z. Li, Spectrally Resolved Ultraviolet (UV) Absorption Cross-Sections of Alkali Hydroxides and Chlorides Measured in Hot Flue Gases, *Appl Spectrosc*. 72 (2018) 1388–1395.
- [119] W. Weng, Z. Li, H. Wu, M. Aldén, P. Glarborg, Quantitative K-Cl-S chemistry in thermochemical conversion processes using in situ optical diagnostics, in: *Proceedings of the Combustion Institute*, Elsevier Ltd, 2021: pp. 5219–5227.
- [120] O. Karlström, M. Perander, N. DeMartini, A. Brink, M. Hupa, Role of ash on the NO formation during char oxidation of biomass, *Fuel*. 190 (2017) 274–280.
- [121] M. José Illán-Gómez, A. Linares-Solano, L.R. Radovic, C. Salinas-Martínez De Lecea, NO Reduction by Activated Carbons. 2. Catalytic Effect of Potassium, *Energy & Fuels*. 9 (1995) 97–103.
- [122] M. José Illán-Gómez, A. Linares-Solano, L.R. Radovic, C. Salinas-Martínez De Lecea, NO Reduction by Activated Carbons. 4. Catalysis by Calcium, *Energy & Fuels*. 9 (1995) 112–118. <https://pubs.acs.org/sharingguidelines> (accessed December 20, 2022).
- [123] R. Zevenhoven, M. Hupa, The reactivity of chars from coal, peat and wood towards NO, with and without CO, *Fuel*. 77 (1998) 1169–1176.
- [124] M. José Illán-Gómez, A. Linares-Solano, L.R. Radovic, C. Salinas-Martínez De Lecea, NO Reduction by Activated Carbons. 5. Catalytic Effect of Iron, *Energy & Fuels*. 9 (1995) 540–548.
- [125] D. Chen, A. Gao, K. Cen, J. Zhang, X. Cao, Z. Ma, Investigation of biomass torrefaction based on three major components: Hemicellulose, cellulose, and lignin, *Energy Convers Manag*. 169 (2018) 228–237.
- [126] S. Yuan, Z.J. Zhou, J. Li, X.L. Chen, F.C. Wang, HCN and NH₃ released from biomass and soybean cake under rapid pyrolysis, *Energy and Fuels*. 24 (2010) 6166–6171.
- [127] T. Räisänen, D. Athanassiadis, Basic chemical composition of the biomass components of pine, spruce and birch, (2013). <https://jukuri.luke.fi/handle/10024/517814> (accessed December 21, 2022).

- [128] M. Kapoor, D. Panwar, G.S. Kaira, Bioprocesses for Enzyme Production Using Agro-Industrial Wastes: Technical Challenges and Commercialization Potential, *Agro-Industrial Wastes as Feedstock for Enzyme Production: Apply and Exploit the Emerging and Valuable Use Options of Waste Biomass*. (2016) 61–93.
- [129] I.A. Müller, B. Brunner, C. Breuer, M. Coleman, W. Bach, The oxygen isotope equilibrium fractionation between sulfite species and water, *Geochim Cosmochim Acta*. 120 (2013) 562–581.
- [130] E. Rolla, C.L. Chakrabarti, Kinetics of Decomposition of Tetrathionate, Trithionate, and Thiosulfate in Alkaline Media, *Environ. Sci. Technol.* 16 (1982) 852–857.
- [131] R.E. Davis, Displacement Reactions at the Sulfur Atom Displacement Reactions at the Sulfur Atom. I. An Interpretation of the Decomposition of Acidified Thiosulfate, *J. Amer. Chem. Soc.* 80 (1958) 3565–3569.
- [132] W.A. Pryor, The Kinetics of the Disproportionation of Sodium Thiosulfate to Sodium Sulfide and Sulfate polysulfide and sulfite are formed + HS-+ H+ (1A), *J. Amer. Chem. Soc.* 82 (1960) 4794–4797.
- [133] M. Steinberg, K. Schofield, The chemistry of sodium with sulfur in flames, *Prog Energy Combust Sci.* 16 (1990) 311–317.
- [134] K.A. Christensen, H. Livbjerg, A Field Study of Submicron Particles from the Combustion of Straw, *Aerosol Science and Technology*. 25 (1996) 185–199.

Appendix I



NaCl and NaOH concentrations from NaCl sulfation experiments at 850 – 1475 °C: measured concentrations (symbols), kinetic modeling (continuous lines) and chemical equilibrium (dashed lines); (a) NaCl and NaOH as function of temperature (no SO₂) and (b-f) NaCl and NaOH in sulfation experiment with 0 – 150 ppm SO₂.

PUBLICATIONS

D. Schmid, O. Karlström, P. Yrjas.

Release of NH₃, HCN and NO during devolatilization and combustion of washed and torrefied biomass.

Fuel 280 (2020), 118583.



Full Length Article

Release of NH₃, HCN and NO during devolatilization and combustion of washed and torrefied biomass

Daniel Schmid*, Oskar Karlström, Patrik Yrjas

Johan Gadolin Process Chemistry Centre, Åbo Akademi University, Piiispankatu 8, Turku, Finland

ARTICLE INFO

Keywords:

Torrefied biomass
Combustion
Nitrogen oxide
NO_x precursors
NH₃
HCN

ABSTRACT

The influence of two different biomass pre-treatment methods (torrefaction and combined treatment of washing and torrefaction) on the formation of NO and its precursors, NH₃ and HCN, during combustion has been studied. Experiments were conducted in an electrically heated single particle reactor under well-controlled conditions in N₂ and O₂/N₂ at 850 °C. NO concentrations of the product gases were measured during devolatilization and char oxidation, and the total amounts of released NH₃ and HCN were determined during devolatilization. The results show that the conversion of vol-N and char-N to NO changed due to the pre-treatments, influencing the NO emission factor (released NO/energy content) of the fuel. For torrefied straw, the NO emission factor was significantly higher than for raw straw. The change in NO formation can partly be explained by how the nitrogen contents change due to the pre-treatments: both for bark and straw, around 20% of the initial fuel-N was removed during the torrefaction; for straw, 50% of the initial fuel-N was removed during the combined torrefaction and washing. In addition, the changes in the NO formation can be explained by the release of NH₃ and HCN during devolatilization. The HCN/NH₃ ratio increased with increasing N content and decreasing H/N ratio due to the pre-treatments. The conversion of vol-N to NH₃ increased with increasing Ca content and decreasing K content. In general, the devolatilization of the pre-treated biomass samples resulted in a higher conversion of vol-N to NH₃ and HCN as compared to the raw biomasses.

1. Introduction

The European Union has a 32% renewable energy target by 2030 [1]. In 2018, around 50% of the primary renewable energy production in the EU was based on wood and other solid biomasses [2]. The presence of nitrogen is a concern in thermal conversion of biomass due to the formation of NO_x and NO_x emission regulations are becoming increasingly stricter [3]. NO_x emissions can be divided into NO (> 90%), NO₂ and N₂O [4]. Both NO and NO₂ are acid rain precursors while N₂O is a greenhouse gas and ozone destroyer [5]. NO_x formation in solid fuel combustion is a complex process which has been studied widely [3,5,6]. The fuel-N is typically divided into nitrogen released during devolatilization (vol-N) and nitrogen released during char conversion (char-N). Vol-N compounds comprise NH₃, HCN, N₂, NO and HCNCO. For high-rank coals, the vol-N is partly bound to tars [3]. Biomass tar-N can be observed at lower temperatures than temperatures typical of industrial biomass combustion, i.e. above 800 °C.

NH₃ and HCN are NO_x precursors, but can also act as reducing agents to reduce NO to N₂. NH₃ has a higher tendency to reduce NO to N₂ as compared to HCN [4]. Hence, the split of NH₃ and HCN is crucial

in order to understand and predict the formation of NO and has, as a result, been studied widely [7,8,9,10,11]. For spruce bark, NH₃ has been reported to be the major N-species while equal amounts of NH₃ and HCN have been formed during devolatilization of straw [12]. Besides the fuel type, the split is influenced by various factors such as temperature and heating rate: an increased heating rate has been shown to enhance the HCN release, while an increased particle size, i.e., a lower heating rate, has been shown to enhance the NH₃ release [5].

In biomass the nitrogen is mostly bound to proteins and, consequently, pyrolysis of various proteins and amino acids has been investigated. Chen et al. identified 17 different amino acids in a range of biomasses [13]. The carbohydrates in biomass (cellulose, hemicellulose and lignin) have different effects on pyrolysis of amino acids, possibly explaining why the NH₃/HCN split differs for various biomasses [12]. In addition, ash forming elements such as K and Ca have been reported to show catalytic effects on the formation of HCN and NH₃ during devolatilization [10,14,15,16]. Potassium has been reported to promote the formation of NH₃ and to inhibit the release of HCN during pyrolysis of 2,5-diketopiperazine, while Ca had an enhancing effect on HCN and an inhibitory effect on NH₃ [15]. During the pyrolysis of proteins and

* Corresponding author.

E-mail address: daniel.schmid@abo.fi (D. Schmid).<https://doi.org/10.1016/j.fuel.2020.118583>

Received 16 March 2020; Received in revised form 14 May 2020; Accepted 29 June 2020

Available online 10 July 2020

0016-2361/© 2020 The Authors. Published by Elsevier Ltd. This is an open access article under the CC BY-NC-ND license (<http://creativecommons.org/licenses/by-nc-nd/4.0/>).

amino acids, on the other hand, Ca showed an enhancing effect on the formation of NH_3 , while it reduced the HCN formation [16]. For the pyrolysis of straw and corn cob it was found that K promotes, while Ca inhibits, the formation of both NH_3 and HCN [17].

Ash forming matter also influences the nitrogen chemistry during the char oxidation. During char conversion, char-N reacts with O_2 , mainly forming NO [18]. The formed NO can then be heterogeneously reduced by the char-C to N_2 [19]. A study with raw and demineralized biomass showed that significantly more NO was released for demineralized biomasses as compared to raw biomasses [20]. Ca and K in the char may influence the conversion of char-N, by catalysing the reduction reaction between NO and char [21].

From the discussion above, it can be expected that fuel pre-treatment methods, such as torrefaction and washing (which influence the elemental composition) will influence the NO formation. Fuel pre-treatments, such as washing and torrefaction may be used to improve fuel quality and to reduce operating problems [22,23,24,25,26,27]. For example, torrefaction may result in a biomass with an improved grindability, a higher heating value and a hydrophobic surface. Water washing is a pre-treatment method which may partly remove harmful ash forming compounds [28,29]. Yet, little is known regarding how fuel pre-treatments for biomass influence the fate of the fuel-N [30].

In the present work, the release of NH_3 , HCN and NO during devolatilization and combustion of raw, torrefied and washed and torrefied bark and straw have been investigated. The objective was to clarify how these pre-treatments influence the fate of the fuel-N.

2. Experimental

2.1. Fuels

Spruce bark and wheat straw were used in raw and pre-treated forms (raw bark = RB, raw straw = RS). The pre-treatment methods were torrefaction (torrefied bark = TB, torrefied straw = TS) and a combined treatment of washing followed by torrefaction (washed & torrefied bark = WTb, washed & torrefied straw = WTS). The fuel samples were obtained from two different pilot plants and were used as received. For the washing treatment, the biomass was water washed at 50 °C for one hour. Afterwards, it was sprayed with additional water and kept for drying until the moisture content was below 15%. For the torrefaction, the bark samples were pre-dried in a first step at 150 °C and the straw samples were pre-dried at 180 °C. In a second step the spruce bark and the straw were torrefied at 230 and 250 °C, respectively, resulting in mass yields of 65 and 69%. All fuel samples were analysed on their elemental composition with a CHNS analyser, and ICP-AES for the ash forming elements. The biomass samples were pulverized in the laboratory and were pressed to uniform pellets with a diameter of 8 mm and a mass of 100 mg.

2.2. Single particle reactor

The experiments were performed in an electrically heated single particle reactor (SPR) made of quartz glass (see Fig. 1) at 850 °C. In the setup, gases are fed from the bottom with a flow of 100 l/h at NTP and inert gas (nitrogen) from the sides with 120 l/h at NTP resulting in a total flow of 220 l/h. The fuel particle is put to the centre of the reactor via an insertion tube. Initially, the temperature of the particle increases rapidly. During the initial devolatilization, temperature gradients are present in the particle due to the large particle size, the heat transfer to the particle, the thermal conductivity of the particle and exothermal oxidation reactions. Note that this is typical for devolatilization of large biomass particle at high combustion temperature. Fuel particles with a uniform size were used in all experiments to minimize the effects of varying temperature gradients for different fuel samples. Concentrations of O_2 , NO, CO and CO_2 in the product gases were continuously measured. NO was measured using a chemiluminescence analyser, CO

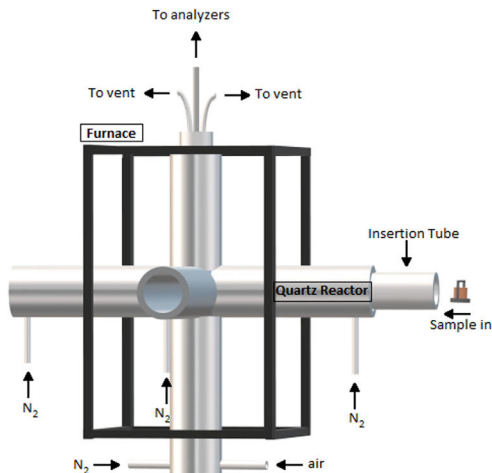


Fig. 1. Åbo Akademi single particle reactor (the black frame illustrates the electric furnace).

and CO_2 using on-dispersive infrared analyser and O_2 using a combined infrared + paramagnetic analyser.

The residence time from the reactor to the gas analysers was around 3 s. By comparing the fuel-C content to a carbon content based on the measured CO and CO_2 signals the carbon balance can be determined: in the experiments, the carbon balance is typically higher than 90%. The reactor system has been used in several previous studies which provides more detailed experimental descriptions, e.g. [20,31,32]. In the present study, an additional setup was used for the quantification of NH_3 and HCN based on a wet chemistry method. The flue gas was channelled to a 1 M HCl solution to collect NH_3 in the form of NH_4^+ or to a 5 wt% aqueous NaOH solution to collect HCN. Ammonium and cyanide ions were then quantified with spectrophotometry.

2.3. Combustion and devolatilization experiments

Two types of thermal experiments were performed: combustion and devolatilization experiments. In a combustion experiment, one single particle (placed on a sample holder (see Fig. 1)) was inserted into the heated reactor in 10 vol-% O_2/N_2 and left there until the combustion ended. The reason for using an oxygen concentration of 10 vol-% in the combustion experiments was to ensure that the volatile nitrogen compounds were oxidized to NO. Each experiment was repeated three times: the deviation of NO concentrations varied < 5% for repeated runs.

Devolatilization experiments were conducted in a pure N_2 atmosphere for 60 s. The experiments were conducted 30 times to collect sufficient amounts of HCN and NH_3 . The experiments (i.e. 30 repetitions) were repeated twice. The distributions of nitrogen in the volatiles (vol-N) and in the char (char-N) were determined from the devolatilization experiments. The char-N was determined from the remaining nitrogen in the char and the vol-N by the difference between fuel-N and char-N.

2.4. Quantification of NO, NH_3 and HCN

Fig. 2 exemplifies the NO release curve from a devolatilization experiment in 100% N_2 and from a combustion experiment in 10% O_2/N_2 . The curve obtained from the combustion test includes both devolatilization and char conversion, as marked in the figure. NO concentrations

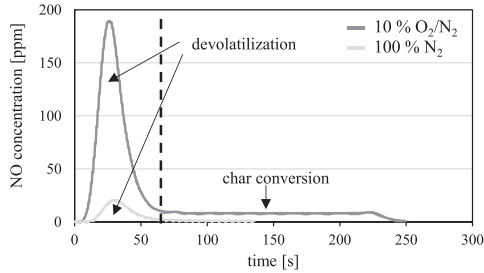


Fig. 2. NO release during combustion and devolatilization of spruce bark at 850 °C.

of the product gas increase rapidly during the devolatilization and drop rapidly after reaching a maximum after approximately 30 s. During the char oxidation, however, the NO concentrations in the product gas are much lower and on a constant level until the char oxidation has ended and the NO concentration drops to 0. The curve obtained from the devolatilization experiments in inert atmosphere only includes devolatilization as char oxidation does not take place under these conditions. The total amount of released NO during the devolatilization and during the char conversion was determined by integrating the devolatilization part and the char conversion part, respectively, while NH₃ and HCN were quantified by spectrophotometry.

3. Results and discussion

3.1. Fuel composition

Table 1 gives the proximate and ultimate analysis of the fuels. The pre-treated samples have higher carbon contents, and higher heating values, as compared to the raw biomasses. The pre-treated samples have, in general, higher nitrogen contents. The difference in the ash forming matter varies dependent on the elements. For example, the torrefied samples have higher concentrations of Ca and K, although the washed and torrefied samples have lower concentrations of K, possibly explained by element-specific differences in the water solubility.

Table 1 Proximate and ultimate analysis of the fuel samples.

| | RB | TB | WTB | RS | TS | WTS |
|--------------------------------|-------|--------|--------|--------|--------|--------|
| Moisture, wt% | 7.4 | 1.5 | 1.8 | 3.4 | 2.4 | 2.4 |
| Volatile matter wt% ds, 850 °C | 79.4 | 68.1 | 68.3 | 85.0 | 78.2 | 78.7 |
| HHV, MJ/kg ds | 19.03 | 20.82 | 20.71 | 16.22 | 16.86 | 16.83 |
| Ultimate analysis, wt% ds | | | | | | |
| C | 51.6 | 55.1 | 54.5 | 43.1 | 44.6 | 44.5 |
| H | 6.0 | 5.3 | 5.4 | 5.5 | 5.3 | 5.4 |
| N | 0.38 | 0.47 | 0.45 | 0.67 | 0.72 | 0.51 |
| S | 0.022 | 0.023 | 0.021 | 0.106 | 0.107 | 0.063 |
| O* | 40.4 | 37.1 | 37.9 | 44.6 | 42.8 | 43.8 |
| Ash wt% ds, 550 °C | 4.0 | 4.9 | 4.4 | 12.3 | 12.9 | 11.9 |
| Ash forming elements, mg/kg ds | | | | | | |
| Si | 2640 | 1490 | 550 | 44,900 | 49,300 | 46,900 |
| Al | 434 | 329 | 178 | 396 | 385 | 262 |
| Ca | 8880 | 14,200 | 13,700 | 3660 | 4180 | 4100 |
| Fe | 227 | 194 | 120 | 245 | 233 | 140 |
| K | 1760 | 2010 | 1120 | 7390 | 7780 | 3290 |
| Mg | 602 | 895 | 829 | 790 | 890 | 720 |
| Mn | 529 | 525 | 530 | 15.5 | 14.3 | 12.5 |
| Na | 148 | 109 | 203 | 160 | 166 | 277 |
| P | 398 | 491 | 436 | 760 | 721 | 575 |
| Cl | 110 | < 80 | < 80 | 1320 | 956 | 248 |

*By difference.

Note that Table 1 presents the actual contents in each fuel sample on a dry solid basis. Fig. 3, on the other hand, shows the relative contents of the pre-treated samples compared to the initial raw samples and, thus, how much of the original elements remaining after the treatment. For TB and WTB, the relative concentrations of the major elements (C, H, N, S and O) are between 60 and 80% which is approximately proportional to the total mass loss during torrefaction. The ash forming elements behave differently. For instance, for the bark, nearly all of the Ca and Mg remained after the pre-treatments while the contents of the other ash forming elements decreased.

Fig. 4a shows the split of vol-N and char-N, and also the amount of N removed during the pre-treatment. For clarification, Fig. 4b illustrates the fate of nitrogen during pre-treatment, devolatilization and char conversion. For bark and straw, the initial splits vol-N/char-N were 69/31 and 90/10; for torrefied bark and straw, the splits were 51/30 and 60/14; and for washed and torrefied bark and straw, the splits were 53/23 and 42/10, respectively. Thus, around 20% of the initial N was lost in the pre-treatments, expect for the washed and torrefied bark: almost 50% of the initial N was removed. Thus, a significant amount of nitrogen was removed due to the pre-treatments.

3.2. NO release from combustion experiments

Fig. 5 shows the amount of released NO from the combustion experiments. For RB, the amount of released NO is around 4 g NO/kg fuel, which corresponds to an emission factor of 0.22 g NO/MJ. For TB, the amount of released NO increased to 4.6 g NO/kg fuel, which is around 15% higher as compared to that of RB. However, the emission factor is almost unchanged as TB has a higher heating value than RB. The amount of released NO was slightly higher for WTB than for RB, although the emission factor was slightly lower. For RS, the amount of released NO was around 3.3 g NO/kg, resulting in an emission factor of 0.20 g NO/MJ. The amount of released NO from TS was higher, 4.1 g NO/kg, which represents an increase of around 25% as compared to RS. In addition, the emission factor for TS was around 20% higher as compared to RS. WTS, on the other hand, only had slightly higher emissions, 3.4 g NO/kg, and the same emission factor as RS.

It is important to emphasize the amounts of released NO of the straw clearly do not correlate with the nitrogen contents. TS has only a slightly higher fuel-N content than RS (see Table 1), although the amount of released NO was significantly higher. The fuel-N content of WTS is around 25% lower than that of RS, although the amounts of released NO were almost identical. For the bark samples, on the other hand, the amounts of released NO correlate with the fuel-N contents. An earlier study presented by Ren et al. also reported varying trends for the NO emissions from different biomass fuels after torrefaction [30]. For instance, NO emissions during the combustion of corn straw and beech wood were much higher when the samples were torrefied, while olive residue and rice hush had much lower NO emissions when torrefied.

Fig. 6 shows the conversion of fuel-N to NO from the combustion experiments (a) and the conversion of vol-N (b) and char-N (c) during the devolatilization stage and the char oxidation, respectively. For RB, 51% of the fuel-N formed NO during the combustion. For TB and WTB, the conversion of fuel-N to NO was 45%. This can mainly be explained by that the conversion of the vol-N to NO during devolatilization decreased. The conversion of the fuel-N to NO is mainly influenced by the conversion of vol-N to NO since the majority of the NO is formed during the devolatilization stage (70% for bark and 80% for straw). Interestingly, for straw, the opposite trend can be observed as compared to bark. The pre-treated straw samples showed higher conversions of the vol-N to NO, hence also for the conversion of fuel-N to NO. For the conversion of char-N to NO, similar observations can be done for RB and RS. For both bark and straw, the torrefied samples showed the lowest conversion of char-N to NO, while the washed and torrefied samples showed the highest conversion. This observation is in line with observation from earlier studied on the char conversion of biomass

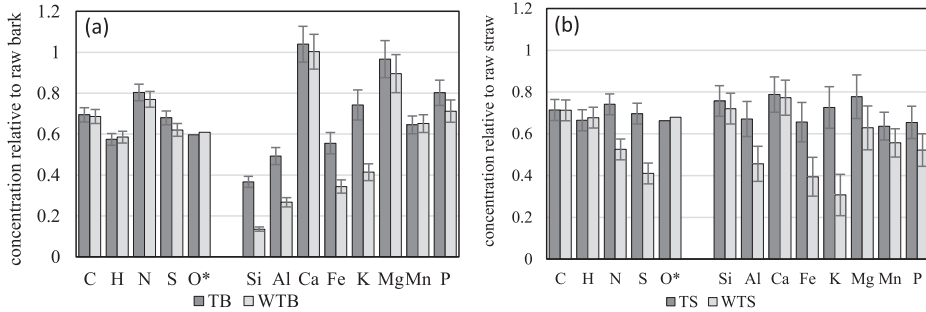


Fig. 3. Relative concentrations in pre-treated bark (a) and straw (b); 1 = concentration in untreated sample (TB = torrefied bark, WTB = washed & torrefied bark, TS = torrefied straw, WTS = washed & torrefied straw).

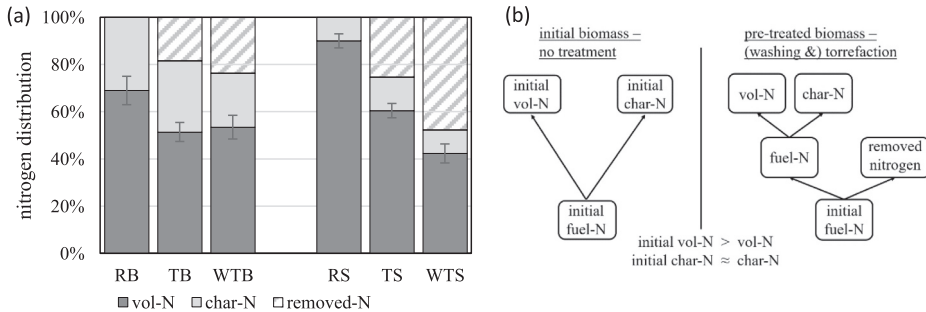


Fig. 4. Distribution of vol-N, char-N and removed-N (removed during pre-treatment) based on the fuel-N content in the raw biomass (a) and illustrative figure on the fate of initial fuel-N (b) (RB = raw bark, TB = torrefied bark, WTB = washed & torrefied bark, RS = raw straw, TS = torrefied straw, WTS = washed & torrefied straw).

[20].

In the torrefied samples, ash forming elements, e.g. K, are enriched, which might promote the catalytic reduction of NO during char oxidation. In washed and torrefied samples, however, the ash forming elements are partly leached, which might inhibit the catalytic reduction of NO to N₂ by the char surface.

3.3. Formation of NH₃, HCN and NO during devolatilization

Fig. 7 shows the conversion of vol-N to NH₃, HCN and NO during devolatilization at 850 °C. For RB, the conversion of vol-N to NH₃ was 21%, the conversion of vol-N to HCN was 8%, and the conversion of vol-N to NO was 6%. The conversion of vol-N to NO for the pre-treated bark and RB were similar. In addition, the conversions of vol-N to NH₃ and HCN from WTB and RB were similar as well. However, for TB an increased conversion of vol-N to NH₃ and HCN can be observed: 27%

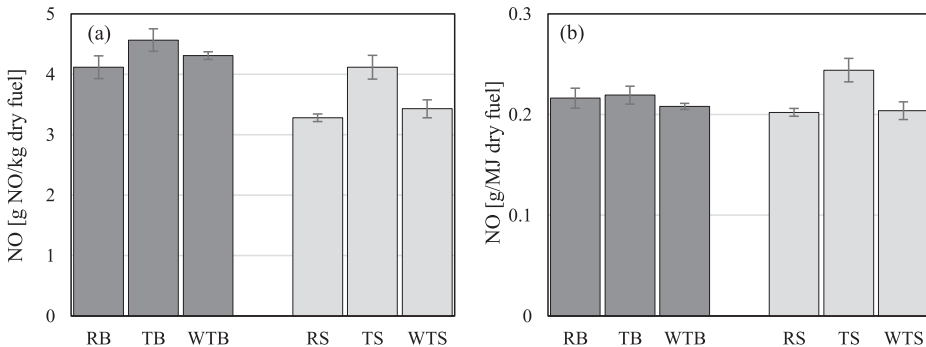


Fig. 5. NO emission based on fuel mass [g/kg] (a) and NO emission factors based on heating values of the fuel samples [g/MJ] (b) in 10% O₂ at 850 °C (RB = raw bark, TB = torrefied bark, WTB = washed & torrefied bark, RS = raw straw, TS = torrefied straw, WTS = washed & torrefied straw).

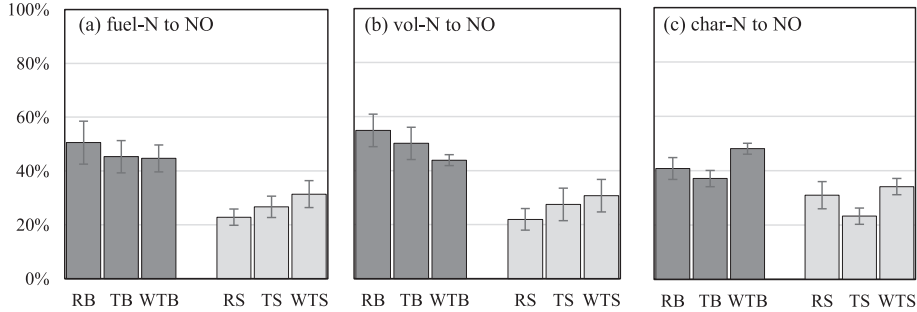


Fig. 6. Conversion of a) fuel-N to NO, b) vol-N to NO and c) char-N to NO in the combustion experiments at 850 °C (RB = raw bark, TB = torrefied bark, WTB = washed & torrefied bark, RS = raw straw, TS = torrefied straw, WTS = washed & torrefied straw).

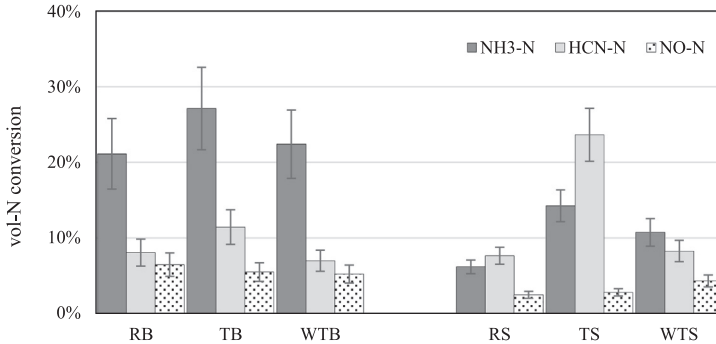


Fig. 7. Conversion of vol-N to NH₃, HCN and NO during devolatilization in pure N₂ at 850 °C (RB = raw bark, TB = torrefied bark, WTB = washed & torrefied bark, RS = raw straw, TS = torrefied straw, WTS = washed & torrefied straw).

and 11% respectively.

For RS, on the other hand, the conversion of vol-N to NH₃ is in general significantly lower as compared to RB, but the conversions of vol-N to HCN are similar in both cases. The conversion of vol-N to NH₃ was 6%, the conversion of vol-N to HCN was 8% and the conversion of vol-N to NO was 3%. The conversions of vol-N to NO are similar for the raw and the pre-treated straw. Also, the conversion of vol-N to HCN for WTS and RS are similar while the conversion of vol-N to NH₃ increased to 8% for WTS. For TS, a significant increase can be observed for the conversion to NH₃ and HCN. The conversion of vol-N to NH₃ and HCN are here 14% and 24% respectively.

The results emphasize that, in general, higher amounts of NO precursors are formed during devolatilization for the pre-treated samples as compared to the raw samples. The NO formation during devolatilization, on the other hand, is similar for raw and pre-treated samples. These results help to explain the NO trends discussed previously in Fig. 5 and Fig. 6. TB forms more NH₃ and HCN during devolatilization and it can also be seen that the NO formation from the corresponding combustion experiment is higher. For TS, the conversion of vol-N to NH₃ and HCN increased significantly and so did also the NO formation in the combustion experiment. The effect of pre-cursors is further illustrated in Fig. 8, which shows the NO formation during combustion as a function of the amount of precursors formed during the devolatilization experiments. In general, more NO is formed from the samples with a higher amount of formed precursors.

As discussed previously, the split of HCN and NH₃ influence formation of NO in oxidizing environments. Fig. 9a shows the molar HCN/

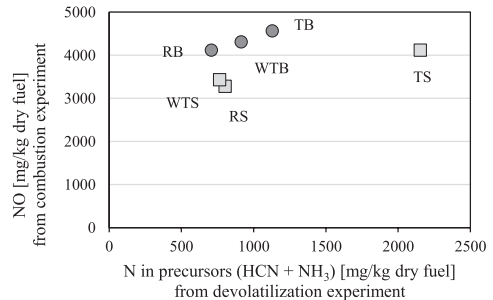


Fig. 8. Correlation between NO formation from combustion experiments in 10% O₂ and HCN and NH₃ from devolatilization experiments in pure N₂ (RB = raw bark, TB = torrefied bark, WTB = washed & torrefied bark, RS = raw straw, TS = torrefied straw, WTS = washed & torrefied straw).

NH₃ ratio for the various samples as a function of the fuel-N content, while in Fig. 9b the ratio is plotted against the molar H/N ratio in the fuel. These results are in line with results from an earlier study reporting that an increased fuel-N content and decreased H/N ratio resulted in a higher HCN/NH₃ ratio [7]. This can partly be explained by the formation mechanisms of HCN and NH₃. For instance, HCN can partly be converted to NH₃ when hydrogen is present. Hence, biomass pre-treatments have a significant influence on the HCN/NH₃ ratio when

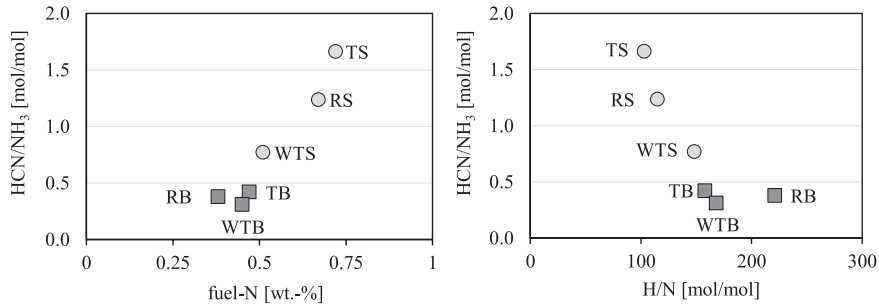


Fig. 9. Molar HCN/NH₃ ratio versus fuel-N (a) and molar H/N (b) (RB = raw bark, TB = torrefied bark, WTB = washed & torrefied bark, RS = raw straw, TS = torrefied straw, WTS = washed & torrefied straw).

the H/N ratio changes during the pre-treatment.

An additional explanation for the increased HCN/NH₃ ratios could be variations in the amount of the biomass components cellulose, hemicellulose and lignin. It has been shown, that lignin can lead to polymerization reactions during pyrolysis between cellulose, hemicellulose and proteins [33]. A plausible results from this is that heterocyclic nitrogen more likely forms HCN than NH₃. A recent study investigated effects of torrefaction on cellulose, hemicellulose and lignin at different temperatures [34]. It was shown, that large parts of the hemicellulose are removed, while most of the cellulose and lignin is left, thus lignin is enriched. This might lead to an increased polymerization and hence to increased HCN formation. This might also explain why the HCN/NH₃ ratio is so much higher in straw as compared to bark, since the lignin content of straw is significantly higher than the lignin content of bark [35,36].

As mentioned above, ash forming matter also may influence the formation of NH₃ and HCN. However, opposing effects of K and Ca have been reported. Fig. 10 shows the conversion of vol-N to HCN and NH₃ as functions of the calcium content (a) and the potassium content (b). Generally, the changes in HCN formation are rather small as compared to the changes in Ca and K contents, with TS as the only exception, and no obvious trend can be observed. For NH₃, on the other hand, the results imply that more NH₃ is formed in the samples with a higher calcium content and a lower potassium content.

4. Conclusions

The formation of NH₃, HCN and NO during devolatilization and

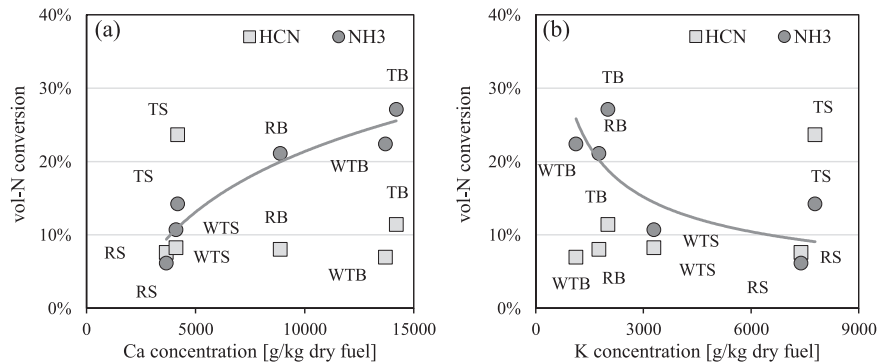


Fig. 10. Conversion of vol-N to HCN and NH₃ versus Ca (a) and K (b) concentration in the fuel samples (RB = raw bark, TB = torrefied bark, WTB = washed & torrefied bark, RS = raw straw, TS = torrefied straw, WTS = washed & torrefied straw).

combustion of raw, torrefied and washed and torrefied biomass fuels has been studied. The following conclusions can be drawn:

- The pre-treatments resulted in a higher conversion of vol-N to NH₃ and HCN as compared to the raw biomass fuels. The highest amounts of NH₃ and HCN were formed for torrefied straw.
- NO conversion was lower for pre-treated bark samples than raw bark, although the NO emission factor did not differ significantly.
- NO conversion was higher for pre-treated straw samples in comparison with raw straw. Torrefied straw had a significantly higher emission factor than raw straw.
- The contents of ash forming elements, the fuel-N content and the molar H/N ratio was significantly influenced by the pre-treatments. The results support the hypothesis that the HCN/NH₃ ratio increases with increasing N content and decreasing H/N ratio. In addition, the conversion of vol-N to NH₃ increased with decreasing K content and increasing Ca content.

CRediT authorship contribution statement

Daniel Schmid: Conceptualization, Methodology, Investigation, Writing - original draft. **Oskar Karlström:** Conceptualization, Writing - review & editing, Supervision, Funding acquisition. **Patrik Yrjas:** Writing - review & editing, Resources, Funding acquisition.

Declaration of Competing Interest

The authors declare that they have no known competing financial interests or personal relationships that could have appeared to influence the work reported in this paper.

Acknowledgements

This work has been done within the *Highly efficient biomass CHP plants by handling ash related problems* project within Horizon2020. Project acronym: Bioefficiency, EU grant agreement 727616. Furthermore, Dr Arno Janssen and Dr Pedro Abelha from TNO, the Netherlands, as well as Dr Tero Joronen from Valmet Technologies, Finland, are acknowledged for providing us with the pre-treated fuels.

This study was partly financed by the Academy of Finland financed project with no. 321598 Chemical challenges in gasification of biomass and waste.

References

- [1] EU. Conclusion of the European Council, 2030 climate and energy policy framework. October 2014, revised in 2018.
- [2] Pelkmans L. European Union – 2018 update Bioenergy policies and status of implementation; 2018. <https://www.ieabienergy.com/iea-publications/country-reports/2018-country-reports/>.
- [3] Glarborg P, Jensen A, Johnsson J. Fuel nitrogen conversion in solid fuel fired systems. *Prog Energy Combust Sci* 2003;29:89–113.
- [4] Mladenovic M, Dakic D, Nemoda S, Paprika M, Komatina M, Repic B, et al. The combustion of biomass – the impact of its types and technologies on the emission of nitrogen oxide. *Hemijiska Industrija* 2016;70:287–98.
- [5] Hansson K-M, Samuelson J, Tullin C, Åmand L-E. Formation of HNCO, HCN and NH₃ from the pyrolysis of bark and nitrogen-containing model compounds. *Combust Flame* 2004;137:265–77.
- [6] Giuntoli J, de Jong W, Verkooijen A, Pietrowska P, Zevenhoven M, Hupa M. Combustion characteristics of biomass residues and biowastes: fate of fuel nitrogen. *Energy Fuels* 2010;24:5309–19.
- [7] Anca-Couce A, Sommersacher P, Evic N, Mehrabian R, Scharler R. Experiments and modelling of NO_x precursor release (NH₃ and HCN) in fixed-bed biomass combustion conditions. *Fuel* 2018;529–37.
- [8] Becidan M, Skreiberg Ø, Hustad J. NO_x and N₂O precursors (NH₃ and HCN) in pyrolysis of biomass residues. *Energy Fuels* 2007;1173–80.
- [9] Leppälahti J. Formation of NH₃ and HCN in slow-heating-rate inert pyrolysis of peat, coal and bark. *Fuel* 1995;9:1363–8.
- [10] Liu H, Yi L, Hu H, Xu K, Zhang Q, Lu G, et al. Emission control of NO_x precursors during sewage sludge pyrolysis using an integrated pretreatment of Fenton peroxidation and CaO conditioning. *Fuel* 2017;195:208–16.
- [11] Hansson K-M, Åmand L-E, Habermann A, Winter F. Pyrolysis of poly-L-leucine under combustion-like conditions. *Fuel* 2003;82:653–60.
- [12] Ren Qiangqiang, Zhao Changsui. Evolution of fuel-N in gas phase during biomass pyrolysis. *Renew Sustain Energy Rev* 2015;50:408–18. <https://doi.org/10.1016/j.rser.2015.05.043>.
- [13] Chen Hanping, Si Yaohui, Chen Yingquan, Yang Haiping, Chen Deming, Chen Wei. NO_x precursors from biomass pyrolysis: distribution of amino acids in biomass and Tar-N during devolatilization using model compounds. *Fuel* 2017;187:367–75. <https://doi.org/10.1016/j.fuel.2016.09.075>.
- [14] Ren X, Zhao C. NO_x and N₂O precursors (NH₃ and HCN) from biomass pyrolysis: interaction between amino acid and mineral matter. *Appl Energy* 2013;21:170–4.
- [15] Zhou J, Gao P, Dong C, Yang Y. Effect of temperature and mineral matter on the formation of NO_x precursors during fast pyrolysis of 2,5-diketopiperazine. *Energies* 2018;6:29.
- [16] Yi L, Liu H, Lu G, Zhang Q, Wang J, Hiu H, et al. Effect of mixed Ca/Fa additives on nitrogen transformation during protein and amino acid pyrolysis. *Energy Fuels* 2017;31:9484–90.
- [17] Ren Q, Zhao C, Wu X, Liand C, Chen X, Shen J, et al. Effect of mineral matter on the formation of NO_x precursors during biomass pyrolysis. *J Anal Appl Pyroly* 2009;85:447–53.
- [18] Winter F, Wartha C, Hofbauer H. NO and N₂O formation during the combustion of wood, straw, male waste and peat. *Bioresour Technol* 1999;39–49.
- [19] Pereira F, Beer J, Gibbe B, Hedley A. NO_x emissions from fluidized-bed coal combustion. *Symp (Int) Combust* 1975;15:1149–56.
- [20] Karlström Oskar, Perander Magnus, DeMartini Nikolai, Brink Anders, Hupa Mikko. Role of ash on the NO formation during char oxidation of biomass. *Fuel* 2017;190:274–80. <https://doi.org/10.1016/j.fuel.2016.11.013>.
- [21] Ulusoy B, Wu H, Lin W, Karlström O, Li S, Song W, et al. Reactivity of sewage sludge, RDF and straw chars towards NO. *Fuel* 2019;236:297–305.
- [22] Chen Dengyu, Mei Jiaming, Li Haiping, Li Yiming, Lu Mengting, Ma Tingting, Ma Zhongqing. Combined pretreatment with torrefaction and washing using torrefaction liquid products to yield upgraded biomass and pyrolysis products. *Bioresour Technol* 2017;228:62–8. <https://doi.org/10.1016/j.biortech.2016.12.088>.
- [23] Davidsson K, Korsgren J, Pettersson J, Jäglid U. The effects of fuel washing techniques on alkali release from biomass. *Fuel* 2002;81:137–42.
- [24] Tan H, Wang S. Experimental study of the effect of acid-washing pretreatment on biomass pyrolysis. *J Fuel Chem. Techn.* 2009;37(6):668–72.
- [25] Batidzirai B, Mignot A, Schakel W, Junginger H, Faaij A. Biomass torrefaction technology: techno-economic status and future prospects. *Energy* 2013;62:196–214.
- [26] Rentizelas A, Li J. Techno-economic and carbon emission analysis of biomass torrefaction downstream in international bioenergy supply chains for co-firing. *Energy* 2016;114:129–42.
- [27] Uslu A, Faaij A, Bergman P. Pre-treatment technologies, and their effect on international bioenergy supply chains logistics. Techno-economic evaluation of torrefaction, pyrolysis and pelletisation. *Energy* 2008;33:1206–23.
- [28] Turn S, Kinoshita C, Ishimura D. Removal of inorganic constituents of biomass feedstocks by mechanical dewatering and leaching. *Biomass Bioenergy* 1997;12:241–52.
- [29] Jenkins B, Bakker R, Wei J. On the properties of washed straw. *Biomass Bioenergy* 1996;10:177–200.
- [30] Ren Xiaohan, Sun Rui, Meng Xiaoxiao, Vorobiev Nikita, Schiemann Martin, Leventis Yiannis A. Carbon, sulfur and nitrogen oxide emissions from combustion of pulverized raw and torrefied biomass. *Fuel* 2017;188:310–23. <https://doi.org/10.1016/j.fuel.2016.10.017>.
- [31] Karlström O, Wu H, Glarborg P. Influence of H₂O on NO formation during char oxidation of biomass. *Fuel* 2019;1260–5.
- [32] Karlström O, Hupa L. Conversion of biomass char: Oxidation rates in mixtures of O₂/CO₂/H₂O. *Energy* 2019;181:615–24.
- [33] Yuan S, Zhou Z, Li J, Chen X, Wang F. HCN and NH₃ released from biomass and soybean cake under rapid pyrolysis. *Energy Fuels* 2010;24:6166–71.
- [34] Chen D, Gao A, Cen K, Zhang J, Cao X, Ma Z. Investigation of biomass torrefaction on three major components: hemicellulose, cellulose and lignin. *Energy Convers Manage* 2018;169:228–37.
- [35] Kapoor M, Panwar D, Kaira G. Bioprocesses for enzyme production using agro-industrial wastes: technical challenges and commercialization potential. *Agro-Industrial Wastes as Feedstock for Enzyme Production*. Elsevier Inc.; 2016.
- [36] Räisänen T, Athanassiadis D. Basic chemical composition of the biomass components of pine, spruce and birch; 2013.

O. Karlström, D. Schmid, M. Hupa, A. Brink.
Role of CO₂ and H₂O on NO Formation during Biomass Char Oxidation.
Energ. Fuel 35(9) (2021), 7058-7064.



Role of CO₂ and H₂O on NO Formation during Biomass Char Oxidation

Oskar Karlström,* Daniel Schmid, Mikko Hupa, and Anders Brink



Cite This: *Energy Fuels* 2021, 35, 7058–7064



Read Online

ACCESS |

Metrics & More

Article Recommendations

ABSTRACT: We have investigated how CO₂ and H₂O influence NO release rates during char oxidation of biomass. In addition, the role of catalytic elements in these processes has been studied. NO release rates were determined from single-particle experiments of softwood and straw at 900 °C, in CO₂/O₂ (34/3%) and H₂O/O₂ (17/3%), with N₂ as the balance gas. The NO release profiles differed in CO₂/O₂ and H₂O/O₂. In CO₂/O₂, the NO release increased as the char conversion proceeded. On the other hand, in H₂O/O₂, the NO release decreased as the char conversion proceeded. In neither of these cases, the conversion rates of char-N to NO were proportional to the conversion rates of char-C. To investigate how the ash-forming matter influenced the NO release rates, the biomasses were demineralized and the experiments were repeated. For the chars of the demineralized biomasses, the NO release profiles were almost identical in CO₂/O₂ and H₂O/O₂. In addition, for the demineralized chars, the conversion rates of char-N to NO were proportional to the conversion rates of char-C. The conversions of char-N to NO were significantly higher for the demineralized chars. For softwood, the total conversion of char-N to NO was as high as 85%. These results show that (i) CO₂ and H₂O influence the formation of char-N to NO in different ways and (ii) the ash-forming matter contributes to the differences in the NO release rates.

1. INTRODUCTION

Combustion and gasification of biomass generate NO_x emissions. For biomass, most NO_x originates from fuel-bound nitrogen (fuel-N).¹ Certain biomasses, such as pine or birch wood, have low nitrogen contents, while, for example, algae or annual crops may have high nitrogen contents.² However, as a result of very strict NO_x legislations, even biomasses with low N contents may give rise to too high NO_x emissions, requiring expensive cleaning strategies, such as ammonia-based selective non-catalytic reduction (SNCR),^{3,4} selective catalytic reduction (SCR), or oxidation of NO to NO₂ using ozone or ClO₂, followed by absorption of NO₂.⁵ These expensive cleaning strategies are difficult to implement because of the complex NO_x chemistry. A better fundamental understanding on the fate of fuel N may improve the implementation of various NO_x cleaning strategies.

For biomasses, volatile N (vol N) accounts for typically 70–90% of fuel N, while char-N accounts for 10–30% of fuel N.⁶ For certain biomass-based fuels, such as black liquor, char-N may account for more than 50% of fuel N.⁷ Vol N is released as NH₃, HCN, HNCN, NO, N₂O, N₂, and tar N.^{8–10} The N species distribution depends upon a range of factors, such as the nitrogen content of the fuel, volatile matter, heating rate, final temperature, surrounding gas atmosphere, metals with catalytic effects, such as Ca and Mg, and how nitrogen is bound to the biomass.

Char-N reacts with O₂, forming mainly NO.^{1,8} In coal combustion, N₂O is also formed during the char oxidation stage.¹¹ For biomass, some N₂O is formed during the char oxidation stage, but reported concentrations of N₂O from biomass char combustion experiments are typically low

compared to concentrations of NO (e.g., ref 8), with some exceptions. Ulusoy et al.¹² showed recently that biomasses with high nitrogen contents form notable amounts of N₂O during the char oxidation stage.

The initial NO formed from char-N does not correspond to the release of NO from the char particle, because the initially formed NO can be reduced to N₂ within the pore system.^{13,14} Interestingly, the fractional conversion of char-N to NO increases with a decreasing particle size.^{15–17} This particle-size-dependent conversion of char-N to NO has been experimentally shown and also by means of single-particle modeling.^{13–17} The reduction potential of biomass char can be explained by the large internal surface area, the catalytic species in the ash-forming matter, such as K, and possibly also the char-N content.^{12,18}

In all solid fuel combustion and gasification systems, significant concentrations of CO₂ and H₂O exist in the gas. However, the influence of CO₂ and H₂O on NO formation is poorly understood. Park et al. suggested that coal char-N reacts with CO₂, forming NO, which reacts further to N₂.¹⁹ They showed experimentally that char-N reacts with H₂O, forming NH₃, HCN, and N₂. In a more recent study, it was suggested that char-N reacts with H₂O, forming HCN, which reacts

Special Issue: In Memory of Mario Costa

Received: October 16, 2020

Revised: November 12, 2020

Published: December 4, 2020

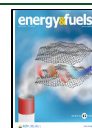


Table 1. Organic Element Analysis of Biomasses and Chars^a

| | N (wt % of dry biomass) | C (wt % of dry biomass) | H (wt % of dry biomass) | S (wt % of dry biomass) | O (wt % of dry biomass) | sum (wt % of dry biomass) | N (wt % of char) | C (wt % of char) | H (wt % of char) | char yield (%) |
|-------------|-------------------------|-------------------------|-------------------------|-------------------------|-------------------------|---------------------------|------------------|------------------|------------------|----------------|
| straw | 0.56 | 46.91 | 6.01 | 0.091 | 43.01 | 96.58 | 1.18 | 71.13 | 0.51 | 18 |
| AW straw | 0.50 | 47.45 | 5.99 | n.d. | 44.17 | 98.12 | 1.19 | 76.57 | 0.58 | 12 |
| softwood | 0.14 | 50.20 | 6.27 | 0.005 | 44.48 | 101.10 | 0.17 | 92.05 | 0.44 | 12 |
| AW softwood | 0.11 | 49.79 | 6.26 | n.d. | 44.94 | 101.09 | 0.15 | 86.44 | 0.53 | 8 |

^aAW = acid washed.**Table 2. ICP–OES Results of Ash-Forming Elements in Straw and Softwood^a**

| | Na (mg/kg of dry biomass) | Mg (mg/kg of dry biomass) | Al (mg/kg of dry biomass) | Si (mg/kg of dry biomass) | P (mg/kg of dry biomass) | K (mg/kg of dry biomass) | Ca (mg/kg of dry biomass) | Mn (mg/kg of dry biomass) | Fe (mg/kg of dry biomass) | Zn (mg/kg of dry biomass) |
|-------------|---------------------------|---------------------------|---------------------------|---------------------------|--------------------------|--------------------------|---------------------------|---------------------------|---------------------------|---------------------------|
| straw | 206 | 560 | 150 | 658 | 692 | 7792 | 925 | 18 | 163 | 7 |
| AW straw | 1 | 16 | 92 | 634 | 250 | 21 | 0 | 1 | 95 | 0 |
| softwood | 4 | 100 | 46 | 81 | 21 | 447 | 286 | 83 | 45 | 10 |
| AW softwood | 3 | 4 | 30 | 58 | 0 | 5 | 14 | 1 | 17 | 0 |

^aAW = acid washed.

further to NH₃.²⁰ Recently, it was suggested on the basis of density functional theory computations that NO is a primary reaction product in the reaction between char-N and CO₂.²¹ For spruce bark, it has been shown that H₂O reacts with char-N, forming NH₃.²² In many industrial combustion and gasification systems, CO₂ and H₂O concentrations can be adjusted, for example, via flue gas recirculation. Consequently, it is crucial to clarify how these gaseous compounds influence the fate of char-N. The influence of CO₂ on the NO formation from biomass chars in oxidative environments has not to the knowledge of the authors been investigated previously.

In this study, single biomass particles were oxidized in CO₂/O₂/N₂, H₂O/O₂/N₂, and O₂/N₂. NO release rates during the char oxidation stage of single biomass particles were determined. The objective is to clarify how CO₂ and H₂O influence the release of NO during char conversion in gases with O₂. To clarify how the ash-forming elements influence the NO formation chemistry, the biomasses were demineralized and the NO release rate experiments were repeated.

2. EXPERIMENTAL SECTION

2.1. Fuels. Two biomasses were investigated: softwood (Norwegian spruce) and straw. The samples were ground and sieved to a size fraction of 0.25–1 mm. The biomasses were also demineralized by washing with a dilute acid to leach off most of the ash-forming elements. These biomasses are hereafter referred to as demineralized or AW biomasses. Single-particle samples were prepared by pressing 200 mg of each biomass and demineralized biomass into cylindrical pellets (referred later to as single particles) with a diameter of 8 mm and a length of around 4 mm. The pellets were produced by pressing samples at 100 bar for 5 s. No binder was used. Char samples for analysis were prepared in the single-particle reactor from pellets of the fuels. These chars were produced at 900 °C in 100 vol % N₂ for 180 s.

The following procedure based on the study by Aho et al.²³ was used in preparing the samples. The pH was adjusted to 2 with HNO₃, and the mixture was stirred for 1 h at 60 °C. The biomass was then filtered and washed thoroughly with 4 × 200 mL of ion-exchange water and filtering after every 200 mL of washed water. The procedure was repeated, and the sample was finally dried at 105 °C. The metal content of the biomass and demineralized biomass samples (see Table 2) were analyzed by inductively coupled plasma optical emission spectroscopy (ICP–OES). As seen in Table 2, K, Ca, Mg,

and Mn were almost totally removed by the acid washing. The carbon, hydrogen, nitrogen, sulfur, and oxygen contents of the samples and chars (produced at 900 °C in N₂) were determined from three repetitions with a Thermo Scientific Flash 2000 organic element analyzer (Flash 2000) (see Table 1). It is possible that the acid washing influenced the internal structure of the resulting biomass chars, as pointed out by Ulusoy et al.¹² Aho et al.²³ showed that sugars were not removed by the same washing procedure for wood, indicating that the organics are not significantly affected. Possible effects of the washing on, for example, the internal surface area were not investigated here.²³

The contents of carbon and nitrogen in the chars (on the basis of initial fuel) are obtained by multiplying the carbon and nitrogen contents by the char yield. For both straw and softwood, the amount of carbon (on the basis of initial fuel) decreased as a result of acid washing. A plausible reason is that the ash-forming matter influenced the amount of carbon released during devolatilization.

2.2. Single-Particle Reactor. The char oxidation experiments were conducted using a single-particle reactor in CO₂/O₂/N₂ (34/3/63 vol %), H₂O/O₂/N₂ (17/3/80 vol %), and O₂/N₂ (3/97 vol %) at 900 °C. For simplicity, these gas mixtures are hereafter referred to as CO₂/O₂, H₂O/O₂, and O₂/N₂. The reason for not using the same CO₂ and H₂O concentrations is that the char reactivity toward H₂O is slightly higher than toward CO₂.²⁴ Figure 1 shows a schematic picture of the reactor. A detailed description of the reactor can be found elsewhere.^{25,26} The single-particle reactor consists of a quartz tube reactor, with an inner diameter of 44 mm, inserted in a ceramic furnace. Gas mixtures of synthetic air, nitrogen, CO₂, and steam were inserted in the bottom of the reactor system, and the product gases exited the reactor from the top of the reactor system. The total gas flow was 220 L/h at normal temperature and pressure (NTP). The gas flow of each gas is obtained by multiplying the concentration of a given gas by the total gas flow. A sample was inserted into the reactor using a movable probe that could be inserted from room temperature into the heated reactor within 1 s. The movable probe with the sample holder was horizontally inserted into the reactor. The sample holder consisted of a thin net on which a single fuel pellet was placed (illustration shown in Figure 1).

Concentrations of NO, CO₂, and CO in the outlet gases were continuously measured. NO was measured with a continuous chemiluminescence analyzer. Figure 2 shows an example of measured NO concentrations and the CO + CO₂ concentration from three repetitions of straw oxidized at 900 °C with 3 vol % O₂ (N₂ as balance gas). As seen, there are very small differences between repeated runs. From the mass flow rate and the measured concentrations, the NO

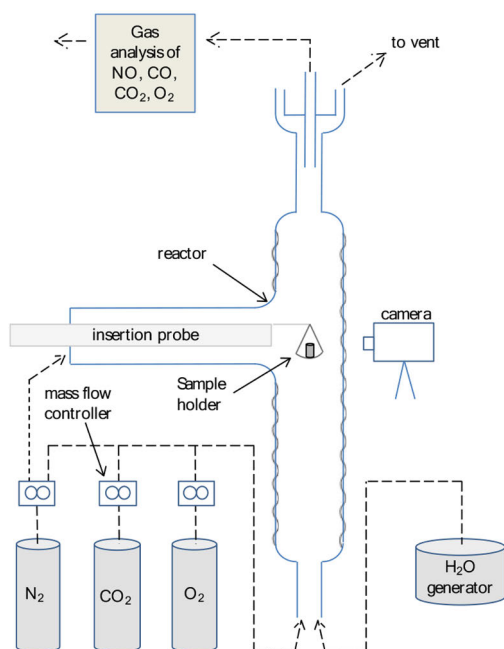


Figure 1. Åbo Akademi single-particle reactor.

release from the particle can be calculated. The NO release is proportional to the measured NO concentrations, and NO concentrations and NO release are used interchangeably hereafter. In this study, the NO release only during the char oxidation stage (marked in Figure 2) is considered. NH_3 and HCN are not measured during the char conversion stages in these experiments, because the nitrogen species are rapidly oxidized to NO (see, for example, ref 22). The starting time of the char conversion have been estimated from the CO analyzer. The residence time from the gases leaving the particle to the CO analyzer is around 3 s. The error margin of the devolatilization time (needed to determine the starting point of char conversion) is estimated to ± 3 s, i.e., around 1% of the total char conversion time.

It may be expected that devolatilization products form deposits (on reactor surfaces), which are oxidized during char conversion, and,

thus, influence the char oxidation results. Interrupted experiments (char sample removed after devolatilization) showed, however, that oxidation of potential devolatilization products on the reactor surface is not occurring.

3. RESULTS AND DISCUSSION

3.1. NO Release Rates in CO_2/O_2 , $\text{H}_2\text{O}/\text{O}_2$, and O_2/N_2 .

Figures 3 and 4 show NO release rates of char from straw and softwood in CO_2/O_2 , $\text{H}_2\text{O}/\text{O}_2$, and O_2/N_2 . In the figures, also the carbon conversion rate is given (as concentrations of CO and CO_2). Note that these curves are not based on averages but are taken from single runs. For the carbon conversion, the trends are similar for both straw and softwood: the carbon conversion rate decreases as a function of time for all conditions. On the other hand, the NO release profile in $\text{H}_2\text{O}/\text{O}_2$ differs from that in CO_2/O_2 for the raw biomasses.

In CO_2/O_2 and O_2/N_2 , the NO release is gradually increasing for the raw biomasses, culminating in a NO concentration peak just before the end of the char oxidation. Similar trends have been observed previously during char oxidation in O_2/N_2 of several biomasses and can be attributed to the fact that less and less of initially formed NO is reduced as the char oxidation proceeds.^{15–17} Thus, the increasing NO release profile can be explained by the change of the NO reduction rate.

While the NO release rate increases with time in CO_2/O_2 , the NO release rate decreases with time in $\text{H}_2\text{O}/\text{O}_2$. In addition, the NO release rates are initially significantly higher in $\text{H}_2\text{O}/\text{O}_2$ than in O_2/CO_2 and O_2/N_2 . These differences have to the knowledge of the authors not been observed previously. One explanation for the initially high NO release in $\text{H}_2\text{O}/\text{O}_2$ is that char-N is not initially forming NO in the reaction between char-N and H_2O but instead forming a NO_x precursor, such as NH_3 .²² A result from this is that the heterogeneous NO reduction step is eliminated: the NO_x precursor would be oxidized to NO in the boundary layer of the particle, and formed NO cannot be reduced by the char. As a result, the NO release rate is not increasing in $\text{H}_2\text{O}/\text{O}_2$ as in CO_2/O_2 . With the assumption that the initial conversion of char-N to NH_3 is proportional to the conversion of char-C, it may be expected that the NO release decreases as a function of conversion (as seen in Figures 3 and 4 for raw fuel chars in $\text{O}_2/\text{H}_2\text{O}$).

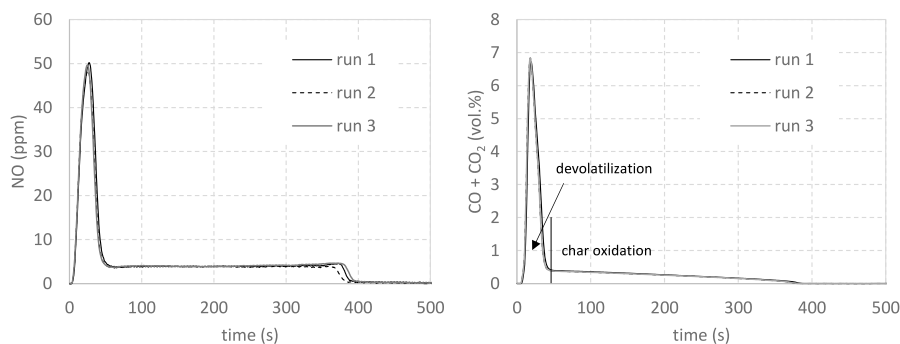


Figure 2. Three repetitions of (A) NO release and (B) CO + CO_2 release from combustion of a single 8 mm biomass (softwood) particle at 900 °C in O_2/N_2 .

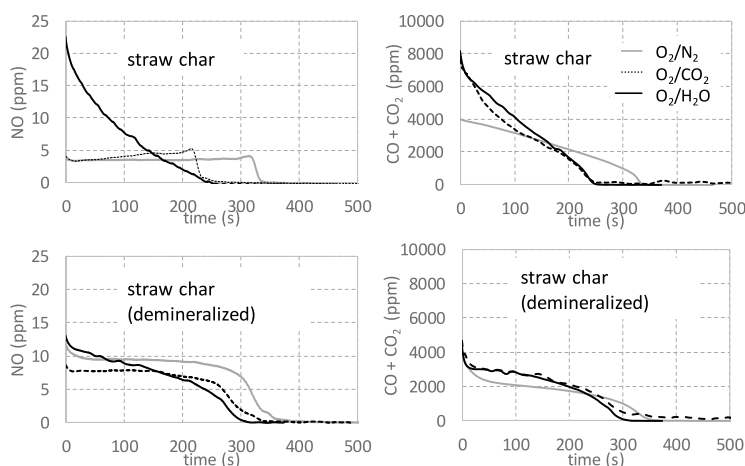


Figure 3. NO release during char oxidation of a single particle in O_2/N_2 , O_2/CO_2 , and O_2/H_2O at $900\text{ }^\circ\text{C}$ for straw and demineralized straw.

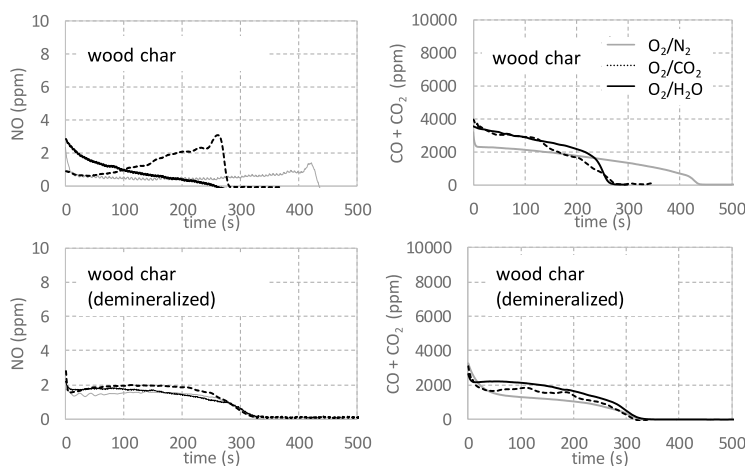


Figure 4. NO release during char oxidation of a single particle in O_2/N_2 , O_2/CO_2 , and O_2/H_2O at $900\text{ }^\circ\text{C}$ for softwood and demineralized softwood.

It should be noted the total char conversion times are significantly shorter when CO_2 or H_2O is present in the gas. The increased carbon conversion rates as a result of H_2O and CO_2 can be explained by the presence of catalytic elements, i.e., K and Ca (see Table 2).²⁷ In addition, the figures show that an addition of 17% H_2O versus 34% CO_2 has similar effects on reducing char conversion times. This can be explained by the fact that the char is more reactive toward H_2O than toward CO_2 .²⁴ The influence of CO_2 and H_2O on the mass loss of carbon has been investigated in numerous other publications (e.g., ref 26) and will not be discussed further here.

3.2. Role of Demineralization on NO Release Rates.

Figures 3 and 4 also show the NO release rates during the char conversion of the demineralized biomasses. The difference in the NO release behavior in CO_2/O_2 and H_2O/O_2 , which could be observed for the raw biomasses, cannot be seen for the

demineralized biomasses. In fact, for all investigated atmospheres, the NO release rates are similar for the demineralized biomass chars. A possible reason for the similarities is that CO_2 and H_2O are inactive because most of the catalytic elements have been removed. It is well-known that char-C of demineralized biomass, i.e., without catalytic elements, has a low reactivity toward CO_2 and H_2O (e.g., refs 23, 27, and 28). The results support this as, for the demineralized biomasses, the char gasification times being almost the same in CO_2/O_2 , H_2O/O_2 , and O_2/N_2 . It should be noted that the total char conversion times for raw versus demineralized fuels cannot be directly compared because both the char yields and the carbon contents differ slightly. The similar NO release rates of the demineralized biomass chars imply that also char-N of the demineralized biomass chars have a low reactivity toward CO_2 and H_2O .

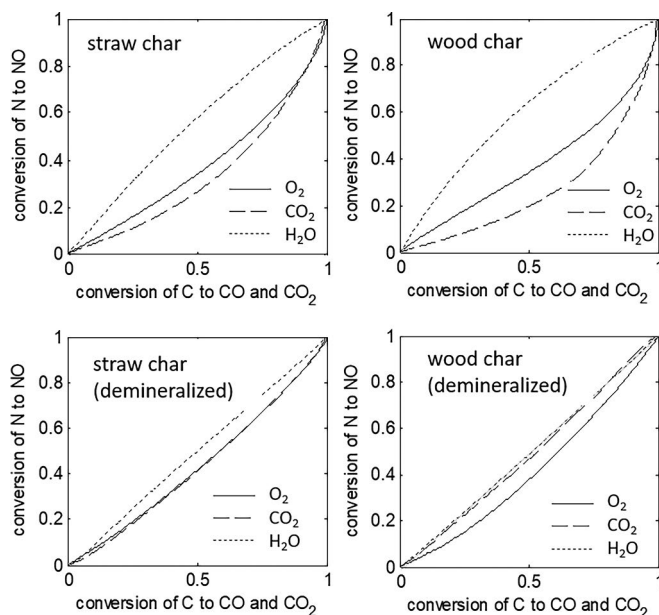


Figure 5. Cumulative conversion of char-N to NO versus char-C to CO and CO₂ for straw, wood, demineralized straw and demineralized wood in O₂/CO₂, O₂/H₂O, and O₂/N₂.

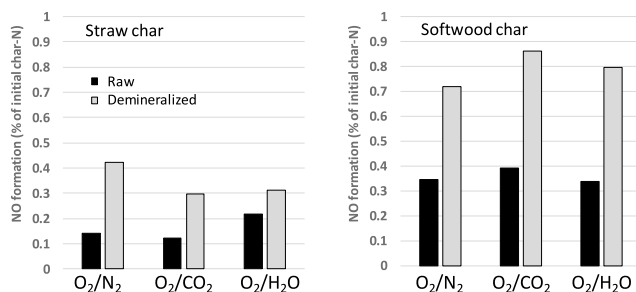


Figure 6. Total conversion of char-N to NO during oxidation in O₂/N₂, O₂/CO₂, and O₂/H₂O at 900 °C for straw and softwood.

3.3. Conversion of Char-N to NO versus Char-C to CO and CO₂. Figure 5 shows the nitrogen conversion (N to NO) versus the carbon conversion for the raw and demineralized biomass chars. As expected, on the basis of Figures 3 and 4, the conversion rate of N to NO is almost proportional to the conversion rate of C for the demineralized chars. On the contrary, the conversion rate of N to NO is not proportional to the conversion rate of char-C for the raw biomass chars. On the basis of this, (i) it cannot be expected that the release of NO is proportional to the conversion rate of carbon, which is a frequent modeling assumption,²⁹ and (ii) the correlation between NO release and carbon conversion is strongly dependent upon both the gas atmosphere and ash-forming elements.

3.4. Total Conversion of Char-N to NO. Figure 6 plots the total conversion of char-N to NO. The total conversions of char-N to NO are, for straw, 0.15, 0.12, and 0.23 and, for softwood, 0.35, 0.39, and 0.31 in O₂/N₂, CO₂/O₂, and H₂O/O₂

O₂, respectively. The conversions of char-N to NO are thus significantly higher for softwood than for straw. There are several possible explanations for this difference, such as the fact that the reduction of initially formed NO to N₂ may be more significant for straw than for softwood as a result of differences in the ash-forming matter and internal surface area (see, e.g., ref 12).

For the demineralized straw and softwood, the char-N values are 0.42, 0.30, and 0.31 and 0.73, 0.86, and 0.80 in O₂/N₂, CO₂/O₂, and H₂O/O₂. Thus, the conversions of char-N to NO were significantly higher for the demineralized chars. The conversion of char-N to NO has been found to be lower, in general, than 50% in environments of O₂/N₂.⁸ The char-N to NO conversion of 86% is the highest reported for biomass, to the knowledge of the authors.

4. CONCLUSION

The NO release during char oxidation of biomass differed in CO₂/O₂ and H₂O/O₂. In CO₂/O₂, the NO release rate increased as the char conversion proceeded, while in H₂O/O₂, the NO release rate decreased as the char conversion proceeded.

After demineralization, the NO release profiles were, on the other hand, similar in CO₂/O₂ and H₂O/O₂. The conversions of char-N to NO were significantly higher for the demineralized chars. For softwood, the total conversion of char-N to NO was as high as 86%.

These results show that CO₂ and H₂O influenced the formation of char-N to NO differently. A plausible explanation for the initially high NO release rates in H₂O/O₂ is that H₂O reacts with char-N, forming a NO_x precursor, such as NH₃, which reacts further to NO. The influence of CO₂ and H₂O on the release of NO can be partly explained by the ash-forming matter.

■ AUTHOR INFORMATION

Corresponding Author

Oskar Karlström – Johan Gadolin Process Chemistry Centre, Åbo Akademi University, 20500 Turku, Finland;
● orcid.org/0000-0002-3133-5677; Email: okarlstr@abo.fi

Authors

Daniel Schmid – Johan Gadolin Process Chemistry Centre, Åbo Akademi University, 20500 Turku, Finland
Mikko Hupa – Johan Gadolin Process Chemistry Centre, Åbo Akademi University, 20500 Turku, Finland
Anders Brink – Johan Gadolin Process Chemistry Centre and Process and System Engineering, Åbo Akademi University, 20500 Turku, Finland

Complete contact information is available at:
<https://pubs.acs.org/10.1021/acs.energyfuels.0c03471>

Notes

The authors declare no competing financial interest.

■ ACKNOWLEDGMENTS

This study was financed by the Academy of Finland (Project 321598, Chemical Challenges in Gasification of Biomass and Waste).

■ REFERENCES

- (1) Glarborg, P.; Jensen, A.; Johnsson, J. E. Fuel nitrogen conversion in solid fuel fired systems. *Prog. Energy Combust. Sci.* **2003**, *29*, 89–113.
- (2) Hupa, M.; Karlström, O.; Vainio, E. Biomass combustion technology development—It is all about chemical details. *Proc. Combust. Inst.* **2017**, *36*, 113–134.
- (3) Leckner, B.; Karlsson, M.; Dam-Johansen, K.; Weinell, C. E.; Kilpinen, P.; Hupa, M. Influence of Additives on Selective Noncatalytic Reduction of NO with NH₃ in Circulating Fluidized Bed Boilers. *Ind. Eng. Chem. Res.* **1991**, *30*, 2396–2404.
- (4) Arand, J. K.; Muzio, L. J.; Sotter, J. G. Urea reduction of NO_x in combustion effluents. U.S. Patent 4,208,386 A, June 17, 1980.
- (5) Senjo, T.; Kobayashi, M. Process for removing nitrogen oxides from gas. U.S. Patent 3,957,949 A, May 18, 1976.
- (6) Konttinen, J.; Kallio, S.; Hupa, M.; Winter, F. NO formation tendency characterization for solid fuels in fluidized beds. *Fuel* **2013**, *108*, 238–246.

(7) Vähä-Savo, N. Behavior of black liquor nitrogen in combustion: Formation of cyanate. Doctoral Thesis, Åbo Akademi University, Turku, Finland, 2014.

(8) Winter, F.; Wartha, C.; Hofbauer, H. NO and N₂O formation during combustion of wood straw, malt waste and peat. *Bioresour. Technol.* **1999**, *70*, 39–49.

(9) Yu, Q. Z.; Brage, C.; Chen, K.; Sjöström, K. The fate of fuel-nitrogen during gasification of biomass in a pressurized fluidized bed gasifier. *Fuel* **2007**, *86*, 611–618.

(10) Ren, Q.; Zhao, C. NO_x and N₂O precursors (NH₃ and HCN) from biomass pyrolysis: Interactions between amino acid and mineral matter. *Appl. Energy* **2013**, *112*, 170–174.

(11) Goel, S.; Zhang, B.; Sarofim, A. NO and N₂O formation during char combustion: Is it HCN or surface attached nitrogen? *Combust. Flame* **1996**, *104*, 213–217.

(12) Ulusoy, B.; Lin, W.; Karlström, O.; Li, S.; Song, W.; Glarborg, P.; Dam-Johansen, K.; Wu, H. Formation of NO and N₂O during Raw and Demineralized Biomass Char Combustion. *Energy Fuels* **2019**, *33*, 5304–5315.

(13) Song, Y. H.; Beer, J. M.; Sarofim, A. F. Oxidation and devolatilization of nitrogen in coal char. *Combust. Sci. Technol.* **1982**, *28*, 177–183.

(14) De Soete, G. G. Heterogenous N₂O and NO formation from bound nitrogen atoms during coal char combustion. *Symp. (Int.) Combust., [Proc.]* **1991**, *23*, 1257–1264.

(15) Saastamoinen, J. J.; Taipale, R. NO_x formation in grate combustion of wood. *Clean Air* **2003**, *4*, 239–268.

(16) Karlström, O.; Brink, A.; Hupa, M. Biomass char nitrogen oxidation—Single particle model. *Energy Fuels* **2013**, *27*, 1410–1418.

(17) Karlström, O.; Brink, A.; Hupa, M. Time dependent production of NO from combustion of large biomass char particles. *Fuel* **2013**, *103*, 524–532.

(18) Karlström, O.; Perander, M.; DeMartini, N.; Brink, A.; Hupa, M. Role of ash on the NO formation during char oxidation of biomass. *Fuel* **2017**, *190* (15), 274–280.

(19) Park, D. C.; Day, S.; Nelson, P. F. Nitrogen release during reaction of coal char with O₂, CO₂ and H₂O. *Proc. Combust. Inst.* **2005**, *30*, 2169–2175.

(20) Park, D.-C.; Day, S. J.; Nelson, P. F. Formation of N-containing gas-phase species from char gasification in steam. *Fuel* **2008**, *87*, 807–814.

(21) Zhao, S.; Sun, R.; Bi, X.; Pan, X.; Su, Y. Density functional theory study of the heterogenous interaction between char-bound nitrogen and CO₂ during oxy-fuel coal combustion. *Combust. Flame* **2020**, *216*, 136–145.

(22) Karlström, O.; Wu, H.; Glarborg, P. Influence of H₂O on NO formation during char oxidation of biomass. *Fuel* **2019**, *235*, 1260–1265.

(23) Aho, A.; DeMartini, N.; Pranovich, A.; Krogell, J.; Kumar, N.; Eränen, K.; Holmbom, B.; Salmi, T.; Hupa, M.; Murzin, D. Y. Pyrolysis of pine and gasification of pine chars—Influence of organically bound metals. *Bioresour. Technol.* **2013**, *128*, 22–29.

(24) Di Blasi, C. Combustion and Gasification Rates of Lignocellulosic Chars. *Prog. Energy Combust. Sci.* **2009**, *35*, 121–140.

(25) Giuntoli, J.; de Jong, W.; Verkooijen, A. H. M.; Piotrowska, P.; Zevenhoven, M.; Hupa, M. Combustion characteristics of biomass residues and biowastes: Fate of fuel nitrogen. *Energy Fuels* **2010**, *24*, 5309–5319.

(26) Karlström, O.; Hupa, L. Energy conversion of biomass char: Oxidation rates in mixtures of O₂/CO₂/H₂O. *Energy* **2019**, *181*, 615–624.

(27) Kannan, M. P.; Richards, G. N. Gasification of biomass chars in carbon dioxide: Dependence of gasification rate on the indigenous metal content. *Fuel* **1990**, *69* (6), 747–753.

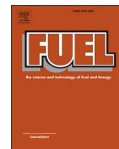
(28) Perander, M.; DeMartini, N.; Brink, A.; Krumb, J.; Karlström, O.; Hemming, J.; Moilanen, A.; Konttinen, J.; Hupa, M. Catalytic effect of Ca and K on CO₂ gasification of spruce wood char. *Fuel* **2015**, *150* (15), 464–472.

(29) Jones, J. M.; Patterson, P. M.; Pourkashanian, M.; Williams, A. Approaches to modelling heterogeneous char NO formation/destruction during pulverized coal combustion. *Carbon* **1999**, *37*, 1545–1552.

D. Schmid, W. Weng, S. Li, O. Karlström, M. Hupa, Z. Li, P. Glarborg, P. Marshall,
M. Aldén.

**Optical in-situ measurements and modeling of post-flame sulfation of NaOH(g)
and NaCl(g).**

Fuel 332(2) (2023), 126337.



Full Length Article

Optical in-situ measurements and modeling of post-flame sulfation of NaOH (g) and NaCl(g)

Daniel Schmid^{a,*}, Wubin Weng^b, Shen Li^b, Oskar Karlström^{a,c}, Mikko Hupa^a, Zhongshan Li^b, Peter Glarborg^d, Paul Marshall^e, Marcus Aldén^b^a Group of Inorganic Chemistry, Johan Gadolin Process Chemistry Centre, Åbo Akademi University, Henrikinkatu 2, 20500 Turku, Finland^b Division of Combustion Physics, Lund University, P.O. BOX 118, SE-221 00 Lund, Sweden^c Industrial Engineering and Management, Department of Mechanical and Materials Engineering, University of Turku, Finland^d Department of Chemical Engineering, Technical University of Denmark, Kgs. Lyngby DK-2800, Denmark^e Department of Chemistry and Center for Advanced Scientific Computing and Modeling, University of North Texas, Denton, TX 76203-5070, USA

ARTICLE INFO

Keywords:

Sodium sulfation

Alkali sulfation

UV absorption spectroscopy

Chemical kinetic modeling

ABSTRACT

Post-flame sulfation of gaseous sodium hydroxide (NaOH) and sodium chloride (NaCl) was investigated with optical in situ measurements at 850 to 1475 °C. A multi-jet burner was used to generate well-controlled combustion environments. The multi-jet burner also enabled the separate feeding of the sodium species and SO₂ to the combustion environment where the sulfation reactions occurred. Concentrations of NaOH(g) and NaCl(g) were measured in the product gas using broadband UV absorption spectroscopy to follow the degree of sulfation. At 1475 and 1275 °C almost no sulfation occurred with an initial NaOH(g) concentration of 20 ppm and SO₂ concentrations between 0 and 150 ppm. At 985 °C, the NaOH(g) concentration decreased to less than 5 ppm with SO₂ concentrations above 50 ppm and at 850 °C almost all NaOH(g) was sulfated under these conditions. The experimental results for the gas-phase sulfation of NaOH were compared to previous results for the sulfation of KOH under the same conditions and the results were shown to be similar for NaOH and KOH under these conditions. Sulfation of NaOH(g) generally occurred to a more significant extent than the sulfation of NaCl(g). At 1115 to 1475 °C, no sulfation of NaCl(g) was observed. At the lowest investigated temperature, 850 °C, the NaCl (g) concentration decreased from 20 ppm to 12 ppm after the addition of 150 ppm SO₂. Chemical equilibrium calculations and kinetic modeling using an updated kinetic model for the detailed Na-Cl-S chemistry were compared to the experimental results. Above 1100 °C, the system can be described by chemical equilibrium, implying that equilibrium is reached in less than 100 ms. At temperatures below 1100 °C, the measured concentration indicated kinetic control. Under these conditions, the kinetic model was in good agreement with the experimental results for NaOH(g) but over-predicted the sulfation of NaCl(g). The combined experimental data, chemical equilibrium calculations and kinetic modeling of the present study support that sulfation of alkali species can occur in the gas phase through homogeneous reactions.

1. Introduction

High-temperature chemistry of alkali species is of interest due to its importance in aerosol formation, deposition, and corrosion in combustion and gasification of challenging fuels such as solid biomass, a range of various waste side streams and black liquor [1–4]. This range of fuels often contain high amounts of alkali, sulfur and chlorine, which can be released as alkali chloride, alkali hydroxides, hydrogen chloride (HCl) and sulfur dioxide (SO₂) [5–8]. Alkali compounds, such as alkali

chlorides, contribute to slagging, fouling and corrosion [9,10,11]. Both sodium chloride (NaCl) and potassium chloride (KCl) are highly corrosive towards conventional heat exchanger materials [12]. Corrosion on metal surfaces can be minimized and even eliminated when the alkali compounds are converted to alkali sulfates due to their higher melting points. The sulfation reactions can occur with SO₂ released from the fuel. If the sulfur content in the fuel is low, however, additional sulfur-containing compounds can be added to increase the degree of sulfation. One possibility is the addition of elemental sulfur, which is then

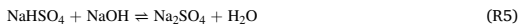
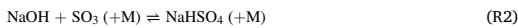
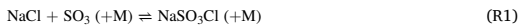
* Corresponding author.

E-mail address: dschmid@abo.fi (D. Schmid).

oxidized to SO₂ in thermal conversion [13], or the co-combustion with sulfur-rich fuels like peat [14]. Another possibility is the introduction of sulfates, e.g. ammonium or ferric sulfate, which will decompose to SO₃, which has been shown to be more efficient for sulfation reactions with alkali as compared to SO₂ [15–17].

The formation of alkali sulfates is believed to occur both in the gas phase and in the condensed phase, dependent on the temperature [18–20]. Sulfation in the gas phase may be expected to occur at faster rates than in the solid and liquid phases [18]. Glarborg and Marshall [21] proposed a detailed kinetic mechanism for the formation of gaseous alkali sulfates, including reactions between gaseous alkali chlorides and hydroxides with sulfur oxides. Predictions based on this mechanism for the sulfation of KCl were in good agreement with experimental results from an entrained flow reactor of Iisa et al. at 900–1100 °C [18]. Results of that study suggest that most of the potassium sulfation at temperatures above 900 °C occurs in the gas phase.

In the sulfation of KCl, SO₃ plays a key role [18]. Jiménez and Ballesler emphasized that the kinetics of the oxidation of SO₂ to SO₃ has been the main obstacle for the complete description of sulfate formation [22]. SO₃ initiates sulfation of alkali species [21]:



Hindiyarti et al. [1] suggested that the rate of SO₂ oxidation to SO₃ may be too slow at lower temperatures and presented alternative sulfation pathways. Accordingly, sulfation can be initiated by a direct reaction between NaOH and SO₂, forming a sulfite species (R6) which can then be oxidized to bisulfate (R7), with the oxidation of the sulfite as the rate-limiting step.



Various studies have investigated the details of the K-Cl-S chemistry, both with experimental work and modeling in laboratory and larger scale [23–25]. Weng et al. developed an experimental measurement system to study gas-phase sulfation and homogeneous nucleation of alkali compounds, based on a novel multi-jet burner being able to provide well-controlled conditions, using optical in situ measurements to quantify relevant species [26–28]. Sulfation experiments were performed feeding K₂CO₃ or KCl together with SO₂ to a hot and stable gas environment. Key species such as KOH, KCl and K atoms were quantified in the gas phase to determine their formation and consumption, and the sulfation was indirectly determined based on measured concentrations of KOH and KCl. The experimentally determined concentrations were compared to predictions by a detailed K-Cl-S mechanism based mostly on the work by Glarborg and Marshall [21]. The model predictions were in satisfactory agreement with the experimental results.

Previous work on gas-phase sulfation of alkali salts have largely focused on potassium, which is the dominating alkali element in most biomass fuels. Besides high potassium contents, many biomasses and wastes (and also some coals [29]) have high sodium contents, e.g. algae and black liquor (one of the most used biomass based fuels) have high sodium contents.

The objective of the present work is to clarify the homogeneous Na-Cl-S chemistry in the gas phase at high temperatures between 850 and 1475 °C. This temperature range is relevant for most combustion processes, ranging from grate fired combustion and fluidized bed combustion to pf combustion. The sulfation of NaOH and NaCl was investigated experimentally in a multi-jet burner, and the consumption of NaOH and

NaCl in the gas phase by reaction with SO₂ was determined using UV absorption spectroscopy. The sulfation reactions of sodium species have not been investigated previously under such conditions. A new updated kinetic Na-S-Cl model is also tested under the investigated conditions. The model is based on the work of Glarborg and Marshall [21], but updated in the present work with novel thermodynamic data and added reaction pathways. In addition, chemical equilibrium calculations are performed to evaluate whether the set-up operates at non-equilibrium conditions.

2. Experimental

A multi-jet burner (see Fig. 1) was used to create well-controlled high temperature conditions for the sodium sulfation experiments. A more detailed description of the reactor setup can be found elsewhere [31]. The multi-jet burner consists of 181 jet tubes through which a gas mixture of methane, oxygen and air was fed. Above each jet, a laminar conical flame is formed. A co-flow is introduced through a perforated mask and several layers of glass beads with a diameter of 1 mm, which is evenly mixed with the hot gas products from the jet tubes, creating a fairly homogeneous hot flue gas environment above the burner outlet for a given temperature and oxygen concentration, depending on the composition of the used gas mixtures. The burner outlet is 29 mm above the front of the jet tubes. The burner walls are insulated to minimize heat loss.

Table 1 lists the compositions of the used gas mixtures and temperatures and concentrations in the zone above the burner where the optical measurements took place. The temperature was measured using two-line atomic fluorescence (TLAF) thermometry using indium atoms, with a reported accuracy of ~ 2.7 % [32]. Additional measurements were obtained with a B-type thermocouple (OMEGA) with a wire diameter of 0.25 mm [26], corrected for radiation loss based on a model reported by Weng et al. [31]. The emissivity of the thermocouple was adjusted so that the thermocouple gave the same temperature at 40 mm height as the temperature from the TLAF measurement. The temperature was measured in the hot flue gas without NaOH, NaCl or SO₂ seeding to avoid any particle deposition effect and to minimize catalytic effects of the thermocouple. The temperature profiles along the vertical axis and adiabatic flame temperatures can be found in the supplementary material.

For the experiments with NaCl and NaOH, respectively, 1.0 M NaCl or 0.5 M Na₂CO₃ solutions were fed to the jet chamber. The Na₂CO₃ was rapidly converted to NaOH by reaction with H₂O when the temperature increased. An ultrasonic fog generator was placed in the flask with the Na-containing solution, and the fog was then transported to the jet chamber via an air flow of 0.5 Nl/min. In the jet chamber, the Na-containing fog was mixed with the methane/air/oxygen mixture and fed to the jet outlet, where NaOH(g) or NaCl(g) was formed after passing the flame. To prevent SO₂ and sodium reacting already in the jet chamber, SO₂(g) was fed to the burner via the co-flow and the sulfation reaction was limited by the mixing rate. For each experiment, the NaOH or NaCl concentration in the hot flue gas was measured by the below described UV absorption spectroscopy, before, while and after SO₂ has been added. This was to ensure that the volume fraction of NaOH or NaCl transported into the flame is the same as set. Since the seeding of SO₂ was conducted only for a short time period, the seeding fluctuation should be small when the NaOH or NaCl was the same for the measurement before and after the SO₂ addition.

NaOH(g) and NaCl(g) were quantified 5 mm above the burner outlet (about 4 cm downstream of the small jet flames) using broadband UV absorption spectroscopy (see Fig. 1c). At this stage the gases were fully mixed and the gaseous NaOH and NaCl were distributed evenly, hence it is reliable to use the line-of sight measurement for the quantification of NaOH and NaCl concentrations in the flame. The distribution has been investigated previously [33]. The UV beam had a diameter of 10 mm and was generated by a deuterium lamp (L1313, Hamamatsu). The beam

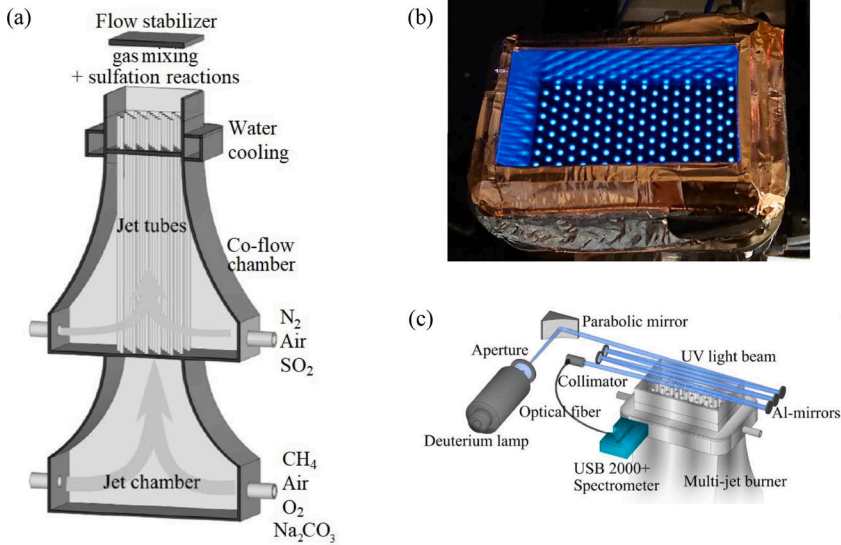


Fig. 1. Schematic picture of the Multi-Jet Burner at Lund University (a) (reproduction from [28]), top view on pre-mixed flames on the outlets of the jet tubes (b) and setup for broadband UV absorption spectroscopy system (c) (reproduction from [30]).

Table 1

Gas-flow composition and gas product temperature 5 mm above the burner outlet; temperature and gas concentration refer to the zone where the sulfation experiments take place.

| Temp. [°C] | Fuel-oxygen ratio ϕ | Gas flow rate [NL/min] | | | | | | | | | |
|------------|--------------------------|------------------------|-------|----------------|----------------|----------------|-----------------|------------------|----------------|----|--|
| | | Jet-flow | | | | | Co-flow | | | | |
| | | CH ₄ | Air | O ₂ | N ₂ | Air | Gas conc. [%] | | | | |
| | | | | | | O ₂ | CO ₂ | H ₂ O | N ₂ | | |
| 1475 | 0.74 | 2.66 | 17.34 | 1.89 | 10.83 | 7.74 | 4.5 | 6.5 | 13.2 | 75 | |
| 1275 | 0.70 | 2.47 | 12.23 | 2.58 | 18.97 | 8.90 | 4.6 | 5.4 | 11.0 | 79 | |
| 1115 | 0.67 | 2.38 | 11.89 | 2.26 | 22.69 | 9.83 | 4.6 | 4.6 | 9.4 | 81 | |
| 985 | 0.63 | 2.09 | 10.90 | 2.07 | 26.50 | 10.66 | 5.2 | 3.9 | 7.9 | 83 | |
| 850 | 0.60 | 1.71 | 8.91 | 1.69 | 26.92 | 10.25 | 4.6 | 3.4 | 6.9 | 85 | |

was passed five times through the hot flue gas by five UV-enhanced aluminium mirrors to achieve a high sensitivity with a long optical path length. The light was then collected and analyzed with a spectrometer (USB 2000+, Ocean Optics). 200 scans were performed for each experiment with an integration time of 2 ms and each experiment was repeated 20 times.

The concentrations of NaOH (g) and NaCl (g) were determined using the Beer-Lambert law.

$$\text{Absorbance}(\lambda) = N_A \sigma_A(\lambda) L = -\ln\left(\frac{I_s(\lambda)}{I_0(\lambda)}\right) \quad (1)$$

where λ is the wavelength; $I_s(\lambda)$ and $I_0(\lambda)$ are the intensities of the UV light after the hot flue gas and the UV light source, respectively, at a given wavelength; N_A is the number density of the gas species; $\sigma_A(\lambda)$ is the absorption cross section at a given wavelength and L is the optical path length.

The cross-section data used in the present study is based on previous work from Weng et al. [27,34] The absorption cross sections for NaOH and NaCl were determined between 1125 and 1575 °C [27]. The temperature dependence of the absorption cross section in this temperature range is weak and, thus, it is reasonable to also use the same absorption cross section for 850 and 985 °C. Almost the same concentrations for

NaOH or NaCl were measured at different temperatures with the same feeding rate of alkali, which supports that the value for the absorption cross sections measured at 1125–1575 °C can be used for the investigated temperature range in the present study. For NaOH, the absorption peaks occur at 230 and 320 nm with $\sigma_{230} = 1.67 \cdot 10^{-17} \text{ cm}^2/\text{molecule}$ and $\sigma_{320} = 1.29 \cdot 10^{-17} \text{ cm}^2/\text{molecule}$.

According to the Beer-Lambert law, the uncertainty of the measurement originated from the uncertainty of the cross section data, optical path length and the measurement of the absorbance. The uncertainty of the cross-section data is about $\pm 5\%$ [34]. The optical path length was estimated based on previous visualization of KOH distribution [33], adding an additional uncertainty of $\pm 10\%$ due to uneven distribution at the edge of the flue gas. The uncertainty from the absorbance measurement is small compared to the uncertainties for the cross section and optical path length and is hence neglected for the overall uncertainty. The reaction influence by the UV radiation is negligible as well. Since the UV light beam had a diameter of about 10 mm and the hot flue gas was flowing at a speed of around 1 m/s, the molecules and radicals only experiences 10 ms radiation from the UV light, and the UV light only had an irradiance below $0.1 \mu\text{W cm}^{-2} \cdot \text{nm}^{-1}$. It was estimated that only about 0.001 % of the NaOH molecules were excited by the UV light in the experiment. Summing up,

the uncertainty of the measurement was estimated to be $\pm 15\%$.

Fig. 2a shows the absorption spectrum of NaOH and Fig. 2b shows the overlapping absorption spectrum of NaCl and NaOH present in the NaCl seeded flame at 1275 °C with the addition of 20 ppm SO₂. Corresponding figures at same conditions without addition of SO₂ are shown in Fig. 2 and Fig. 3 of the supplementary material to illustrate that SO₂ does not interfere with the measurement as it is subtracted from the spectrum via background measurements. To quantify NaCl and NaOH simultaneously, in a first step the NaOH concentration was determined from the peak at 320 nm of the 'raw data (NaOH + NaCl spectrum)', as this peak is not overlapping with the spectrum of NaCl. Based on this NaOH concentration, the entire spectrum for NaOH ('NaOH (fitted based on absorption at 320 nm)' in Fig. 2b) was fitted using the cross section at different wavelengths obtained from [27]. In a second step, the NaOH absorbance was then subtracted from the combined spectrum ('raw data (NaOH + NaCl spectrum)' in Fig. 2b) to obtain the absorbance for NaCl ('NaCl (difference between raw data and NaOH fit)' in Fig. 2b). The NaCl concentration was then determined from the absorption peak at 238 nm with the absorption cross section $\sigma_{238} = 2.5 \cdot 10^{-17} \text{ cm}^2/\text{molecule}$.

3. Model

The thermodynamic data and reaction mechanism for sulfation of NaCl and NaOH were based on the work by Glarborg and Marshall [21], but updated as part of the present work. Glarborg et al. emphasized the importance of alkali hydrogen sulfates as gas-phase precursors of A₂SO₄, and estimated the thermodynamic properties of KHSO₄ and NaHSO₄, as well as chlorinated intermediates, from ab initio computations. In a later work, Hindiyarti et al. [1] proposed a number of additional pathways to sulfation of KCl and KOH, involving KHSO₃ and KOSO₃, and more recently, additional modifications were made to the potassium subset [25,26,28]. In the present work, these modifications have been applied also to the sodium subset. Using the methods described in ref. [21], with G3 theory replaced by G4 [35], properties for species added to the mechanism, i.e., NaHSO₃ and NaOSO₃ were calculated in the present work, and data for NaSO₃Cl were updated. For the added reactions, rate constants were assumed to be similar for corresponding sodium and potassium reactions in the exothermic direction. Compared to the model of Glarborg and Marshall [21], the thermodynamic data for NaOH was replaced with data from the reference [36]. The novel calculated thermodynamic properties are listed in Table 2. In the Na-mechanism, a check was made to ensure that rate constants in both the forward and reverse direction were below the collision frequency.

The kinetic modeling was done with Chemkin-Pro. In a first step, a one-dimensional free propagation model was used to determine the

composition of the post-flame gases. The mixture of these post-flame gases and the co-flow was used as the inlet gases for the plug flow reactor model that was used to model the sulfation reactions. In this step, 20 ppm NaOH or NaCl was added together with 0–150 ppm SO₂ to the hot gas products. For the plug flow model it was assumed that the post-flame gases and co-flow gases are mixed rapidly. The temperature profile in the model was adopted from the measured values.

FACTSAGE 7.3 was used for the equilibrium calculations. The "Equilib" module within the FACTSAGE software calculated the equilibrium concentrations by minimizing the Gibbs energy. All species that were considered for the kinetic model were also considered in the equilibrium calculations. The thermodynamic data was taken from the FACTSAGE database and extended with thermodynamic data for the following sodium species from reference [21] and from the present work: NaSO₂, NaSO₃, NaSO₄, NaHSO₃, NaHSO₄ and NaSO₃Cl.

4. Experimental results

It is a limitation in the present reactor setup, from a kinetic point of view, that the species could only be quantified 5 mm above the burner outlet and not close to the jet tubes due to the walls of the burner that are needed to stabilize the flames. Nevertheless, the measurements provide the first direct characterization of sulfation of sodium salts, and allow for an assessment of the relative importance of kinetic and equilibrium constraints.

Fig. 3a presents the measured NaOH(g) concentrations above the burner outlet during the sulfation experiments at 850 to 1475 °C and for SO₂ concentrations between 0 and 150 ppm. The NaOH(g) concentration, without SO₂, is 20 ppm. The error bars in Fig. 3 are derived from the deviation of repeated experiments and from the uncertainty of the measurement method. At the highest investigated temperature, 1475 °C, the NaOH(g) concentration remains constant at 20 ppm, indicating that no sulfation reactions take place under these conditions. When the temperature is reduced to 1275 °C, the NaOH(g) concentration decreases slightly with the addition of > 50 ppm SO₂. At 1115 °C, only little NaOH(g) was consumed with 20 ppm SO₂, but up to 40 % of the NaOH(g) was consumed with 100 or 150 ppm SO₂. Also at the lowest temperatures, 985 and 850 °C an increased NaOH(g) consumption with increased SO₂ concentration can be observed. At 850 °C, almost all NaOH(g) is consumed at SO₂ concentrations > 50 ppm. For comparison, experimental results from KOH sulfation under the same conditions, published by Weng et al [28], are shown in Fig. 3b. It can be seen that the consumption of the two alkali hydroxides is almost identical under same conditions. The consumption of NaOH(g), similar to KOH(g), can be explained by the sulfation of the NaOH(g) into gaseous Na₂SO₄ and

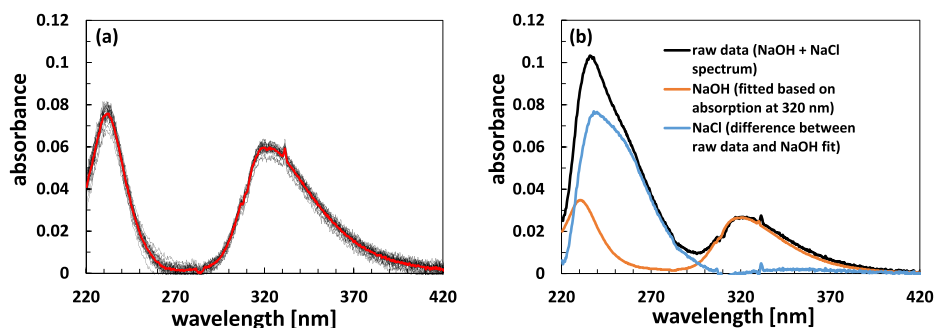


Fig. 2. (a) Measured absorbance of NaOH at 1275 °C adding 20 ppm NaOH and 20 ppm SO₂ to the flame (20 repetitions, red line showing the average absorbance) and (b) measured absorbance of combined NaOH and NaCl and calculated absorbance for NaOH and NaCl determined from the combined spectrum at 1275 °C adding 20 ppm NaCl and 20 ppm SO₂ to the flame. (For interpretation of the references to colour in this figure legend, the reader is referred to the web version of this article.)

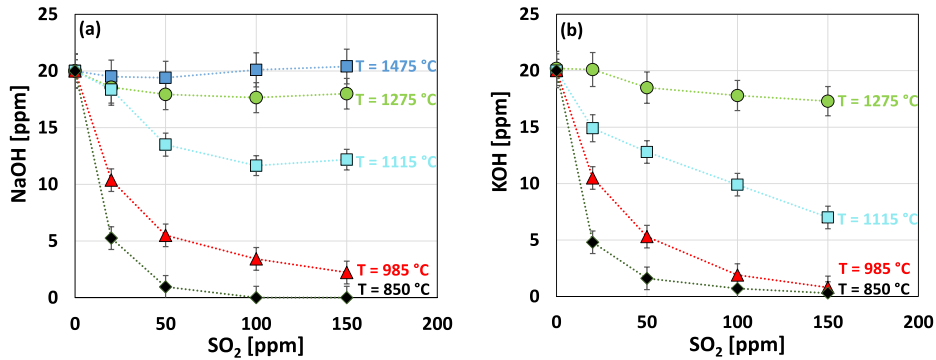


Fig. 3. (a) NaOH concentrations from sulfation experiments at various temperatures with 20 ppm NaOH inlet concentration and SO₂ concentrations between 0 and 150 ppm and (b) KOH concentrations from previous sulfation experiments under same conditions for comparison (KOH results reproduced from [28], dotted lines for clarity only).

Table 2

Thermodynamic properties calculated in the present work for selected alkali species. Units are cal, mol, K.

| Species | H _{r,298} | S ₂₉₈ | C _{p,300} | C _{p,400} | C _{p,500} | C _{p,600} | C _{p,800} | C _{p,1000} | C _{p,1500} |
|----------------------|--------------------|------------------|--------------------|--------------------|--------------------|--------------------|--------------------|---------------------|---------------------|
| NaHSO ₃ | -159.84 | 78.54 | 21.25 | 23.66 | 25.32 | 26.46 | 27.82 | 28.66 | 29.92 |
| NaOSO ₃ | -159.88 | 79.27 | 22.07 | 24.80 | 26.69 | 27.97 | 29.42 | 30.19 | 31.08 |
| NaSO ₃ Cl | -178.68 | 82.80 | 22.74 | 25.04 | 26.74 | 27.98 | 29.45 | 30.15 | 31.00 |

Na₂SO₄ aerosols, as proposed by Glarborg and Marshall [21].

The formation of sulfate aerosols from the sulfation of KOH(g) was detected previously at 985 and 850 °C by elastic scattering measurements [28]. Due to the similar experimental results for NaOH(g) and KOH(g), it is assumed that aerosol formation also takes place at these temperatures in the sulfation of NaOH(g). These results are also in agreement to results by Jiménez and Ballester [37]. In their study on pulverized olive residue combustion, it was observed that KOH was consumed in the presence of SO₂, and the nucleation of the formed K₂SO₄ started when temperatures decreased below 1000 °C.

Fig. 4 shows the concentrations of NaCl(g) and NaOH(g) above the burner outlet from the experiments with NaCl-seeding without SO₂. At

low temperatures, all sodium in the gas-phase is present as NaCl(g). At increasing temperatures however, NaCl was partly converted to NaOH(g). At 1475 °C, around 50 % of the NaCl reacted to NaOH(g).

The NaCl(g) concentration for the sulfation experiments with NaCl-feeding are presented in Fig. 5. For the temperatures between 1115 and 1475 °C, it can be seen that the NaCl(g) concentration is not influenced by SO₂, hence no sulfation of NaCl(g) occurred under these conditions. At 985 °C, the NaCl(g) concentration decreased from roughly 17 ppm without SO₂ to roughly 12 ppm with 150 ppm SO₂. At lower SO₂ concentrations, the concentration remained at around 17 ppm. Only at the lowest temperature, i.e. at 850 °C, a continuous decrease in the NaCl(g) concentration with increasing SO₂

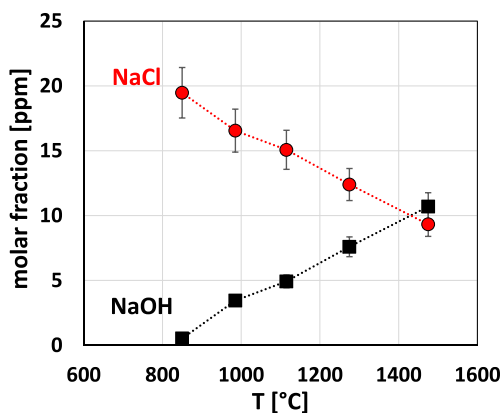


Fig. 4. Concentrations of NaCl and NaOH at 850–1475 °C measured in tests without SO₂ inlet concentration in all cases 20 ppm NaCl (dotted lines for clarity only).

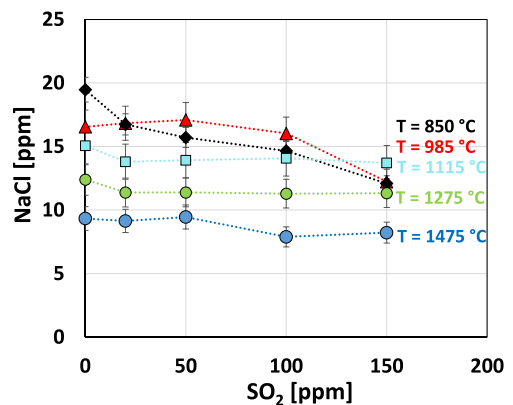


Fig. 5. NaCl concentrations from sulfation experiments at various temperatures with 20 ppm NaCl inlet concentration and SO₂ concentrations between 0 and 150 ppm (dotted lines for clarity only).

concentrations can be observed. The concentration decreases continuously from 20 ppm without SO_2 addition to roughly 12 ppm with 150 ppm SO_2 , which corresponds to a reduction of around 40 %. It can be concluded that the sulfation of NaCl(g) occurs to a much lower extent as compared to the sulfation of NaOH(g) under the investigated conditions.

5. Modeling

Kinetic modeling and equilibrium calculations were made to further interpret the reactions occurring during the gas phase sulfation of NaOH and NaCl . Fig. 6 compares NaOH concentrations (a) and NaCl concentrations (b) from chosen experiments with predictions from the kinetic model and the thermodynamic model. In these sulfation tests, it can be seen that predictions from the kinetic model and the equilibrium calculations are almost identical at 1275 and 1475 °C, indicating that the system is already at equilibrium under the used conditions. For the cases at 1115 °C and below, the system seems not to be at equilibrium under the present conditions. At these temperatures, NaOH(g) are close to the values obtained from the kinetic model as compared to the equilibrium calculations. NaCl(g) concentrations in Fig. 6b are given for the cases at 985 and 850 °C, which are the only temperatures at which NaCl(g) sulfation was observed in the experiment. According to the modeling, the system is almost at equilibrium at 985 °C, but far from equilibrium at 850 °C. This is in agreement with previous findings for the sulfation of alkali chlorides, e.g. in the field study by Christensen and Livbjerg focusing on the sulfation of KCl , which also was far from equilibrium according to their model [38]. At 850 °C, where reactions seem to be limited by kinetics, the kinetic model does not give a good prediction and deviates significantly from the observations in the experiment.

A sensitivity analysis has been performed to illustrate the effects of uncertainties in the experimental setup and their effect on the modeling results. The results are shown in Fig. 4 of the supplementary material. In addition to the SO_2 inlet level, the flame temperature was found to be the most sensitive input parameter with a change of 40 °C sufficient to significantly alter the predicted NaOH concentration.

Generally, the model gives a good description of the observed sodium sulfation reaction. However, due to the fact that reactions occur rapidly, the current set-up cannot be used to fully validate the kinetic model. Nevertheless, the model gives a good kinetic description for most of the cases.

Fig. 7 shows concentrations of relevant species during NaOH(g) sulfation at 1115 °C with 50 ppm SO_2 as a function of time (logarithmic plot) and as a function of the distance from the jet-tubes (linear plot). It can be seen some reactions occur rapidly within the first 1 ms/ few

millimeters above the burner outlet. After the rapid reactions in the beginning, NaOH is slowly consumed, while the concentration of Na_2SO_4 is steadily increasing. The range in which the optical measurement takes place (after roughly 30 ms reaction time) is marked by the dotted lines. Even beyond that range sulfation reactions seem to continue, indicating that indeed kinetics is investigated under these conditions and equilibrium has not been reached.

To clarify whether sulfation reactions take place in the gas phase and if stable gaseous products can be formed under these conditions, equilibrium calculations have been made to determine the ratio between gaseous and condensed Na_2SO_4 . Fig. 8 shows the ratio of $\text{Na}_2\text{SO}_4(\text{g})$ and $\text{Na}_2\text{SO}_4(\text{l})$ between 890 and 1130 °C. Above 1080 °C, only the gaseous product seems to be stable. At below 1000 °C, almost all Na_2SO_4 is expected to be in the condensed phase. This is in agreement with the observations made by Weng et al. [28], reporting aerosol formation in alkali sulfation experiments at similar temperatures. The combined experimental data, chemical equilibrium calculations and kinetic modeling of the present study support that sulfation of alkali species can occur in the gas phase through homogenous reactions, in contrast to earlier reports [39].

6. Conclusions

Post-flame sulfation of NaOH(g) and NaCl(g) was investigated with optical in-situ measurements under well-defined combustion environments. Experiments were performed under oxidizing conditions at 850 to 1475 °C with initial concentrations of 20 ppm for the Na-species and 0–150 ppm SO_2 . The concentrations of NaOH(g) and NaCl(g) were quantified using UV absorption spectroscopy. Additionally, an updated model for the detailed Na-Cl-S chemistry was used to describe the sulfation reactions.

At the highest investigated temperatures 1475 and 1275 °C almost no sulfation of NaOH(g) was observed in the experiments while almost all NaOH(g) was consumed with 50 ppm SO_2 . The experimental results for the sulfation of NaOH(g) were compared to previous results for the sulfation of KOH(g) under the same conditions. The results for NaOH(g) were shown to be similar to those of KOH(g) , indicating that the kinetics and thermodynamics are similar for those species under the investigated conditions.

Sulfation of NaCl(g) occurred to a much lower extent under the investigated conditions as compared to sulfation of NaOH(g) . Sulfation of NaCl(g) was observed at 985 and 850 °C. At 850 °C the NaCl(g) concentration decreased from 20 to 12 ppm after the addition of 150 ppm SO_2 .

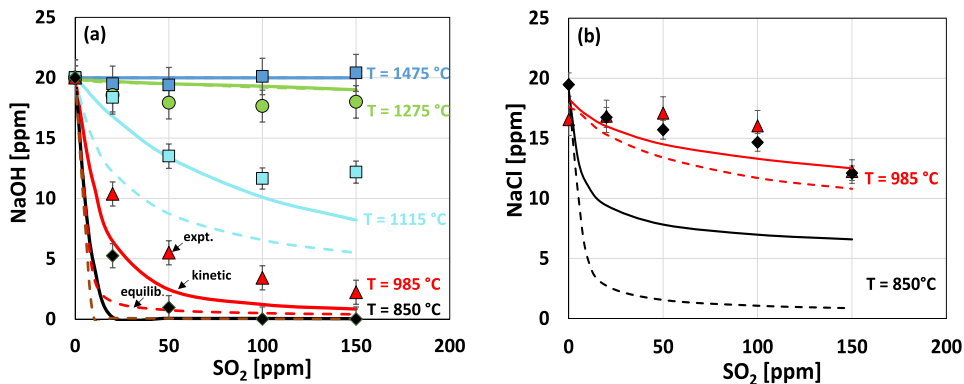


Fig. 6. (a) NaOH and (b) NaCl concentrations for sulfation experiments at 850 to 1475 °C and varying SO_2 concentrations; inlet concentration 20 ppm NaOH or 20 ppm NaCl respectively (dotted lines = equilibrium calculations, continuous lines = kinetic modeling and symbols = experimental results).

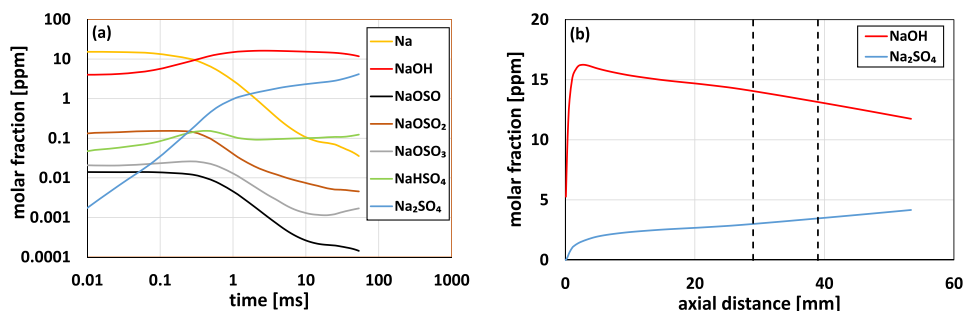


Fig. 7. (a) Molar fractions of relevant species as a function of time (logarithmic scale) and (b) molar fraction of NaOH and Na₂SO₄ (linear scale) from kinetic modeling of NaOH-sulfation experiments at 1115 °C as a function of the vertical distance from the jet-tubes (linear); inlet concentration 20 ppm NaOH and 50 ppm SO₂. The dotted lines indicate the area in which the optical measurement of NaOH was performed.

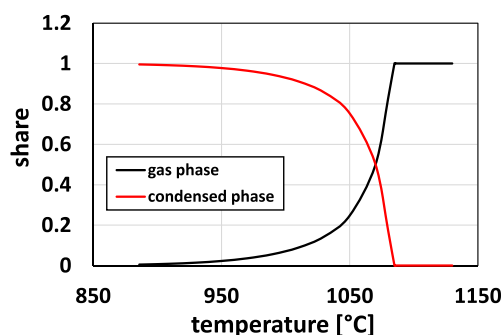


Fig. 8. Equilibrium ratio of Na₂SO₄(g) and Na₂SO₄(l) for NaOH sulfation at 890 to 1130 °C; inlet concentration 20 ppm NaOH, 50 ppm SO₂, 4.7 % CH₄ and 13.9 % O₂ (N₂ as balance).

Chemical equilibrium calculations and kinetic modeling using an updated kinetic model for the detailed Na-Cl-S chemistry were compared to the experimental results. Above 1275 °C, the system can be described by chemical equilibrium, implying that equilibrium is reached in less than 50 ms. At 1115 °C and below, the measured concentrations were in good agreement to the updated chemical kinetic model. Under these conditions, the kinetic model was in good agreement with the experimental results for NaOH(g) but over-predicted the sulfation of NaCl(g). The combined experimental data, chemical equilibrium calculations and kinetic modeling support that sulfation of alkali species can occur in the gas phase through homogenous reactions.

CRediT authorship contribution statement

Daniel Schmid: Investigation, Writing – original draft. **Wubin Weng:** Methodology, Writing – review & editing. **Shen Li:** Investigation. **Oskar Karlström:** Writing – review & editing, Supervision, Project administration. **Mikko Hupa:** Conceptualization. **Zhongshan Li:** Supervision. **Peter Glarborg:** Methodology, Writing – review & editing. **Paul Marshall:** Methodology. **Marcus Aldén:** Project administration.

Declaration of Competing Interest

The authors declare that they have no known competing financial interests or personal relationships that could have appeared to influence the work reported in this paper.

Data availability

Data will be made available on request.

Acknowledgment

This study was financed by the Academy of Finland through the project Chemical challenges in gasification of biomass and waste (321598 and 353318) and Swedish Energy Agency through the KC-CECOST project (22538-4, biomass). PM acknowledges computational facilities provided by the National Science Foundation, Grant CHE-1531468.

Appendix A. Supplementary data

Supplementary data to this article can be found online at <https://doi.org/10.1016/j.fuel.2022.126337>.

References

- [1] Hinidyarti L, Frandsen F, Livbjerg H, Glarborg P, Marhsall P. An exploratory study of alkali sulfate aerosol formation during biomass combustion. *Fuel* 2008;87: 1591–600.
- [2] Christensen KA, Livbjerg H. A Plug Flow Model for Chemical Reactions and Aerosol Nucleation and Growth in an Alkali-Containing Flue Gas. *Aerosol Sci Tech* 2000;33(6):470–89.
- [3] Jensen JR, Nielsen LB, Schultz-Møller C, Wedel S, Livbjerg H. The Nucleation of Aerosols in Flue Gases with a High Content of Alkali – A Laboratory Study. *Aerosol Sci Technol* 2000;33(6):490–509.
- [4] Hupa M, Karlström O, Vainio E. Biomass combustion technology development – It is all about chemical details. *Proceeding of the Combustion Institute* 2017:113–34.
- [5] Paulauskas R, Striugas N, Sadeckas M, Sommersacher P, Retschitzegger S, Kienzl N. Online determination of potassium and sodium release behaviour during single particle biomass combustion by FES and ICP-MS. *Sci Total Environ* 2020;746: 141162.
- [6] Olsson JG, Jäglid U, Pettersson JBC. Alkali Metal Emission during Pyrolysis of Biomass. *Energy Fuel* 1997;11:779–84.
- [7] Backman R, Frederick WJ, Hupa M. Basic Studies on Black-Liquor Pyrolysis and Char Gasification. *Bioresour Technol* 1993;46:153–8.
- [8] Dayton DC, Frederick WJ. Direct Observation of Alkali Vapor Release during Biomass Combustion and Gasification. 2. Black Liquor Combustion at 1100 °C. *Energy Fuel* 1996;10:284–92.
- [9] Gilbe C, Öhman M, Lindström E, Boström D, Backman R, Samuelsson R, et al. Slagging Characteristics during Residential Combustion of Biomass Pellets. *Energy Fuel* 2008;22:3536–43.
- [10] Lapuerta M, Acosta A, Pazo A. Fouling Deposits from Residual Biomass with High Sodium Content in Power Plants. *Energy Fuel* 2015;29:5007–17.
- [11] Niu Y, Tan H, Hui S. Ash-related issues during biomass combustion: Alkali-induced slagging, silicate melt-induced slagging (ash fusion), agglomeration, corrosion, ash utilization, and related countermeasures. *Prog Energy Combust* 2016;52:1–61.
- [12] Enestam S, Bankiewicz D, Tuiremo J, Mäkelä K, Hupa M. Are NaCl and KCl equally corrosive on superheater materials of steam boilers? *Fuel* 2013;104:294–306.
- [13] Wu H, Yrjas P, Vainikka P, Lindberg D, Hupa M. Sulfation of alkali halides in a bench-scale bubbling fluidized bed reactor. *Fuel* 2016:173–9.

- [14] Kassman H, Pettersson J, Steenari B-M, Åmand L-E. Two strategies to reduce gaseous KCl and chlorine in deposits during biomass combustion – injection of ammonium sulphate and co-combustion with peat. *Fuel Process Technol* 2013;105:170–80.
- [15] Wu, H.; Wang, G.; Jensen, P. A.; Jappe Frandsen, F.; Glarborg, P. Reactive additives for alkali capture in biomass combustion. *Paper presented at 27th International Conference on the Impact of Fuel Quality on Power Production and the Environment*, 2018.
- [16] Aho M, Paakinen K, Taipale R. Destruction of alkali chlorides using sulphur and ferric sulphate during grate combustion of corn stover and wood chip blends. *Fuel* 2013;103:562–9.
- [17] Aho M, Vainikka P, Taipale R, Yrjas P. Effective new chemicals to prevent corrosion due to chlorine in power plant superheaters. *Fuel* 2008;87:647–54.
- [18] Iisa K, Lu Y, Salmenoja K. Sulfation of Potassium Chloride at Combustion Conditions. *Energy Fuel* 1999;13:1184–90.
- [19] Boonsongsup L, Iisa K, Frederick WJ. Kinetics of the Sulfation of NaCl at Combustion Conditions. *Ind Eng Chem Res* 1997;36:4212–6.
- [20] Capablo J, Ballester J. Experimental study of the kinetics of sulfation of alkali chloride deposits. *Fuel Process Technol* 2015;140:215–21.
- [21] Glarborg P, Marshall P. Mechanism and modeling of the formation of gaseous alkali sulfates. *Combust Flame* 2005;141:22–39.
- [22] Jiménez S, Ballester J. Influence of operating conditions and the role of sulfur in the formation of aerosols from biomass combustion. *Combust Flame* 2005;140:346–58.
- [23] Ekvall T, Andersson K, Leffler T, Berg M. K-Cl-S chemistry in air and oxy-combustion atmospheres. *Proceeding of the Combustion Institute* 2017;36:4019–26.
- [24] Ekvall T, Normann F, Andersson K, Johnsson F. Modeling the Alkali Sulfation Chemistry of Biomass and Coal Co-firing in Oxy-fuel Atmospheres. *Energy Fuel* 2014;28:3486–94.
- [25] Li B, Sun Z, Li Z, Aldén M, Jakobsen FG, Hansen S, et al. Post-flame gas-phase sulfation of potassium chloride. *Combust Flame* 2013;160:959–69.
- [26] Weng W, Chen S, Wu H, Glarborg P, Li Z. Optical Investigation of gas-phase KCl/KOH sulfation in post flame conditions. *Fuel* 2018;224:461–8.
- [27] Weng W, Leffler T, Brackmann C, Aldén M, Li Z. Spectrally Resolved Ultraviolet (UV) Absorption Cross-Sections of Alkali Hydroxide and Chlorides Measured in Hot Flue Gases. *Appl Spectrosc* 2018;72(9):1388–95.
- [28] Weng W, Li Z, Wu H, Aldén M, Glarborg P. Quantitative K-Cl-S chemistry in thermochemical conversion processes using in situ optical diagnostics. In: *Proceeding of the Combustion Institute* 38th; 2021. p. 5219–27.
- [29] Li, K.; Yan, W.; Yu, L.; Huang, X.; Chen, Y.; Zhou, H.; Zheng, S.; Lou, C. Simultaneous Determination of Na Concentration and Temperature during Zhundong Coal Combustion using the Radiation Spectrum. *Energy Fuel*, 2021, 31, 3348–3359.
- [30] Weng W. *Optical Diagnostics for Quantitative Potassium Chemistry in Biomass Thermochemical Conversion Processes* [Doctoral Thesis]. Department of Physics: Lund University, Lund; 2020.
- [31] Weng W, Borggren J, Li B, Aldén M, Li Z. A novel multi-jet burner for hot flue gases of wide range of temperatures and compositions for optical diagnostics of solid fuels gasification/combustion. *Rev Sci Instrum* 2017;88:045104.
- [32] Borggren J, Weng W, Hosseinnia A, Bengtsson P-E, Aldén M, Li Z. Diode laser-based thermometry using two-line atomic fluorescence of indium and gallium. *Appl Phys B* 2017;123:278.
- [33] Weng W, Chang Y, Wu H, Glarborg P, Li Z. Optical measurements of KOH, KCl and K for quantitative K-Cl chemistry in thermochemical conversion processes. *Fuel* 2020;271:117643.
- [34] Weng W, Brackmann C, Leffler T, Aldén M, Li Z. Ultraviolet Absorption Cross Sections of KOH and KCl from Nonintrusive Species-Specific Quantitative Detection in Hot Flue Gases. *Anal Chem* 2019;91(7):4719–26.
- [35] Curtiss LA, Pedfern PC, Raghavachari K. Gaussian-4 theory. *J Chem Phys* 2007;126:084108.
- [36] Chase MW. NIST-JANAF Thermodynamic Tables. *J Phys Chem Ref Data* 1998; 1–1951.
- [37] Jiménez S, Ballester J. Formation and Emission of Submicron Particles in Pulverized Olive Residue (Orujillo) Combustion. *Aerosol Sci Technol* 2004;38:707–23.
- [38] Christensen K, Livbjerg H. A Field Study of Submicron Particles from the Combustion of Straw. *Aerosol Sci Technol* 1996;25:185–99.
- [39] Steinberg M, Schofield K. The chemistry of sodium with sulfur in flames. *Prog Energy Combust Sci* 1990;16(4):311–7.

D. Schmid, O. Karlström, V. Kuvaja, I. Vuorinen, M. Paavola, M. Hupa.
Role of Sulfite Oxidation in NO₂ Absorption in a pH-Neutral Scrubber Solution.
Energ. Fuel 36(5) (2022), 2666-2672.

Role of Sulfite Oxidation in NO₂ Absorption in a pH-Neutral Scrubber Solution

Daniel Schmid,* Oskar Karlström, Virva Kuvaja, Ilari Vuorinen, Mikko Paavola, and Mikko Hupa



Cite This: *Energy Fuels* 2022, 36, 2666–2672



Read Online

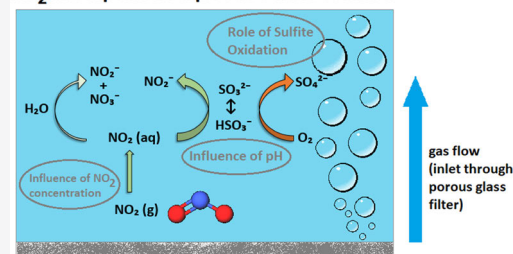
ACCESS |

Metrics & More

Article Recommendations

ABSTRACT: Nitrogen dioxide (NO₂) absorption in aqueous sulfite solutions has recently gained more attention to reduce NO_x emissions. The NO₂ removal efficiency is strongly influenced by the competing reactions of NO₂ absorption and sulfite oxidation. The present study investigates the role of sulfite oxidation in NO₂ absorption at neutral pH. The effects of sulfite concentration, thiosulfate, pH, NO₂ inlet concentration, oxygen concentration on NO₂ absorption efficiency, and sulfite oxidation rates were investigated under well-controlled conditions at 25 °C in a laboratory-scale wet scrubbing system. NO₂ absorption rates showed a strong dependence on the sulfite concentration and increased linearly with increasing NO₂ inlet concentrations between 25 and 150 ppm. At the highest investigated sulfite concentration, 20 mM, the NO₂ removal efficiency was around 80%. Oxidation rates of sulfite during NO₂ absorption in the presence of 5 vol % O₂ increased with increasing sulfite concentrations in the scrubbing solution and ranged from 20 mg·L⁻¹·min⁻¹ with 1 mM sulfite to 200 mg·L⁻¹·min⁻¹ with 20 mM sulfite. The oxidation rate decreased significantly when thiosulfate was added, while the oxidation rates were independent of the oxygen concentration between 2–10 vol % O₂. The NO₂ absorption rate decreased with decreasing pH between pH 6 and 8 proportionally to the sulfite concentration as predicted by the sulfite–bisulfite equilibrium. The implication from these results is that significantly less sulfite feeding is needed in industrial NO₂ absorption if the pH can be maintained at neutral pH, instead of lower pH such as in simultaneous SO₂ and NO₂ scrubbing.

NO₂ absorption in aqueous sulfite solution



1. INTRODUCTION

NO_x emissions resulting from thermal conversion of solid and liquid fuels, and also from other industrial processes, continue to be a major challenge for environmental reasons and due to increasingly strict emission limits. In the last 50 years, numerous studies investigated the formation and chemistry of NO_x emissions experimentally, computationally, and at an industrial scale.^{1–8} NO_x emissions can be reduced by selective noncatalytic reduction (SNCR)^{9–11} and selective catalytic reduction (SCR).^{12,13} In the SNCR process, NO and NO₂ are reduced to N₂ by injecting ammonia (NH₃) or urea (CO(NH₂)₂) in the presence of oxygen. The main disadvantages of SNCR are the ammonia slip, that there should be little or no hydrocarbons or CO present, and the narrow temperature range (900–1050 °C when using urea) for its maximum efficiency.⁷ In SCR, the ammonia is chemisorbed on a catalyst and reacts with NO or NO₂ from the gas phase, enabling operation at lower temperatures, usually between 250 and 400 °C,¹¹ but the SCR technique is limited due to poisoning of the catalyst, particularly, in flue gases containing high amounts of fly ash or dust.

One alternative NO_x reduction strategy is based on absorption in aqueous solutions.^{14,15} The solubility of NO in

water is low, but various additives have been investigated to improve the solubility and removal of NO.^{16–20} Alternatively, to the direct absorption of NO, NO can be selectively oxidized to NO₂, which has a higher solubility in water.^{16,21,22} NO can be selectively oxidized to NO₂ by, e.g., ClO₂, NaClO, NaClO₂, NaClO₃, O₃, etc.^{23–27} However, even with the higher solubility of NO₂, NO₂ absorption rates may be too low. Various chemical compounds have been investigated as additives to further improve the absorption rates of NO₂. One possible additive that has been investigated for that purpose is sodium sulfide (Na₂S), which has also been demonstrated on the industrial scale.^{28–30} Sulfide reacts with NO₂(aq) forming sulfite (SO₃²⁻) and nitrogen (N₂). Shen and Rochelle showed that >95% of the initial NO₂ could be removed in a stirred cell contactor with sulfide concentrations of 0.1 M and higher for

Received: November 17, 2021

Revised: January 19, 2022

Published: February 17, 2022

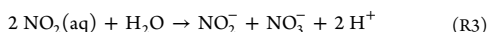
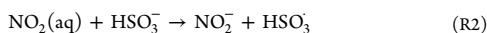
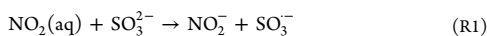


NO₂ inlet concentrations between 20 and 500 ppm.²⁹ One drawback of using sulfide is that a high pH is required since H₂S is formed if the pH is below 9, which is typical for a range of processes.

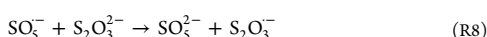
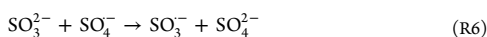
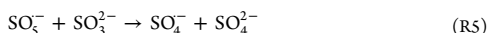
Sulfite (SO₃²⁻) as an additive to improve NO₂ absorption has been studied extensively. The sulfite ion improves the NO₂ absorption rates significantly and can also be used at lower pH as compared to sulfide.^{22,31–33} Similar to the experiments with sulfide,²⁹ Shen and Rochelle investigated the absorption of NO₂ in a stirred cell contactor with concentrations of 1–100 mM sulfite.²² At pH > 7.5, the NO₂ removal efficiency increased linearly with the sulfite concentration, and at 10 mM sulfite, more than 80% of NO₂ was absorbed.

The absorption of NO₂ depends on a complex series of chemical and diffusion steps, where the first two steps are (i) diffusion of NO₂ to and through the gas–liquid film and (ii) NO₂(g) ↔ NO₂(aq). The rapid reactions occurring in the liquid phase (in the presence of sulfite) decrease the distance through which the NO₂ must diffuse in the liquid before it is transformed into ions.

The mechanism of the reaction between NO₂ and aqueous sulfite is complex (see, for e.g., refs 22 and 34). The reaction likely involves charge transfer reactions in a free-radical chain mechanism.³⁴ Three irreversible parallel reactions, depending on the pH, may occur in the boundary layer and enhance NO₂ absorption, following Nash³⁴



In the presence of oxygen, the sulfite radical (SO₃^{•-}) that is formed according to R1 can undergo radical chain reactions R4–R7, oxidizing the sulfite to sulfate.^{21,35,36} The oxidation to sulfate is not desired, as sulfate has no positive effect on NO₂ absorption.



The decrease of NO₂ absorption rates due to sulfite oxidation by O₂(aq) has been studied only to a limited extent, e.g., refs 21 and 37. To prevent oxidation of sulfite to sulfate, free-radical scavengers, such as thiosulfate, can be added to terminate the chain reactions R8–R10.^{21,38} Other additives that may be used to inhibit the oxidation of sulfite to sulfate are, e.g., hydroquinone, thiourea, ascorbic acid, p-phenylenediamine, and *tert*-butylhydroquinone.³⁹

Several previous studies have investigated the chemistry of simultaneous absorption of SO₂ and NO₂.^{24,40–46} Li et al.⁴² investigated the NO₂ absorption in a Na₂CO₃ solution with SO₂ gas concentrations between 500 and 2000 ppm. With 500

ppm SO₂, the NO₂ concentration decreased from 300 to 150 ppm, while with 2000 ppm SO₂, the NO₂ concentration decreased from 300 to 100 ppm. Gaseous SO₂, which forms sulfite ions when absorbed in water, does not only influence the NO₂ absorption but also affects the pH of scrubbing solutions, which is usually around pH 4–6 for the simultaneous removal of SO₂ and NO₂. A range of fuels, such as coals, have high contents of sulfur forming SO₂ influencing NO₂ absorption. On the other hand, many biomass- and waste-derived fuels have almost no or very low contents of sulfur, and, thus, thermal conversion of such fuels does not generate high amounts of SO₂.⁴⁷ As a result, the pH can be maintained at a higher level (such as pH 6–8) in the scrubber solution in NO₂ absorption under such conditions. Additionally, higher sulfite additions might be required due to the lack of SO₂. Johansson et al. performed techno-economic evaluations for the simultaneous absorption of SO₂ and NO_x from various industrial processes.⁴⁶ The presented case of a recovery boiler required the highest sulfite addition as was the case with the lowest SO₂ concentration. In such cases, it is crucial to understand the consumption of sulfite by NO₂ and SO₂ to reduce the overall consumption of chemicals.⁴⁶ Johansson et al.⁴⁵ investigated the simultaneous absorption of NO_x and SO_x from flue gases from a 100 kW gas-fired furnace. The results from experimental measurements were compared to modeling results. Tests were performed with 0–500 ppm SO₂ and 70–350 ppm NO_x in the flue gas and 0–1 g/L Na₂SO₃ in the scrubber solution. The modeled NO₂ removal efficiency was generally in good agreement with the experimental results. In the cases with sulfite addition, the model slightly overpredicted the NO_x absorption, which was attributed to the high rate of sulfite oxidation, which is not yet fully understood.

The present study investigates the role of sulfite oxidation in absorption of NO₂ in aqueous sulfite solutions at neutral pH. Various parameters such as sulfite concentration, the pH of the scrubber solution, and NO₂ inlet concentrations were investigated. NO₂ absorption experiments were performed with and without oxygen in the atmosphere to investigate the role of sulfite oxidation in the overall sulfite consumption and how sulfite oxidation can be prevented by the addition of thiosulfate to the scrubber solution.

2. EXPERIMENTAL METHODS

Figure 1 shows the experimental setup for the NO₂ absorption experiments. The setup consists of a mixing unit for the gas mixtures, a gas washing bottle, and a NO/NO₂ analyzer. Experiments were performed with inlet concentrations of 25–150 ppm NO₂ and 0% O₂ and 50 ppm NO₂ and 2–10% O₂. The balance gas was N₂. The chosen NO₂ concentrations correspond to NO_x concentrations typically found in flue gases from thermal conversion of biomass. The total flow rate was 2 Nl/min at ambient temperature. The gas was bubbled through a sintered glass filter into the scrubber solution to achieve a good contact area between the gas and the liquid. A magnetic agitator in the solution provided continuous stirring at a rate of 300 rpm to minimize concentration gradients within the washing solution. After passing through the scrubber, the gas mixture was analyzed for NO₂. NO₂ concentrations were determined in the following way: NO₂ was converted to NO (SCC-K analyzer), and the NO concentrations were determined using a chemiluminescence analyzer. The setup was also tested without the NO₂ to NO conversion to check whether NO was formed during the experiments, which was not the case.

For the preparation of the aqueous scrubber solutions, sodium sulfite (Na₂SO₃) was dissolved in ultrapure water in concentrations

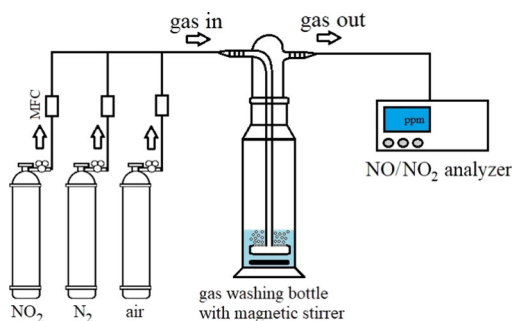


Figure 1. Experimental setup for NO_2 absorption experiments. MFC, mass flow controller.

between 0 and 20 mM. The scrubbing solution in the tests with thiosulfate contained 6 mM sodium thiosulfate ($\text{Na}_2\text{S}_2\text{O}_3$) and 10 mM sulfite. All solutions were buffered with a phosphate buffer ($\text{NaH}_2\text{PO}_4 \cdot 2\text{H}_2\text{O} + \text{KH}_2\text{PO}_4$), and different pH values were obtained by varying the ratios between the weak acid and the conjugate base. Additional absorption tests were performed with pure water and the buffer solution without sulfite to confirm that the buffer did not interfere with the NO_2 reactions (results not shown here).

Some of the solutions were analyzed after the absorption experiments with ion chromatography to quantify nitrite (NO_2^-) and nitrate (NO_3^-) in the solutions. For these analyses, a Metrosep A SUPP 4 column from Metrohm was used with a carbonate/bicarbonate eluent.

3. RESULTS

Figure 2 shows the NO_2 concentrations after the absorption for sulfite concentrations between 0 and 20 mM at pH 8. Table 1 lists the corresponding initial NO_2 absorption rates for each concentration. With 0 mM sulfite, the NO_2 concentration decreased from 50 to 43 ppm. This NO_2 absorption corresponds to previously published values on NO_2 absorption in pure water.³⁵ The measured NO_2 concentration was almost constant throughout the experiment (30 min). With 0.5 mM sulfite, the NO_2 concentration decreased initially from 50 to 35 ppm. This corresponds to an initial NO_2 absorption rate of $25.4 \mu\text{mol}\cdot\text{L}^{-1}\cdot\text{min}^{-1}$. With the highest investigated sulfite

concentration, i.e., 20 mM, the NO_2 concentration initially decreased from 50 to 8 ppm and the initial NO_2 absorption rate increased to $75.6 \mu\text{mol}\cdot\text{L}^{-1}\cdot\text{min}^{-1}$. Thus, higher sulfite concentrations resulted in better NO_2 absorption, as expected. The results show that the highest investigated sulfite concentration of 20 mM already gives more than 80% removal efficiency of the NO_2 inlet of 50 ppm.

From Figure 2, it can be seen that the NO_2 concentrations increased with time when sulfite was initially present, i.e., less NO_2 was absorbed as the sulfite was oxidized to sulfate. With 0.5 mM sulfite, the NO_2 concentration reached the same value as in the test with 0 mM sulfite at 1200 s; hence, it can be assumed that all sulfites were consumed at this point and NO_2 only reacted with water. With increasing sulfite concentration, this effect (NO_2 absorption rates decreasing with time) was less significant. With 1 mM sulfite, the NO_2 concentration increased from the initial 30 ppm to around 38 ppm after 30 min. With 20 mM sulfite, the NO_2 concentration remained almost constant for the entire test. This can be explained by the fact that only a fraction of the sulfite was consumed due to the high initial amounts of sulfite.

Table 2 lists the concentrations of ions for selected tests based on the results from the gas analysis and ion chromatography of the solutions after the test. In general, the mass balances are good. With 1 and 10 mM sulfite, the concentration of the nitrogen-containing ions as determined with IC is slightly higher than what is expected based on the measurements from the continuous gas analyzer. This can be explained by various experimental uncertainties, for e.g., in controlling the gas flow. With 0 mM sulfite, NO_2 only reacted with water, and approximately equal amounts of nitrite (NO_2^-) and nitrate (NO_3^-) were formed, validating reaction R2. With 1 mM sulfite, mostly, nitrite was formed. Small amounts of nitrate were also formed, indicating that reactions R1 and R2 can take place simultaneously when the sulfite concentration was sufficiently low due to the consumption of NO_2 . In the case with 10 mM, only nitrite was formed, which can be explained by the fact that the sulfite concentration was sufficiently high throughout the experiment (reaction R1).

Figure 3 shows NO_2 concentrations (a) and NO_2 absorption rates (b) for the tests with varying NO_2 inlet concentrations between 25 and 150 ppm, and 5 mM sulfite in the scrubber

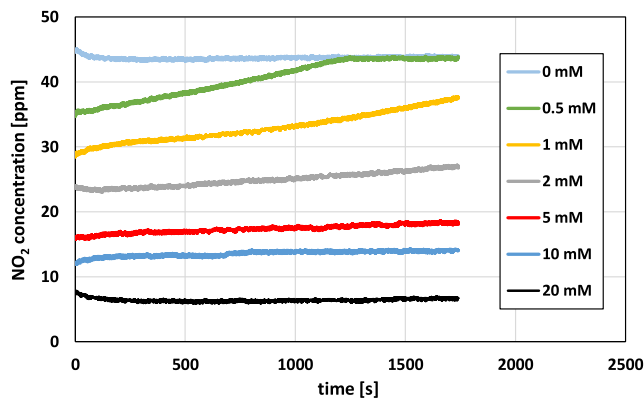


Figure 2. NO_2 concentrations during oxygen-free scrubbing tests with varying sulfite concentrations in 50 mL of buffered solution (pH 8); initial concentration, 50 ppm NO_2/N_2 ; flow rate, 2 NL/min.

Table 1. NO₂ Absorption Rates

| sulfite concentration [mM] | 0 | 0.5 | 1 | 2 | 5 | 10 | 20 |
|---|------|------|------|------|------|------|------|
| NO ₂ absorption rate [$\mu\text{mol}\cdot\text{L}^{-1}\cdot\text{min}^{-1}$] | 11.3 | 25.4 | 35.7 | 44.7 | 56.7 | 63.2 | 75.6 |

Table 2. Mass Balance for NO₂, NO₂⁻, and NO₃⁻

| SO ₃ ²⁻ [mM] | NO ₂ in [μmol] | NO ₂ out [μmol] | NO ₂ abs. [μmol] ^a | NO ₂ ⁻ [μmol] | NO ₃ ⁻ [μmol] | mass balance |
|------------------------------------|--|---|---|--|--|--------------|
| 0 | 81.7 ^b | 63.1 | 18.6 | 9.3 | 8.3 | 0.95 |
| 1 | 122.6 | 82.1 | 40.4 | 45 | 4 | 1.2 |
| 10 | 122.6 | 35.6 | 87 | 107 | <1 | 1.2 |

^aBy difference. ^bLower NO₂ due to the shorter reaction time in the test, where the sample was produced.

solution. With 25, 50, and 100 ppm NO₂, the measured NO₂ concentrations were almost constant throughout the experiment. With 125 and 150 ppm, the NO₂ concentrations increased slightly with time. This can be explained by increasing sulfite consumption due to the higher NO₂ concentrations. Nevertheless, initially, the ratio NO_{2,out}/NO_{2,in} was 0.37 (63% NO₂ absorption) independent of the NO₂ inlet concentration, i.e., the initial NO₂ absorption rate increased linearly with increasing NO₂ inlet concentration.

As discussed above, the pH is also an important factor that may influence the NO₂ absorption. Sulfite can be present as SO₃²⁻ or HSO₃⁻ (bisulfite), depending on the pH.⁴⁸ Figure 4 shows the molar ratio of sulfite and bisulfite based on chemical equilibrium as a function of pH together with the normalized NO₂ absorption efficiency of a sulfite solution between pH 6 and 8. The normalized value of 100% for the relative NO₂ absorption efficiency represents the highest absorption rates at pH 8, i.e., almost all dissolved sulfur is present as sulfite. It can be seen that with decreasing pH, the absorption rates decrease. At pH 6, the molar ratio of sulfite is around 0.7, and also, the normalized absorption rate has been decreased to 70%, implying that sulfite is a significantly more active agent than bisulfite in the reaction with NO₂. This is in agreement with the results by Takeuchi³¹ and Shen,²² reporting roughly 40 times higher rate constants for the reaction between sulfite and NO₂ as compared to the reaction of bisulfite with NO₂. These results explain why significantly more sulfite is needed to obtain similar NO₂ absorption rates at lower pH, say 4, as compared to neutral pH. The positive effect of a higher pH on NO₂ absorption with sulfite has also been demonstrated on a

large scale, showing a sharp increase in NO₂ absorption efficiency when the pH is increased from below 7 to above 8.⁴⁵

Figure 5 shows the NO₂ concentrations from absorption tests with 50 ppm NO₂ and 5% O₂ and varying sulfite concentrations. Similar to the test with 0% O₂ (see Figure 2), it can be seen that the absorption rate improves with increasing sulfite concentration. However, in the presence of O₂, the NO₂ concentrations increased rapidly with time and approached the level representing absorption in pure water (~34 ppm). In the test with 1 mM sulfite and 5% O₂, the NO₂ absorption rate was the same as in pure water already after 100 s. In the test with sulfite and 0% O₂, this level was not reached even after 30 min. With 20 mM sulfite and O₂, the level representing the absorption in water was reached after 520 s.

From the absorption tests under different conditions, it is possible to estimate the sulfite concentration in the solution at any given time point. For instance, when the used gas mixture has an inlet concentration of 50 ppm NO₂ and the concentration is 20 ppm after the scrubber (at pH 8), it can be estimated that the sulfite concentration in the scrubber solution is roughly 3 mM (compare to Figure 3). Based on the increase of the NO₂ concentration during the tests, the sulfite concentration can be estimated and, hence, also the sulfite consumption rates. The consumption of sulfite by NO₂ in the absence of oxygen can be calculated using reaction R1. The difference between the sulfite consumption by NO₂ and the total sulfite consumption from the experiments with O₂ can then be assumed to be the share of sulfite that is oxidized following the radical chain mechanism due to the presence of oxygen. Figure 6 shows the sulfite oxidation rate versus sulfite concentration in the scrubber solution. The error bars represent the deviation between several experimental tests that have been used for the calculations of the oxidation rates. Interestingly, the sulfite oxidation rates show a nearly linear dependence on the sulfite concentration. This shows that sulfite consumption in the presence of oxygen will be much higher using higher sulfite concentrations for the NO₂ absorption. Similar observations were also presented by Sapkota et al, showing that the ratio of oxidized SO₃²⁻ to absorbed NO₂ increased linearly with the sulfite concentration between 7 and 135 mM sulfite.²¹

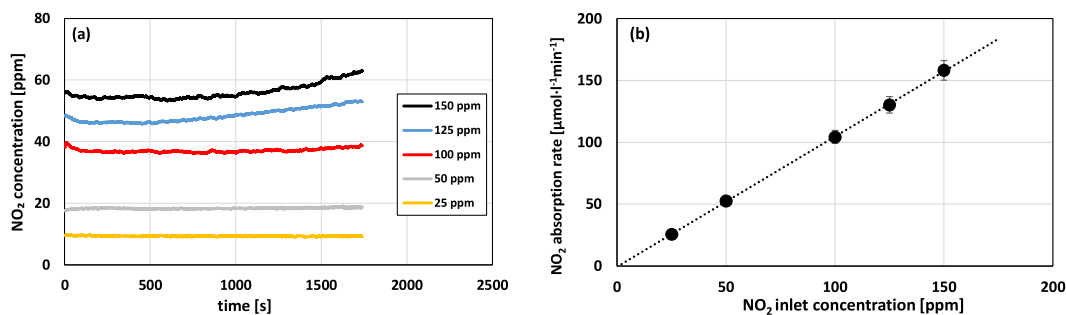


Figure 3. NO₂ concentrations after the laboratory scrubber (a) and initial NO₂ absorption rates (b) with varying NO₂ inlet concentrations (25–150 ppm) in 50 mL of buffered sulfite solution (5 mM sulfite, pH 8); flow rate, 2 NL/min.

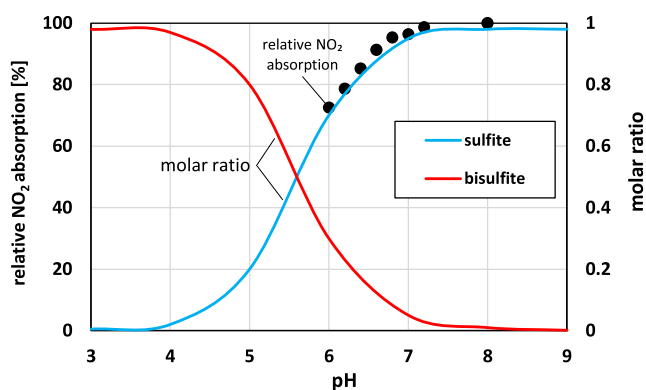


Figure 4. pH dependence of a molar ratio of sulfite species (SO_3^{2-} and HSO_3^-) and NO_2 absorption efficiency (50 ppm NO_2/N_2 , flow rate 2 NL/min, 50 mL of sulfite solution). NO_2 absorption is given relative to absorption at pH 8.

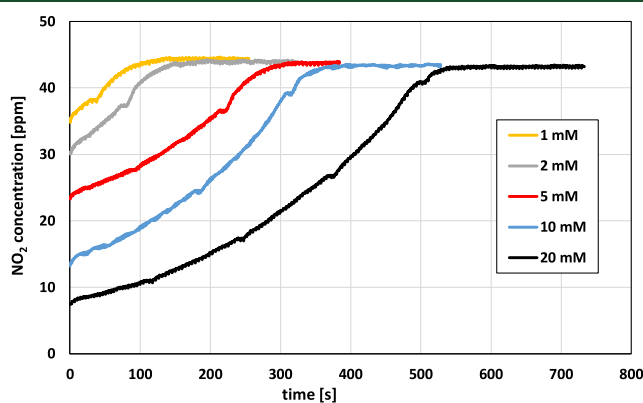


Figure 5. NO_2 concentrations during scrubbing tests with oxygen and varying sulfite concentrations in 50 mL of buffered solution (pH 8); initial concentration, 50 ppm $\text{NO}_2/\text{N}_2 + 5\% \text{O}_2$; flow rate, 2 NL/min at room temperature.

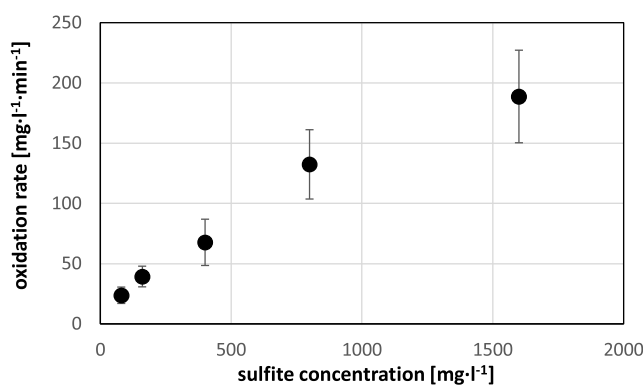


Figure 6. Oxidation rate of sulfite during the NO_2 scrubbing test with oxygen vs sulfite concentration in scrubbing solution; gas inlet 50 ppm $\text{NO}_2/\text{N}_2 + 5\% \text{O}_2$, 2 NL/min, 50 mL of scrubbing solution.

Figure 7 shows the NO_2 concentrations for the absorption tests with 10 mM sulfite and 6 mM thiosulfate, and 2, 5, or 10% oxygen. It can clearly be seen that the NO_2 absorption

rate remains higher with the addition of thiosulfate as compared to the rate in the tests with O_2 and without thiosulfate (see Figure 6). With thiosulfate, the absorption rate

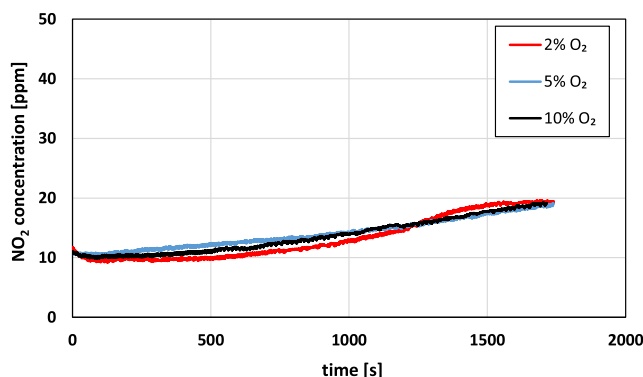


Figure 7. NO₂ concentrations during scrubbing tests with various oxygen concentrations using 6 mM thiosulfate as a stabilizer in the 10 mM sulfite solution; gas inlet concentration, 50 ppm NO₂/N₂ + 5% O₂; flow rate, 2 NL/min at room temperature.

is high even after 30 min, resulting in a sulfite oxidation rate of about 19 mg·L⁻¹·min⁻¹, which is more than 7 times lower than the sulfite oxidation rate in the test without thiosulfate. Interestingly, with 2, 5, or 10% O₂, the NO₂ absorption rate is almost identical, implying that the sulfite oxidation rate (in the presence of thiosulfate) is the same regardless of whether there is 2, 5, or 10% O₂. Thus, the reaction order of the sulfite oxidation with respect to O₂ is zero for these tests.

4. CONCLUSIONS

In the present study, the absorption of NO₂ in aqueous sulfite solutions and the role of sulfite oxidation during NO₂ removal were investigated. Various parameters such as sulfite concentration, the pH of the scrubber solution, and NO₂ inlet concentrations were investigated. NO₂ absorption experiments were performed with and without oxygen in the atmosphere to investigate the role of sulfite oxidation in the overall sulfite consumption and how sulfite oxidation can be prevented by the addition of thiosulfate to the scrubber solution. The following conclusions can be drawn.

The NO₂ removal efficiency increased with increased sulfite concentration. With 20 mM sulfite and 50 ppm NO₂ inlet concentration, the NO₂ removal efficiency was 80%. The NO₂ absorption rates increased linearly with the NO₂ inlet concentration. The NO₂ absorption rates increased with pH. Between pH 6 and pH 8, the absorption rate was proportional to the ratio SO₃²⁻/HSO₃⁻.

Sulfite oxidation rates increased linearly with the sulfite concentration in the scrubber solution during NO₂ absorption in the presence of oxygen. Sulfite oxidation rates decreased when thiosulfate was added. The sulfite oxidation rates were independent of the oxygen concentration in the range of 2–10% O₂. This has a major implication for industrial NO₂ absorption processes: higher thiosulfate concentrations are not needed as the oxygen concentrations increase under conditions similar to the investigated ones.

■ AUTHOR INFORMATION

Corresponding Author

Daniel Schmid – Group of Inorganic Chemistry, Johan Gadolin Process Chemistry Centre, Åbo Akademi University, 20500 Turku, Finland; orcid.org/0000-0002-7786-7134; Email: dschmid@abo.fi

Authors

Oskar Karlström – Group of Inorganic Chemistry, Johan Gadolin Process Chemistry Centre, Åbo Akademi University, 20500 Turku, Finland

Virva Kuvaja – Valmet Technologies Oy, 33900 Tampere, Finland

Ilari Vuorinen – Valmet Technologies Oy, 33900 Tampere, Finland

Mikko Paavola – Valmet Technologies Oy, 33900 Tampere, Finland

Mikko Hupa – Group of Inorganic Chemistry, Johan Gadolin Process Chemistry Centre, Åbo Akademi University, 20500 Turku, Finland

Complete contact information is available at: <https://pubs.acs.org/10.1021/acs.energyfuels.1c03914>

Notes

The authors declare no competing financial interest.

■ ACKNOWLEDGMENTS

This study was financed by the Academy of Finland financed project Chemical challenges in gasification of biomass and waste (321598 and 328952).

■ REFERENCES

- (1) Hood, K. A study of nitrogen oxides emissions from Kraft Recovery Furnaces. *National Council of the Paper Industry For Air and Stream Improvement*, Technical Bulletin No. 105, 1979.
- (2) Miller, J. A.; Bowman, C. T. Mechanism and modeling of nitrogen chemistry in combustion. *Prog. Energy Combust.* **1989**, *15*, 287–338.
- (3) Nichols, K. M.; Thompson, L. M.; Empie, H. J. A review of NO_x formation mechanisms in recovery furnaces. *Tappi J.*, **1993**, *76*, 119–139.
- (4) Glarborg, P.; Jensen, A. D.; Johnsson, J. E. Fuel nitrogen conversion in solid fuel fired systems. *Prog. Energy Combust.* **2003**, *29*, 89–113.
- (5) Leppälähti, J.; Koljonen, T. Nitrogen evolution from coal, peat and wood during gasification: Literature review. *Fuel Process. Technol.* **1995**, *43*, 1–45.
- (6) Hupa, M.; Karlström, O.; Vainio, E. Biomass combustion technology development – It is all about chemical details. *Proc. Combust. Inst.* **2017**, *36*, 113–134.

- (7) Sukumaran, S.; Kong, S.-C. Modeling fuel NO_x formation from combustion of biomass-derived producer gas in a large-scale burner. *Combust. Flame* **2013**, *160*, 2159–2169.
- (8) Schmid, D.; Karlström, O.; Yrjas, P. Release of NH₃, HCN and NO during devolatilization and combustion of washed and torrefied biomass. *Fuel* **2020**, *280*, No. 118583.
- (9) Anichkov, S. N.; Zykov, A. M.; Tumanovskii, A. G.; Kulish, O. N.; Zaporozhskii, K. I. Development of SNCR Technology and Prospects of its application. *Therm. Eng.* **2021**, *68*, 510–515.
- (10) Daoud, S.; Javed, M.; Gibbs, B.; Nimmo, W. NO_x control in coal combustion by combining biomass co-firing, oxygen enrichment and SNCR. *Fuel* **2013**, *105*, 283–292.
- (11) Mahmoudi, S.; Baeyens, J.; Seville, J. P. K. NO_x formation and selective non-catalytic reduction (SNCR) in a fluidized bed combustor of biomass. *Biomass Bioenergy* **2010**, *34*, 1393–1409.
- (12) Mladenović, M.; Paprika, M.; Marinković, A. Denitrification techniques for biomass combustion. *Renewable Sustainable Energy Rev.* **2018**, *82*, 3350–3364.
- (13) Zheng, Y.; Jensen, A. D.; Johnsson, J.-E. Deactivation of V₂O₅-WO₃-TiO₂ SCR catalyst at a biomass-fired combined heat and power plant. *Appl. Catal., B* **2005**, *60*, 253–264.
- (14) Sharif, H. M. A.; Mahmood, N.; Wang, S.; Hussain, I.; Hou, Y.-N.; Yang, L.-H.; Zhao, X.; Yang, B. Recent advances in hybrid wet scrubbing techniques for NO_x and SO₂ removal: State of the art and future research. *Chemosphere* **2021**, *273*, No. 129695.
- (15) Zhao, M.; Xue, P.; Liu, J.; Liao, J.; Guo, J. A review of removing SO₂ and NO_x by wet scrubbing. *Sustainable Energy Technol. Assess.* **2021**, *47*, No. 101451.
- (16) Guo, R.-T.; Hao, J.-K.; Pan, W.-G.; Yu, Y.-L. Liquid Phase Oxidation and Absorption of NO from Flue gas: A Review. *Sep. Sci. Technol.* **2015**, *50*, 310–321.
- (17) Brogren, C.; Karlsson, H.; Bjerle, I. Absorption of NO in an Aqueous Solution of NaClO₂. *Chem. Eng. Technol.* **1998**, *21*, 61–70.
- (18) Chu, H.; Chien, T. W.; Li, S. Y. Simultaneous absorption of SO₂ and NO from flue gas with KMnO₄/NaOH solutions. *Sci. Total Environ.* **2001**, *275*, 127–135.
- (19) Adewuyi, Y. G.; Sakyi, N. Y. Simultaneous Absorption and Oxidation of Nitric Oxide and Sulfur Dioxide by Aqueous Solutions of Sodium Persulfate Activated by Temperature. *Ind. Eng. Chem. Res.* **2013**, *52*, 11702–11711.
- (20) Zheng, C.; Xu, C.; Zhang, Y.; Zhang, J.; Gao, X.; Luo, Z.; Cen, K. Nitrogen oxide absorption and nitrite/nitrate formation in limestone slurry for WFGD system. *Appl. Energy* **2014**, *129*, 187–194.
- (21) Sapkota, V. N. A.; Fine, N. A.; Rochelle, G. T. NO₂-catalyzed sulfite oxidation. *Ind. Eng. Chem. Res.* **2015**, *54*, 4815–4822.
- (22) Shen, C. H.; Rochelle, G. T. Nitrogen Dioxide Absorption and Sulfite Oxidation in Aqueous Sulfite. *Environ. Sci. Technol.* **1998**, *32*, 1994–2003.
- (23) Deshwal, B. R.; Lee, S. H.; Jung, J. H.; Shon, B. H.; Lee, H. K. Study on the removal of NO_x from simulated flue gas using acidic NaClO₂ solution. *J. Environ. Sci.* **2008**, *20*, 33–38.
- (24) Yoon, H. J.; Park, H.-W.; Park, D. W. Simultaneous Oxidation and Absorption of NO_x and SO₂ in an integrated O₃ Oxidation/Wet Atomizing System. *Energy Fuels* **2016**, *30*, 3289–3297.
- (25) Jin, D.-S.; Deshwal, B.-R.; Park, Y.-S.; Lee, H.-K. Simultaneous removal of SO₂ and NO by wet scrubbing using aqueous chlorine dioxide solution. *J. Hazard. Mater.* **2006**, *135*, 412–417.
- (26) Wei, J.; Luo, Y.; Yu, P.; Cai, B.; Tan, H. Removal of NO from flue gas by wet scrubbing with NaClO₂/(NH₂)₂CO solutions. *J. Ind. Eng. Chem.* **2009**, *15*, 16–22.
- (27) Mok, Y. S. Absorption-reduction technique assisted by ozone injection and sodium sulfite for NO_x removal from exhaust gas. *Chem. Eng. J.* **2006**, *118*, 63–67.
- (28) Kaczur, J. Oxidation Chemistry of chloric acid in NO_x/SO_x and air toxic metal removal from gas streams. *Environ. Prog.* **1996**, *15*, 245–254.
- (29) Shen, C.; Rochelle, G. Nitrogen Dioxide Absorption and Sulfite Oxidation in Aqueous Sulfite. *J. Air Waste Manage.* **1999**, *49*, 332–338.
- (30) Gao, X.; Guo, R.; Ding, H.; Luo, Z.; Cen, K. Absorption of NO₂ into Na₂S solution in a stirred tank reactor. *J. Zhejiang Univ.-SC A* **2009**, *10*, 434–438.
- (31) Takeuchi, H.; Ando, M.; Kizawa, N. Absorption of Nitrogen Oxides in Aqueous Sodium Sulfite and Bisulfite Solutions. *Ind. Eng. Chem. Process Des. Dev.* **1977**, *16*, 303–308.
- (32) Nelli, C. H.; Rochelle, G. T. Simultaneous Sulfur Dioxide and Nitrogen Dioxide Removal by Calcium Hydroxide and Calcium Silicate Solids. *J. Air Waste Manage. Assoc.* **1998**, *48*, 819–828.
- (33) Kameoka, Y.; Pigford, R. Absorption of Nitrogen Dioxide into Water, Sulfuric Acid, Sodium Hydroxide, and Alkaline Sodium Sulfite Aqueous Solution. *Ind. Eng. Chem. Fundam.* **1977**, *16*, 163–169.
- (34) Nash, T. The effect of nitrogen dioxide and of some transition metals on the oxidation of dilute bisulfate solutions. *Atmos. Environ.* **1979**, *13*, 1149–1154.
- (35) Huie, R.; Neta, P. Chemical Behaviour of SO₃⁻ and SO₅⁻ Radical in Aqueous Solutions. *J. Phys. Chem. A* **1984**, *88*, S665–S669.
- (36) Neta, P.; Huie, E. Free-Radical Chemistry of Sulfite. *Environ. Health Perspect.* **1985**, *64*, 209–217.
- (37) Zhang, Z.; Zhou, S.; Xi, H.; Shreka, M. A Prospective Method for Absorbing NO₂ by the Addition of NaHSO₃ to Na₂SO₃-based Absorbents for Ship NO_x Wet Absorption. *Energy Fuels* **2020**, *34*, 2055–2063.
- (38) Rochelle, G. T.; Owens, D. R.; Chang, J. C.; Bma, T. G. Thiosulfate as an Oxidation Inhibitor in Flue Gas Desulfurization Processes: A Review of R&D Results. *J. Air Waste Manage. Assoc.* **1986**, *36*, 1138–1146.
- (39) Li, S.; Huang, W.; Xu, H.; Liu, K.; Wang, J.; Sun, Y.; Qu, Z.; Yan, N. Enhanced simultaneous absorption of NO_x and SO₂ in oxidation-reduction-absorption process with a compounded system based on Na₂SO₃. *J. Environ. Sci.* **2022**, *111*, 1–10.
- (40) Guo, Q.; He, Y.; Sun, T.; Want, Y.; Jia, J. Simultaneous removal of NO_x and SO₂ from flue gas using combined Na₂SO₃-based electrochemical reduction and direct electrochemical reduction. *J. Hazard. Mater.* **2014**, *276*, 371–376.
- (41) Shi, F.; Li, K.; Li, J.; Ying, D.; Jia, J.; Sun, T.; Yan, N.; Zhang, X. Simultaneous wet absorption of SO₂ and NO_x with mixed Na₂SO₃ and (NH₄)₂SO₃: Effects of mass concentration ratio and pH. *Chem. Eng. J.* **2021**, *421*, No. 129945.
- (42) Li, S.; Xu, H.; Huang, W.; Sun, Y.; Qiang, J.; Qu, Z.; Yan, N. NO_x Absorption enhancement and Sulfite Oxidation Inhibition via a Match Strategy in Na₂SO₃ Solution from a Wet Flue Gas Denitrification System. *ACS ES&T Engg* **2021**, *1*, 100–109.
- (43) Sun, Y.; Hong, X.; Zhu, T.; Guo, X.; Xie, D. The Chemical Behaviours of Nitrogen Dioxide Absorption in Sulfite Solution. *Appl. Sci.* **2017**, *7*, 377.
- (44) Tumsa, T. Z.; Lee, S. H.; Normann, F.; Andersson, K.; Ajdari, S.; Yang, W. Concomitant removal of NO_x and SO_x from a pressurized oxy-fuel combustion process using a direct contact column. *Chem. Eng. Res. Des.* **2018**, *131*, 626–634.
- (45) Johansson, J.; Normann, F.; Sarajlic, N.; Andersson, K. Technical-Scale Evaluation of Scrubber-Based, Co-Removal of NO_x and SO_x Species from Flue Gases via Gas-Phase Oxidation. *Ind. Eng. Chem. Res.* **2019**, *58*, 21904–21912.
- (46) Johansson, J.; Normann, F.; Andersson, K. Techno-Economic Evaluation of Co-Removal of NO_x and SO_x Species from Flue Gases via Enhanced Oxidation of NO by ClO₂ – Case Studies of Implementation at a Pulp and Paper Mill, Waste-to-Heat Plant and a Cruise Ship. *Energies* **2021**, *14*, 8512.
- (47) Morón, W.; Rybak, W. NO_x and SO₂ emissions of coals, biomass and their blends under different oxy-fuel atmospheres. *Atmos. Environ.* **2015**, *116*, 65–71.
- (48) Müller, I. A.; Brunner, B.; Breuer, C.; Coleman, M.; Bach, W. The oxygen isotope equilibrium fractionation between sulfite species and water. *Geochim. Cosmochim. Acta* **2013**, *120*, 562–581.

D. Schmid, M. Hupa, M. Paavola, I. Vuorinen, A. Lehtikoinen, O. Karlström.
Role of Thiosulfate in NO₂ Absorption in Aqueous Sulfite Solutions.
Ind. Eng. Chem. Res. 62(1) (2023), 150-110.

Role of Thiosulfate in NO₂ Absorption in Aqueous Sulfite Solutions

Daniel Schmid,* Mikko Hupa, Mikko Paavola, Ilari Vuorinen, Arja Lehtikoinen, and Oskar Karlström

Cite This: *Ind. Eng. Chem. Res.* 2023, 62, 105–110

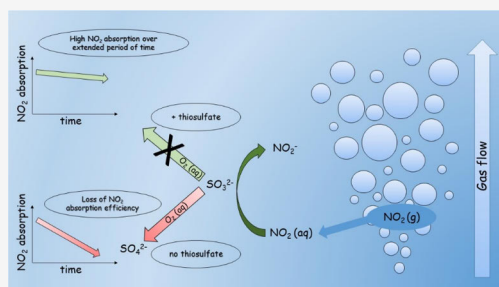
Read Online

ACCESS |

Metrics & More

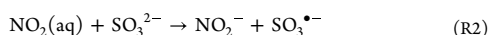
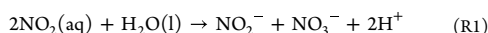
Article Recommendations

ABSTRACT: NO_x emissions continues to be a major challenge in order to reduce the environmental impact of thermal conversion of non-recyclable waste and fuels with high nitrogen contents. Oxidation of NO to NO₂ followed by absorption of NO₂ in aqueous solutions with sulfur compounds as additives has recently gained more attention in order to reduce NO_x emissions from flue gases. One major challenge in NO₂ absorption is the high consumption of sulfite, requiring sulfite oxidation inhibitors such as thiosulfate. The present study clarifies the chemistry and consumption of thiosulfate in wet scrubbing of NO₂ with buffered solutions under well-controlled conditions at neutral pH at 25 °C. Absorption rates for the reaction of thiosulfate and NO₂ in the scrubber were determined, and the ability of thiosulfate to inhibit the sulfite oxidation was investigated and quantified. With 1 mM thiosulfate (no sulfite) in the scrubber solution, the NO₂ absorption rate increased by 30% as compared to pure water and by 160% with 100 mM thiosulfate. The absorption rate increased with time in the presence of oxygen. With 1 mM sulfite (no thiosulfate), the initial NO₂ absorption rate increased by 200% as compared to pure water. However, the absorption rate decreases significantly after short periods of time due to the high consumption of sulfite through undesired oxidation by O₂. In tests with sulfite and thiosulfate as an oxidation inhibitor, high removal efficiencies could be maintained over extended periods of time. With a 10 mM sulfite solution, 1 mM thiosulfate decreased the sulfite oxidation rate from 130 to 31 mg·L⁻¹·min⁻¹, and 2 mM thiosulfate decreased the rate to 16 mg·L⁻¹·min⁻¹. For the investigated conditions, the consumption of thiosulfate did not change significantly when higher sulfite concentrations were used. The results of the study demonstrate high NO₂ absorption rates for low concentrations of sulfite and thiosulfate at neutral pH.



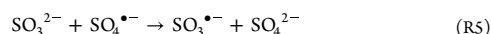
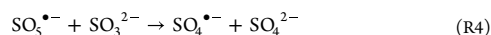
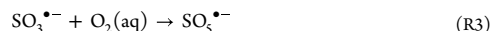
1. INTRODUCTION

NO₂ absorption in aqueous sulfite solutions has recently gained more attention in order to reduce NO_x emissions from thermal conversion of non-recyclable waste and fuels with high nitrogen contents.^{1–4} The NO_x in flue gases consists mostly of NO. Due to the low solubility of NO in water, NO is oxidized to NO₂ which has a higher solubility in water.^{5,6} NO₂ reacts with water forming nitrite and nitrate (see RR1).⁷ In order to further improve NO₂ absorption rates, additives such as sulfite can be used.^{8–10} The sulfite concentration, the oxygen concentration, and the pH of the scrubber solution influence the NO₂ absorption rate.^{11–13} The reaction between sulfite and NO₂ is believed to take place close to the surface of the liquid via charge transfer, forming nitrite (NO₂⁻) and a sulfite radical (SO₃^{•-}) (see RR2).¹⁴



The sulfite radical can undergo a radical chain reaction (see RR3, RR4, RR5, and RR6) which results in a high consumption of sulfite in the presence of oxygen. In this

chain reaction, SO₅^{•-} and SO₄⁻ radicals are formed oxidizing sulfite to sulfate. The kinetics of the sulfite oxidation by oxygen has been studied by Lian et al.¹⁵ The influence of sulfite concentration and NO₂(g) concentration on the sulfite oxidation rate has been investigated showing that the oxidation rate increases with increased sulfite concentrations.^{11,13}



Received: November 29, 2022

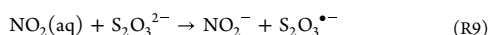
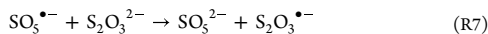
Revised: December 12, 2022

Accepted: December 22, 2022

Published: December 29, 2022



Thiosulfate can be used as a sulfite oxidation inhibitor to reduce the consumption rate of sulfite in the NO₂ absorption process.^{16,17} Thiosulfate acts as a radical scavenger and terminates the chain reaction (see RR7 and RR8). Besides this, thiosulfate can also react with NO₂, similarly to the reaction between sulfite and NO₂, forming nitrite and another radical (see RR9).



The role and chemistry of thiosulfate in NO₂ absorption have only been investigated to a limited extent.^{9,13} Sapkota et al. investigated the kinetics of the NO₂-catalyzed sulfite oxidation at low NO₂ concentrations (2–10 ppm) and sulfite concentrations of around 40 and 25 mM or 100 mM thiosulfate at pH 9.¹³ In their tests with 40 mM sulfite and 25 or 100 mM thiosulfate, the sulfite oxidation rate was reduced by 1 order of magnitude, while a further increase in the thiosulfate concentrations (from 25 to 100 mM thiosulfate) only showed minor improvements. The use of even lower thiosulfate/sulfite ratios under neutral pH has not been investigated previously, which is the aim of the present work. For industrial applications, it is crucial to understand the details of the absorption process with thiosulfate and sulfite in order to minimize the consumption of chemicals and thereby reduce the production of waste products.

The present study investigates the role of thiosulfate in NO₂ absorption in aqueous sulfite solutions. The reactions between thiosulfate and NO₂ and O₂ are investigated to understand the overall contribution of thiosulfate on the NO₂ absorption. In a second step, the role of thiosulfate as a sulfite oxidation inhibitor is investigated. Sulfite oxidation rates in the presence of thiosulfate are determined, as well as the consumption of thiosulfate when used as a sulfite oxidation inhibitor. To understand the thiosulfate and sulfite consumption rates is of great importance in order to minimize the usage of additives for NO₂ absorption, while maintaining a high NO₂ absorption efficiency.

2. EXPERIMENTAL SECTION

The setup used for the NO₂ absorption experiments is shown in Figure 1. The gases used in the experiments were mixed before entering a gas washing bottle in which the gas bubbled

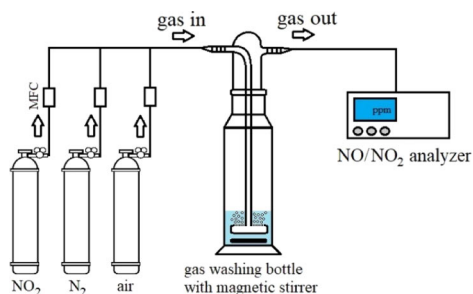


Figure 1. Experimental setup for NO₂ absorption experiments; MFC = mass flow controller.

through a magnetically stirred absorption solution (50 mL) at room temperature. The NO₂ was purchased from Air Products (200 ppm NO₂, N₂ as balance gas). After passing through the absorption solution, the gas passed a SCC-K catalyst from ABB to reduce all NO₂ to NO. The NO was then quantified using a chemiluminescence detector from Teledyne, model 200EM. The total gas flow rate of 2.3 NL/min was controlled with EL-FLOW mass flow meters from Bronkhorst. The inlet gas concentration was either 50 ppm NO₂ without oxygen or 50 ppm + 5% O₂ with nitrogen as the carrier gas.

Absorption tests with only thiosulfate in the absorption solution were performed with thiosulfate concentrations between 0 and 100 mM. The sodium thiosulfate (anhydrous, ≥98%) was purchased from Riedel-de Haën. For the absorption tests with both sulfite and thiosulfate, absorption solutions containing 2–10 mM sulfite and 0–5 mM thiosulfate were used. The sodium sulfite (anhydrous, ≥98%) was purchased from Sigma-Aldrich. The solutions were buffered with a phosphate buffer (NaHPO₄·2H₂O + KH₂PO₄) to maintain stable conditions around pH 7. Ion chromatography was performed for selected absorption experiments to follow the consumption of thiosulfate. For the quantification of thiosulfate, a Metrosep A SUPP 4 column from Metrohm was used with a carbonate/bicarbonate eluent.

3. RESULTS AND DISCUSSION

3.1. NO₂ Absorption with Thiosulfate. Figure 2 shows NO₂ concentrations for the experiments with 0–100 mM thiosulfate (a) or 0–20 mM sulfite (b) (reproduced from¹¹) in the scrubber solution. The corresponding apparent absorption rates are presented in Table 1 (absorption rates marked with * are estimated values for comparison with data from¹¹). Without thiosulfate, that is, pure water, the NO₂ concentration decreased from the initial 50 to 44 ppm. In the experiment with 1 mM thiosulfate, the NO₂ concentration decreased to 42 ppm, that is, the absorption rate increased by 30%. Increasing the thiosulfate concentration from 1 to 2 mM had no observable effect on the NO₂ absorption. With 10 or 100 mM, the NO₂ concentration decreased to 39 or 35 ppm, respectively.

Comparing the NO₂ absorption rates from tests with thiosulfate to the tests with sulfite, it is clear that sulfite has a much stronger effect on the NO₂ absorption rates than thiosulfate, which is in agreement with earlier findings in literature.^{9,18} The apparent reaction rates for the sulfite solutions with 1, 2, or 5 mM concentration are about 2.5–3 times higher as compared to the corresponding thiosulfate solutions. Various reactions might occur simultaneously (NO₂ either reacting with sulfite/thiosulfate or water), hence only apparent reaction rates are given to describe the observed phenomena in our scrubber system. However, ion chromatography analysis of selected tests indicate that NO₂ mainly reacts with thiosulfate and sulfite as only nitrite was found as an absorption product (compare RR2 and RR9).

Figure 3 shows NO₂ concentrations for absorption experiments with 2 mM thiosulfate (no sulfite) with and without O₂(g) in the inlet gas, and Table 2 lists the thiosulfate concentrations in the absorption solution before and after the corresponding experiments. Without oxygen, the NO₂ concentration decreased from the initial 50 ppm to around 40 ppm and remained almost constant during the 30 min period of the experiment. A slight increase of the NO₂ concentration could be observed as the experiment proceeded.

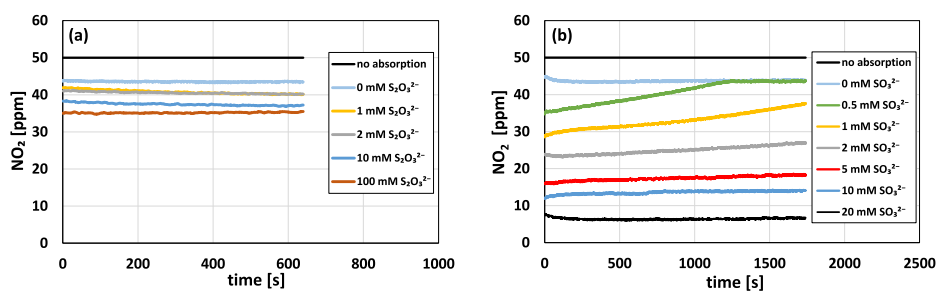


Figure 2. NO_2 concentrations for absorption experiments with (a) 0–100 mM thiosulfate and (b) 0–20 mM sulfite (reproduced from¹¹); inlet gas 50 ppm NO_2 (rest N_2 , no oxygen).

Table 1. Apparent Reaction Rates for Reaction of NO_2 with Thiosulfate or Sulfite Solutions; 50 ppm NO_2 , No Oxygen^a

| additive concn [mM] | NO_2 abs. rate (thiosulfate) [$\text{mol} \cdot \text{dm}^{-3} \cdot \text{s}^{-1}$] | NO_2 abs. rate (sulfite) [$\text{mol} \cdot \text{dm}^{-3} \cdot \text{s}^{-1}$] ¹¹ |
|---------------------|---|---|
| 0 | 1.82×10^{-7} | 1.88×10^{-7} |
| 0.5 | 2.23×10^{-7} * | 4.23×10^{-7} |
| 1 | 2.37×10^{-7} | 5.95×10^{-7} |
| 2 | 2.72×10^{-7} | 7.45×10^{-7} |
| 5 | 3.10×10^{-7} * | 9.46×10^{-7} |
| 10 | 3.50×10^{-7} | 1.05×10^{-6} |
| 20 | 3.93×10^{-7} * | 1.25×10^{-6} |
| 100 | 4.68×10^{-7} | n.i. |

^a*Estimated, n.i. = not investigated.

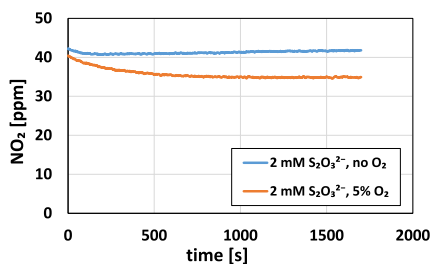


Figure 3. NO_2 concentrations for absorption experiments with 2 mM $\text{S}_2\text{O}_3^{2-}$, 50 ppm NO_2 with or without 5% O_2 .

Table 2. Thiosulfate Consumption Determined by Ion Chromatography

| gas inlet concn. | SO_3^{2-} [mM] | $\text{S}_2\text{O}_3^{2-}$ [mM] | | $\text{S}_2\text{O}_3^{2-}$ consumed [%] |
|---------------------------------------|-------------------------|----------------------------------|--------------|--|
| | | initial concn. | after 30 min | |
| 50 ppm NO_2 | | 2.08 | 1.96 | 5.8 |
| 50 ppm $\text{NO}_2 + 5\% \text{O}_2$ | | 2.10 | 1.74 | 17.1 |

This is likely due to the consumption of thiosulfate by the absorption reaction with NO_2 (compare RR9). In the 30 min test without oxygen, around 6% of the thiosulfate was consumed.

In the presence of oxygen, the thiosulfate consumption increased and also the NO_2 absorption efficiency increased. Initially the NO_2 decreased to 40 ppm, and a further decrease of the NO_2 concentration over time was observed. After

around 700 s, the NO_2 concentration decreased to 35 ppm and remained at this level. One possible explanation for this observation might be the partial oxidation of thiosulfate to sulfite. The oxidation of thiosulfate has been described as a very slow reaction and the final oxidation product is sulfite,^{16,19} which does not react with NO_2 . However, sulfite might be formed as an intermediate in the oxidation of thiosulfate, which is then reacting with NO_2 . Due to the much higher reaction rate for the reaction with sulfite as compared to thiosulfate, a small amount of thiosulfate oxidized to sulfite could explain the improved NO_2 absorption efficiency. As only thiosulfate and sulfite were present in the scrubber solution after the experiment, it is likely that sulfite is consumed rapidly after its formation, which could also explain why the NO_2 concentration in Figure 3 eventually becomes constant, that is, the absorption rate is constant and the rate is limited by the oxidation of thiosulfate to sulfite. Another possibility could be the formation of sulfide by decomposition of thiosulfate. This has previously only been described for acidic solutions at room temperature.²⁰ The formation of sulfide from decomposition of thiosulfate²¹ could also be a possible explanation for the increased absorption as sulfide reacts rapidly with NO_2 ,²² but this would likely lead to H_2S formation at the investigated pH, which was not the case in our experiments.

3.2. NO_2 Absorption with Thiosulfate and Sulfite.

Figure 4 shows the NO_2 concentrations for experiments with 2 or 5 mM thiosulfate and 2, 5, or 10 mM sulfite. The initial NO_2 concentrations for the experiments with same sulfite concentration but different thiosulfate concentration are identical. Also, when comparing the initial NO_2 concentrations to the corresponding tests without thiosulfate in Figure 2b, it can be seen that the initial NO_2 concentrations are identical. Hence, it can be concluded that thiosulfate has no relevant influence on the NO_2 absorption under the investigated conditions in the presence of sulfite. However, thiosulfate has a positive effect as a sacrificial agent on maintaining the absorption efficiency of sulfite over an extended period of time. The increase of the NO_2 concentration over time, that is, the loss of absorption efficiency, was more rapid in the case with 2 mM thiosulfate as compared to 5 mM thiosulfate. With 10 mM sulfite and 2 mM thiosulfate, 76% of the NO_2 is absorbed initially. The absorption efficiency decreased to 60% after 10 min in the case with 2 mM thiosulfate, while it was still at 70% with 5 mM thiosulfate.

In our previous work,¹¹ we determined oxidation rates for sulfite (oxidation by O_2 , excluding oxidation by NO_2) based on multiple absorption tests with and without O_2 . An example of

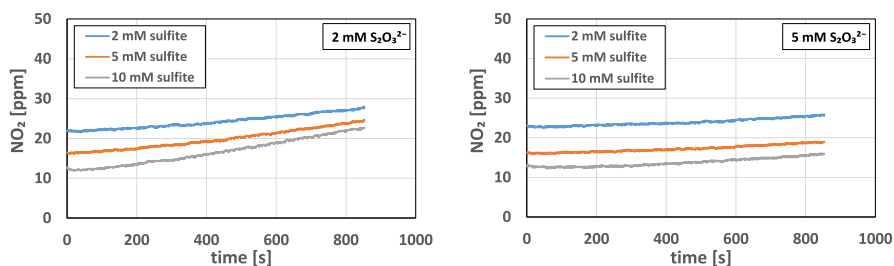


Figure 4. NO₂ concentrations for absorption experiments with 2–10 mM sulfite and 2 or 5 mM thiosulfate; input 50 ppm NO₂ + 5% O₂ (rest N₂).

the sulfite oxidation rate (excluding oxidation by NO₂) with 2 mM sulfite and 1 mM thiosulfate is presented in Figure 5.

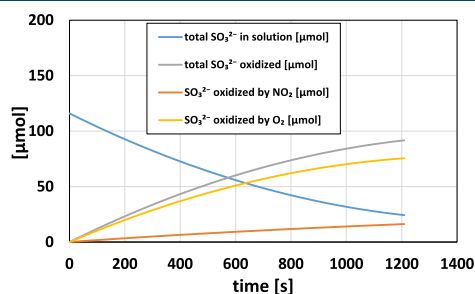


Figure 5. Total amount of sulfite as a function of time (blue line) and amount of consumed sulfite: total consumption (gray), consumed by O₂ (yellow), and consumed by NO₂ (red); test with 2 mM sulfite and 1 mM thiosulfate, input gas 50 ppm NO₂ + 5% O₂ (rest N₂).

Using this approach, the sulfite concentration at each point of time is determined based on the NO₂ absorption efficiency. The amount of sulfite oxidized by NO₂ is then calculated based on the NO₂ absorption up to this point, and the stoichiometric ratio according to RR2. RR1 has been shown to be negligible at sufficient high sulfite concentrations and based on the above results, it is assumed that the reactions of thiosulfate with NO₂ can be neglected for the overall reaction as well with sufficient high sulfite concentrations. The difference between the amount of sulfite oxidized by NO₂ and the total amount of oxidized sulfite is considered to be the amount of sulfite that has been oxidized due to the presence of oxygen through the above described mechanisms (RR3, RR4, RR5, and RR6).

The results for those sulfite oxidation rates based on the above describe approach are shown in Figure 6. Oxidation rates have been determined for 2, 5, and 10 mM sulfite with 0, 1, 2, or 5 mM thiosulfate. Without thiosulfate, sulfite oxidation rates were high and increased with increasing sulfite concentration, which is in agreement to previous studies.^{11,13} With 2 mM sulfite, the oxidation rate was around 40 and 130 mg·L⁻¹·min⁻¹ with 10 mM sulfite. With 1 mM thiosulfate, the oxidation rate decreased notably for all sulfite concentrations, 9 mg·L⁻¹·min⁻¹ for 2 mM sulfite and 31 mg·L⁻¹·min⁻¹ for 10 mM sulfite, respectively. A further increase in the thiosulfate concentration above 2 mM showed only little reduction of the oxidation rate, as it is already low at this point for all cases.

Figure 7 compares NO₂ concentrations from absorption experiments with 10 mM sulfite and various thiosulfate

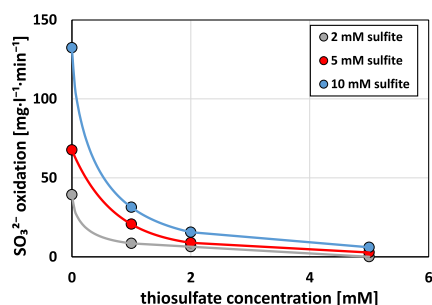


Figure 6. Sulfite oxidation rates (oxidation by O₂; oxidation by NO₂ excluded) vs thiosulfate concentration for 50 ppm NO₂ + 5% O₂ (rest N₂).

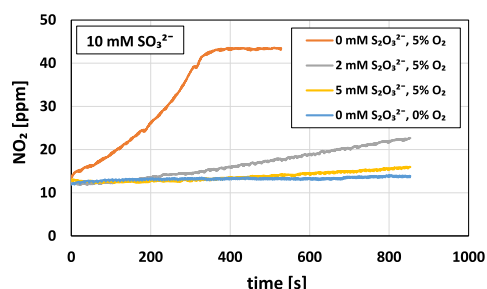


Figure 7. Comparison of NO₂ absorption experiments with 10 mM sulfite and various thiosulfate concentrations with and without oxygen; inlet gas 50 ppm NO₂ or 50 ppm NO₂ + 5% O₂ (rest N₂).

concentrations with and without oxygen in the inlet gas (red line for 0 mM S₂O₃²⁻, 5% O₂ and blue line for 0 mM S₂O₃²⁻, 0% O₂ reproduced from¹¹). This figure illustrates the effect of thiosulfate on the improved NO₂ absorption over extended periods of time. With 2 mM thiosulfate and 5% O₂, the absorption still decreases with time. With 5 mM thiosulfate and 5% O₂, the absorption is almost the same over the investigated period of time as compared to 0 mM thiosulfate and 0% O₂. This indicates that it is possible to inhibit the sulfite oxidation to such an extent that the absorption almost works equally well and long in the presence of oxygen as compared to the absorption without oxygen in the inlet gas when thiosulfate is used as an oxidation inhibitor.

Table 3 presents thiosulfate concentrations from an additional absorption test with 2 or 5 mM sulfite and 2 mM

Table 3. Thiosulfate Consumption Determined by Ion Chromatography

| gas inlet concn | SO ₃ ²⁻ [mM] | S ₂ O ₃ ²⁻ [mM] | | S ₂ O ₃ ²⁻ consumed [%] |
|--|------------------------------------|--|--------------|--|
| | | initial concn | after 30 min | |
| 50 ppm NO ₂ + 5% O ₂ | 2 | 2.00 | 1.24 | 38.0 |
| 50 ppm NO ₂ + 5% O ₂ | 5 | 2.04 | 1.14 | 44.1 |

thiosulfate and 50 ppm NO₂ + 5% O₂ in the inlet gas. The time of the experiment was 30 min, and the thiosulfate concentrations were measured before and after the tests. Interestingly, the consumption of the thiosulfate did not increase significantly when more sulfite is present in the solution. In the test with 2 mM sulfite, around 38% of the thiosulfate was consumed in 30 min, while 44% of the thiosulfate was consumed in the case with 5 mM sulfite. Based on the obtained data, it cannot be clarified to which extent thiosulfate is consumed by oxygen or reaction products from the sulfite oxidation mechanism. The higher sulfite oxidation rates with higher sulfite concentrations may be explained by a higher concentration of sulfite radicals which accelerate the chain mechanism described in RR3, RR4, RR5, and RR6. Based on the suggested mechanism, a higher thiosulfate consumption could be expected for higher sulfite concentrations as more radicals are available for reaction with thiosulfate according to RR7. This, however, was not observed in the experiments. Also, according to RR8, the SO₅²⁻ ion formed in RR7 should still be able to oxidize sulfite to sulfate. In this case, however, sulfite should be consumed at a higher rate than what is observed. Based on our results, it may be concluded that the current understanding about the sulfite oxidation inhibition with thiosulfate requires further research.

4. CONCLUSIONS

The present study investigated the role of thiosulfate in wet scrubbing of NO₂ with aqueous sulfite solutions under buffered conditions. Absorption rates for the reaction of thiosulfate and NO₂ in the scrubber were determined, and the ability of thiosulfate to inhibit the sulfite oxidation was investigated. In addition, NO₂ absorption with only thiosulfate was investigated.

With 1 mM thiosulfate (no sulfite) in the scrubber solution, the NO₂ absorption rate increased by 30% as compared to pure water, and by 160% with 100 mM thiosulfate. With 1 mM sulfite (no thiosulfate), the NO₂ absorption rate increased by 200% as compared to pure water. Interestingly, in tests with thiosulfate (no sulfite) and oxygen, the NO₂ absorption rates improved with time. This effect has previously not been observed to our knowledge and may have a strong influence of future industrial NO₂ absorption processes.


Tests with both sulfite and thiosulfate as an oxidation inhibitor resulted in high removal efficiencies that could be maintained over extended periods of time. With small concentrations of thiosulfate, the sulfite oxidation rates decreased significantly. For a 10 mM sulfite solution, 1 mM thiosulfate decreased the oxidation rate by 75%, and with 2 mM thiosulfate by 88%, respectively.

For the investigated conditions, the consumption of thiosulfate when used as a sulfite oxidation inhibitor did not change significantly when higher sulfite concentrations were

used. For a 2 mM sulfite solution and 2 mM thiosulfate, 38% of the thiosulfate was consumed after 30 min, while 44% was consumed in the corresponding test with 5 mM sulfite. The results demonstrate high NO₂ absorption rates for low concentrations of sulfite and thiosulfate at neutral pH.

■ AUTHOR INFORMATION

Corresponding Author

Daniel Schmid – Johan Gadolin Process Chemistry Centre, Åbo Akademi University, 20500 Turku, Finland;
 orcid.org/0000-0002-7786-7134; Email: dschmid@abo.fi

Authors

Mikko Hupa – Johan Gadolin Process Chemistry Centre, Åbo Akademi University, 20500 Turku, Finland

Mikko Paavola – Valmet Technologies Oy, 33900 Tampere, Finland

Ilari Vuorinen – Valmet Technologies Oy, 33900 Tampere, Finland

Arja Lehtikoinen – Valmet Technologies Oy, 33900 Tampere, Finland

Oskar Karlström – Johan Gadolin Process Chemistry Centre, Åbo Akademi University, 20500 Turku, Finland; Industrial Engineering and Management, Department of Mechanical and Materials Engineering, University of Turku, 20500 Turku, Finland

Complete contact information is available at:
<https://pubs.acs.org/10.1021/acs.iecr.2c04299>

Notes

The authors declare no competing financial interest.

■ ACKNOWLEDGMENTS

This study was financed by the Academy of Finland financed project Chemical challenges in gasification of biomass and waste (355914 and 353318).

■ REFERENCES

- (1) Sharif, H. M. A.; Mahmood, N.; Wang, S.; Hussain, I.; Hou, Y.-N.; Yang, L.-H.; Zhao, B.; Yang, B. Recent advances in hybrid wet scrubbing techniques for NO_x and SO₂ removal: State of the art and future research. *Chemosphere* **2021**, *273*, 129695.
- (2) Zhao, M.; Xue, P.; Liu, J.; Liao, J.; Guo, J. A review of removing SO₂ and NO_x by wet scrubbing. *Sustain. Energy Technol. Assessments* **2021**, *47*, 101454.
- (3) Johansson, J.; Normann, F.; Andersson, K. Techno-Economic Evaluation of Co-Removal of NO_x and SO_x Species from Flue Gases via Enhanced Oxidation of NO by ClO₂ - Case Studies of Implementation at Pulp and Paper Mill, Waste-to-Heat Plant and a Cruise Ship. *Energies* **2021**, *14*, 8512.
- (4) Johansson, J. Absorption Based Systems for Co-removal of Nitrogen Oxides and Sulfur Oxides from Flue Gases. Ph.D Thesis, Chalmers University, 2022.
- (5) Guo, R.; Hao, J.; Pan, W.; Yu, Y. Liquid Phase Oxidation and Absorption of NO from Flue Gas: A review. *Sep. Sci. Technol.* **2015**, *50*, 310–321.
- (6) Brogren, C.; Karlsson, H. T.; Bjerle, I. Absorption of NO in an Aqueous Solution of NaClO₂. *Chem. Eng. Technol.* **1998**, *21*, 61–70.
- (7) Kameoka, Y.; Pigford, R. Absorption of Nitrogen Dioxide into Water, Sulfuric Acid, Sodium Hydroxide, and Alkaline Sodium Sulfite Aqueous Solutions. *Ind. Eng. Chem. Fundam.* **1977**, *16*, 163–169.
- (8) Zhang, Z.; Xi, H.; Zhou, S.; Zhou, W.; Shreka, M. Efficient removal of NO_x from simulated marine exhaust by using O#-

Na₂SO₃: Experimental factors and optimization analysis. *Fuel* **2022**, *313*, 122659.

(9) Shen, C. H.; Rochelle, G. T. Nitrogen Dioxide Absorption and Sulfite Oxidation in Aqueous Sulfite. *Environ. Sci. Technol.* **1998**, *32*, 1994–2003.

(10) Takeuchi, H.; Ando, M.; Kizawa, N. Absorption of Nitrogen Oxides in Aqueous Sodium Sulfite and Bisulfite Solutions. *Ind. Eng. Chem. Process Des. Dev.* **1977**, *16*, 303–308.

(11) Schmid, D.; Karlström, O.; Kuvaja, V.; Vuorinen, I.; Paavola, M.; Hupa, M. Role of Sulfite Oxidation in NO₂ Absorption in a pH-Neutral Scrubber Solution. *Energy Fuels* **2022**, *36*, 2666–2672.

(12) Shi, F.; Li, K.; Li, J.; Ying, D.; Jia, J.; Sun, T.; Yan, N.; Zhang, X. Simultaneous wet absorption of SO₂ and NO_x with mixed Na₂SO₃ and (NH₄)₂SO₃: Effects of mass concentration ratio and pH. *Chem. Eng. J.* **2021**, *421*, 129945.

(13) Sapkota, V. V. A.; Fine, N. A.; Rochelle, G. T. NO₂-catalyzed sulfite oxidation. *Ind. Eng. Chem. Res.* **2015**, *54*, 4815–4822.

(14) Nash, T. The effect of nitrogen dioxide and of some transition metals on the oxidation of dilute bisulphite solutions. *Atmos. Environ.* **1979**, *13*, 1149–1154.

(15) Lian, Z.; Zhu, K.; Zhang, S.; Ma, W.; Zhong, Q. Study on the synergistic oxidation of sulfite solution by ozone and oxygen: kinetics and mechanism. *Chem. Eng. Sci.* **2021**, *242*, 116745.

(16) Mo, J.-S.; Wu, Z.-B.; Cheng, C.-J.; Guan, B.-H.; Zhao, W.-R. Oxidation inhibition of sulfite in dual alkali flue gas desulfurization system. *J. Environ. Sci.* **2007**, *19*, 226–231.

(17) Rochelle, G. T.; Owens, D. T.; Chang, J. C.; Bma, T. G. Thiosulfate as an Oxidation Inhibitor in Flue Gas Desulfurization Processes: A review of R&D Results. *J. Air Pollut. Control Assoc.* **1986**, *36*, 1138–1146.

(18) Clifton, C.; Altstein, N.; Huie, R. Rate constant for the Reaction of NO₂ with Sulfur(IV) over the pH Range of 5.3–13. *Environ. Sci. Technol.* **1988**, *22*, 586–589.

(19) Rolia, E.; Charkrabarti, C. L. Kinetics of Decomposition of Tetrathionate, Trithionate, and Thiosulfate in Alkaline Media. *Environ. Sci. Technol.* **1982**, *16*, 852–857.

(20) Davis, R. E. Displacement reactions at the sulfur atom. I. An Interpretation of the Decomposition of Acidified Thiosulfate. *J. Am. Chem. Soc.* **1958**, *80*, 3565–3569.

(21) Pryor, W. The Kinetics of the Disproportionation of Sodium Thiosulfate to Sulfide and Sulfate. *J. Am. Chem. Soc.* **1960**, *82*, 4794–4797.

(22) Shen, C.; Rochelle, G. Nitrogen Dioxide Absorption and Sulfite Oxidation in Aqueous Sulfite. *J. Air Waste Manage. Assoc.* **1999**, *49*, 332–338.

ISBN 978-952-12-4273-1